

Method for Thoracic Injury Risk Function Development for Human Body Models

A

Thesis

Presented to

the faculty of the School of Engineering and Applied Science
University of Virginia

in partial fulfillment
of the requirements for the degree

Master of Science

by

Shubham Kulkarni

May 2022

APPROVAL SHEET

This
Thesis
is submitted in partial fulfillment of the requirements
for the degree of
Master of Science

Author: Shubham Kulkarni

This Thesis has been read and approved by the examining committee:

Advisor: Dr. Matthew Panzer

Advisor: Dr. Jason Forman

Committee Member: Dr. Robert Salzar

Committee Member:


Committee Member:

Committee Member:

Committee Member:

Committee Member:

Accepted for the School of Engineering and Applied Science:



Jennifer L. West, School of Engineering and Applied Science

May 2022

ACKNOWLEDGMENTS

This study was supported by Toyota Collaborative Safety Research Center (CSRC). The opinions presented here are solely those of the author, and do not necessarily represent the consensus views of the sponsoring organization.

I would like to thank Dr. Jason Forman and Dr. Matthew Panzer for providing the opportunity to learn and research at the University of Virginia's Center for Applied Biomechanics, as well as the members of my thesis committee for their feedback and support throughout this process. I would also like to thank Dr. Daniel Perez-Rapela who has made invaluable contributions to this research and my development as a researcher.

I would also like to thank CAB staff and students for their assistance and collaboration throughout my time here. CAB's greatest strength is its people, and I have benefitted greatly from the relationships and support that I have found here.

Finally, I would like to thank my parents and brother for their love and encouragement throughout this process. I would not have made it here without their support and blessing.

ABSTRACT

Introduction: In recent years, finite element human body models (FE-HBMs or HBMs) have been developed as an evaluation tool for restraint system and safety assessment in virtual simulations. However, for HBMs to be truly useful as a tool, standardized methods need to be developed for translating the outputs from HBM simulations into predicted risk of injury. An important body region of interest for such standardization is the thorax. Although the thorax was one of the first body regions for which anatomical structures were modeled in detail in HBMs, the thorax remains one of the most frequently injured body regions in motor vehicle collisions (MVCs). Thus, there is a need to develop a framework for tuning model-specific thoracic injury risk functions which would drive towards consistent injury risk prediction across various HBMs, despite the differences in the models.

Goals of Study: The main objective of this thesis was to develop a set of guidelines and framework which standardizes the methodology for developing thoracic injury risk functions for human body models in frontal impacts and drives towards consistent injury risk prediction even across different models.

Methods of Study: The framework for developing thoracic injury risk functions for frontal impacts was developed using the THUMS v4.1 M50 model and verified by application to an alternate model, namely the GHBMC v6.0 M50. Simulations targeting test conditions used in past tests with post-mortem human surrogates (PMHS) were performed with the HBMs and further regression and optimization analyses were performed to relate thoracic measures from HBM to injuries observed in matched PMHS tests. Simulations were performed in nineteen frontal-impact loading modes derived from the literature, including hub impact tests, bar impact tests, and table-

top tests with belt loading as well as sled cases. The model input conditions were adjusted based on the input conditions used for each specific PMHS test, resulting in a simulation for each individual PMHS test. In all, approximately 176 individual simulations were performed, distributed across the nineteen loading modes. Various deflection and strain-based outputs from these simulations were examined to determine which measures (or combination of measures) best predicted the rib fracture injuries observed in the PMHS tests. Further, both the models were exercised in a realistic vehicle environment subjected to 56 kph frontal collision. The subsequent injury risk prediction from the models was compared to field data describing risk from comparable collisions.

Results of Study: The study resulted in the formation of a framework and detailed guidelines on setting up simulations and developing thoracic injury risk functions for HBMs in frontal impacts. The framework was demonstrated using the THUMS v4.1 model and verified using the GHBM v6.0 model. A total of 176 unique matched pair simulations (55 impactor cases, 115 table-top cases and 6 sled cases) from 19 different loadcases were performed for THUMS and 170 (excluding the sled cases) for GHBM. Two types of injury risk functions, deflection based and rib strain based were developed. For the strain based IRF, the underlying rib fracture risk curve of Larsson et al. 2021 was calibrated to be used with the specific HBM in the probabilistic rib fracture risk prediction framework developed by Forman et al. 2012. The collision simulations performed in a realistic vehicle environment, showed that using the tuned strain-based chest IRFs, the THUMS and GHBM both predicted rib fracture risks that were generally consistent with the field data for 56 km/h frontal collisions.

Impact of Thesis: The major contribution of this thesis is a set of guidelines and framework which can be used to develop thoracic injury risk functions for human body models from a

consistent dataset and thus drive towards consistent injury risk prediction across various human body models. This thesis is also the first study to tune or calibrate the underlying rib fracture risk curve in the probabilistic rib fracture risk prediction framework of Forman et al. 2012 to be used with a specific HBM. The methodology developed for calibrating the fracture risk curve can be used to develop risk curves for any model. This removes the need for modifying the HBM ribcage (geometry, mesh or material properties) to get the best results in injury prediction with the strain based probabilistic rib fracture risk prediction framework.

TABLE OF CONTENTS

ACKNOWLEDGMENTS	3
ABSTRACT	4
TABLE OF CONTENTS	7
TABLE OF FIGURES	10
TABLE OF TABLES	16
CHAPTER 1: INTRODUCTION	17
1.1 BACKGROUND AND MOTIVATION	17
1.2 OBJECTIVES.....	21
CHAPTER 2: TASK 1 – PMHS DATA AND SIMULATIONS FOR IRF DEVELOPMENT AND VALIDATION	23
2.1 SELECTION OF LOADCASES (PMHS DATA).....	23
2.2 SIMULATIONS	25
2.2.1 <i>HBM Instrumentation</i>	25
2.2.2 <i>Simulations For IRF Development</i>	26
Impactor Cases.....	26
Introduction.....	26
FE Setup	27
HBM Biofidelity.....	38
Test Specific Simulations	42
Table-Top Cases	43
Introduction.....	43
FE Setup	44

HBM Biofidelity	57
Test Specific Simulations	63
2.2.3 <i>Simulations For IRF Validation</i>	63
Sled Cases	63
Introduction	63
FE Setup and HBM Kinematics	64
2.3 SUMMARY	79
CHAPTER 3: TASK 2 – INJURY RISK FUNCTIONS DEVELOPMENT	80
3.1 STRATEGY	80
3.2 DEFLECTION BASED IRF	81
3.2.1 <i>Development of Injury Risk Curves</i>	81
3.2.2 <i>Results</i>	83
3.2.3 <i>Validation with Sled Cases</i>	86
3.2.4 <i>Conclusion</i>	88
3.3 STRAIN BASED IRF	89
3.3.1 <i>Probabilistic Rib Fracture Risk Prediction Framework</i>	89
3.3.2 <i>Optimization of Rib Fracture Risk Curve for HBM</i>	91
3.3.3 <i>Results</i>	93
3.3.4 <i>Validation with Sled Cases</i>	95
3.3.5 <i>Conclusion</i>	98
3.4 SUMMARY	99
CHAPTER 4: TASK 3 – APPLICATION TO ALTERNATE HUMAN BODY MODEL	101
4.1 DEFLECTION BASED IRF	102
4.2 STRAIN BASED IRF	103
4.3 SUMMARY	104

CHAPTER 5: TASK 4 – IN-VEHICLE SIMULATION	106
5.1 SIMULATION SETUP	106
5.1.1 <i>Vehicle Environment and Loadcase</i>	106
5.1.2 <i>HBM Position and Posture in Vehicle</i>	108
5.2 RESULTS	109
5.3 SUMMARY	112
CHAPTER 6: DISCUSSION AND CONCLUSIONS	114
6.1 DISCUSSION	114
6.2 FUTURE RESEARCH DIRECTIONS	125
6.3 CONCLUDING REMARKS.....	126
REFERENCES.....	128
APPENDIX A: PMHS DETAILS AND INJURY INFORMATION FOR ALL TESTS.....	136
APPENDIX B: IMPACTOR MASSES AND VELOCITIES FOR IMPACTOR CASES.....	141
APPENDIX C: MID-STERNUM DEFLECTIONS AND PROBABILITIES OF INJURY CALCULATED WITH DEFLECTION IRF FOR ALL CASES	143
APPENDIX D: NORMALIZED INPUT DISPLACEMENT CURVES FOR TABLE TOP TESTS.....	148

TABLE OF FIGURES

Figure 1 HBM Instrumentation - a) Local coordinate systems on vertebrae T1 - T12 b) skeletal deflection points c) parts for output of strain.....	26
Figure 2 Pretest experimental setup from (Kroell et al., 1974)	28
Figure 3 THUMS v4.1 M50 model posture for Kroell 1974 thorax validation case.....	28
Figure 4 Upper leg (femurs) orientation with reference angle	29
Figure 5 Torso orientation with reference angle.....	30
Figure 6 a) Impactor dimensions and position b) Final FE Setup	31
Figure 7 Final simulation setup for Horsch 1988	32
Figure 8 a) Orientation of impactor and impact velocity b) Final simulation setup.....	33
Figure 9 Free-back, rigid-bar experimental setup from (Hardy et al., 2001).....	34
Figure 10 a) Rigid bar position and impact direction b) Final simulation setup	35
Figure 11 Experimental setup for (Shaw et al., 2004)	36
Figure 12 PMHS spinal mount and fixture used in (Shaw et al., 2004)	36
Figure 13 a) Steering wheel rim position and impact direction b) Final simulation setup.....	37
Figure 14 a) Chest deflection measurement b) Comparison of THUMS thoracic response with PMHS corridor for Kroel 1974.....	38
Figure 15 Force v normalized chest deflection comparison for Horsch 1988.....	39
Figure 16 a) Chest deflection measurement b) Force v normalized deflection comparison for Yoganandan 1997	40
Figure 17 Force v bar penetration comparison for Hardy 2001.....	41

Figure 18 a) Chest deflection measurement b) Force v normalized deflection comparison for Shaw 2004.....	41
Figure 19 Experimental setup and different loading conditions (Kent et al., 2004).....	45
Figure 20 a) Table dimensions from Kent 2004 b) Gravity settling and final HBM settled posture	46
Figure 21 a) Prescribed displacement time history b) Hub impactor position and simulation setup	46
Figure 22 a) Diagonal belt routing over HBM b) Simulation setup	47
Figure 23 a) Fabric material card for 2D belt material b) Loading curve for 1D belt material	48
Figure 24 a) Double diagonal belt routing b) Double diagonal belt simulation setup.....	49
Figure 25 a) Distributed belt routing b) Distributed loading condition simulation setup.....	50
Figure 26 a) Experimental setup for Forman 2005 b) Custom force-limiters c) Belt orientation over subject torso	51
Figure 27 Simulation setup for Forman 2005 case with Force-Displacement curve for spring force-limiters	52
Figure 28a) Experimental setup and b) Spine fixture for Salzar 2009	53
Figure 29 a) Belt orientation and b) Simulation setup for Salzar 2009	54
Figure 30 Experimental setup and spine fixture for Kemper 2011.....	55
Figure 31 Belt orientation and simulation setup for Kemper 2011	55
Figure 32 Experimental setup for Cesari 1990,1994.	56
Figure 33 a) Prescribed velocity time history and b) Simulation setup for Cesari 1990,1994.....	57
Figure 34 Chest deflection measurement for Kent 2004 (hub loading example).....	58

Figure 35 Force v normalized deflection comparison for Kent 2004 (clockwise) a) hub b) single diagonal belt c) distributed and d) double diagonal belt loading condition.....	59
Figure 36 Force v normalized deflection comparison for Forman 2005 600 N force-limit condition.	60
Figure 37 a) Chest deflection and force measurement b) Force v normalized chest deflection comparison for Salzar 2009	61
Figure 38 Force v normalized deflection comparison for Kemper 2011	61
Figure 39 Deflection time histories of torso points and comparison with PMHS range for maximum deflections for Cesari 1990, 1994.....	62
Figure 40 a) Gold Standard sled experiment setup and b) Gold standard impact crash pulses	66
Figure 41 THUMS v4.1 position and posture in Gold Standard sled setup	67
Figure 42 Belt position over torso for THUMS v4.1 in Gold Standard Setup and comparison with PMHS position.....	67
Figure 43 Gold Standard 1 sled setup with THUMS v4.1	68
Figure 44 Occupant kinematics and upper shoulder belt forces comparison for GS1.....	68
Figure 45 Gold Standard 2 setup with THUMS v4.1	69
Figure 46 Occupant kinematics and upper shoulder belt forces comparison for GS2.....	69
Figure 47 Gold Standard 3 sled setup with THUMS v4.1	70
Figure 48 Occupant kinematics and upper shoulder belt forces comparison for GS3.....	70
Figure 49 a) Experiment setup and b) Impact crash pulse for Rear Seat Sled cases	71
Figure 50 Rear seat sled assembly in simulation environment.....	72
Figure 51 a) THUMS v4.1 position and posture in the Rear Seat sled b) Comparison with the PMHS position measurements	72

Figure 52 Belt position over torso for THUMS v4.1 in Rear seat sled Setup and comparison with PMHS position.....	73
Figure 53 Rear seat sled setup with THUMS v4.1 and Force v Belt payout curve for FL+PT cases (Forman 2009)	74
Figure 54 Upper shoulder belt force comparison for Michaelson 2008	75
Figure 55 Upper shoulder belt force comparison for Forman 2009	75
Figure 56 a) Experiment setup and b) Impact crash pulse for low-speed frontal sled tests	77
Figure 57 Sled model used for Low Speed Frontal Sled simulations.....	77
Figure 58 a) THUMS v4.1 position and posture in the Low Speed Frontal sled b) Comparison with the PMHS position measurements	78
Figure 59 Belt position over torso for THUMS v4.1 in Low speed frontal sled Setup and comparison with PMHS position.....	78
Figure 60 a) Final simulation setup for Low speed frontal sled case with THUMSv4.1 b) Upper shoulder belt forces comparison.	79
Figure 61 Measurement locations for deflection-based injury metrics	82
Figure 62 Mid-Sternum deflection metric injury risk curves for 3+ rib fractures injury level.....	85
Figure 63 Mid-Sternum deflection metric injury risk curves for 7+ rib fractures injury level.....	85
Figure 64 Example Reliability Diagram.....	87
Figure 65 Reliability diagrams for Mid-Sternum deflection models. (diameter of the circle indicates the sample size present in that particular loadcase).....	87
Figure 66 Flowchart outlining the probabilistic rib fracture risk prediction framework from Forman 2012 with fracture risk function from Larsson 2021.	90
Figure 67 Equations for fracture risk functions used in Larsson et al 2021.	92

Figure 68 Comparison of original fracture risk curves from Larsson et al. 2021 (red) and calibrated fracture risk curves (dotted black, pink, blue) for THUMS v4.1 model for age of 45 years old..	95
Figure 69 Reliability diagrams for 3+ and 7+ rib fractures injury levels with Combined Optimized Weibull fracture risk function for strain based probabilistic framework.....	97
Figure 70 Reliability diagrams for 3+ and 7+ rib fractures injury levels with Independently Optimized Weibull fracture risk functions for strain based probabilistic framework	97
Figure 71 Comparison of Reliability diagrams with combined optimized and independently optimized Weibull fracture risk functions for strain based probabilistic framework	97
Figure 72 Mid-sternum deflection based thoracic IRF for the GHBM v6.0 model.....	103
Figure 73 Tuned rib strain IRF for the GHBM v6.0 model (red) and original strain IRF from Larsson et al 2021 (black dashed).....	104
Figure 74 Loadcase selected for in-vehicle simulations	107
Figure 75 Reduced sled model with rigid exteriors and deformable interiors.....	107
Figure 76 Transfer of kinematics from full vehicle simulation to sled model: Top view (top), side view (bottom).....	108
Figure 77 HBMs positioned and seated in the sled model.....	109
Figure 78 Ranges of AIS 3+ thoracic injury risk in 56 km/h frontal collision estimated from the strain-based predictions of THUMS and GHBM, compared to risk estimates from field data (Forman et al. 2019 and subsequent follow-up study).....	111
Figure 79 AIS 3+ thoracic injury risk in 56 km/h frontal collision, estimated if the Larsson (2021) strain IRF curves were applied to both HBMs (compared to the field risk estimates).....	112
Figure 80 Comparison of deflection based IRF for 7+ rib fractures tuned for THUMS v4.1 with chest deflection IRFs for PMHS proposed by Kent et al. 2003 and Laituri et al. 2005	117

Figure 81 Comparison of mid-sternum deflection based injury risk curves tuned for THUMS v4.1 model with that developed for the HIII M50 dummy model (Laituri et al. 2005).	118
Figure 82 Comparison between ribcages of THUMS v4.1 and GHBMC v6.0 models.....	120
Figure 83 Comparison of original fracture risk curves from Larsson et al. 2021 and calibrated fracture risk curves for THUMS v4.1 for age of 45 yeas old.	121
Figure 84 Ribcage deformation patterns and generated rib strains in example impactor and table-top simulations with THUMSv4.1.....	123
Figure 85 THUMSv4.1 ribcage deformation and generated strains in Gold Standard sled simulation.....	124

TABLE OF TABLES

Table 1 PMHS test series selected for simulation	24
Table 2 Impactor type PMHS test series.....	26
Table 3 Table-top type PMHS test series	43
Table 4 Sled type PMHS test series	64
Table 5 Comparison of PMHS and THUMS v4.1 posture in Gold Standard sled setup.....	67
Table 6 Deflection Model Coefficients for 3+ rib fracture risk injury levels.....	84
Table 7 Deflection Model Coefficients for 7+ rib fracture risk injury levels.....	84
Table 8 Parameters calibrated for THUMS v4.1 using Combined Optimization.....	94
Table 9 Parameters calibrated for THUMS v4.1 using Independent Optimization for 3+ rib fractures injury level	94
Table 10 Parameters calibrated for THUMS v4.1 using Independent Optimization for 7+ rib fractures injury level	94
Table 11 AUROC values for combined and independently optimized weibull fracture risk functions for strain based probabilistic framework	98
Table 12 Finalized parameters for the Weibull fracture risk functions to be used in the strain-based probabilistic rib fracture prediction framework with the THUMS v4.1 model.....	99
Table 13 Strain IRF parameters (Weibull distribution) tuned for the GHBMC v6.0.....	104
Table 14 Injury risk for THUMS v4.1 using Deflection IRF.....	109
Table 15 Injury risk for THUMS v4.1 using Strain IRF	109
Table 16 Injury risk for GHBMC v6.0 using Strain IRF.....	110

CHAPTER 1: INTRODUCTION

1.1 Background and Motivation

Computer Aided Engineering simulations have provided a new avenue for the study and development of advanced restraint system designs. Novel crash modes pertaining to automated or self-driving vehicles like occupants in reclined or out of position seating and postures can be studied in virtual environment to a larger extent before actual physical crash tests, thus bringing down the costs. Crash simulations have traditionally used virtual models of anthropomorphic test devices to correlate with physical crash tests and evaluate the performance of new systems. In recent years, finite element human body models (FE-HBMs or HBMs) have been developed as an evaluation tool for restraint system and safety assessment in virtual simulations. Because HBMs are developed for the virtual environment, the complexity of these models is only limited by the computational power. With the advancement of computation power and resources, advanced HBM models have been developed – for example the GHBMC family (Gayzik et al., 2012), THUMS family (Iwamoto et al., 2002; Kato et al., 2018; Shigeta et al., 2009) and the SAFER HBM (Pipkorn & Kent, 2011). These models have fairly accurate representation of human anatomical geometry and mechanical material properties of various internal organs and structures as well as well-defined contact interaction between the internal organs. Some HBMs also have active musculature incorporated in them, able to generate muscle forces like a living human being (Kato et al., 2018; Martynenko et al., 2019). As a result of all these details, HBMs also have the potential to predict tissue level injury response and accurate occupant kinematics under different loading conditions.

However, for HBMs to be truly useful as a tool, standardized methods need to be developed for translating the various outputs from HBM simulations into predicted risk for injury types of interest. This is especially important as there are multiple advanced HBMs in the field and for these to be used in virtual assessment, the injury prediction method should be harmonized. An important body region of interest for such standardization is the thorax. Because even after substantial improvements in vehicle occupant safety systems (Kullgren et al., 2019), the thorax still remains one of the most prevalently injured body region at the AIS3+ injury level in motor vehicle collisions (MVCs) (J. Forman et al., 2019; J. L. Forman & McMurry, 2018; Pipkorn et al., 2020).

Thorax was one of the first body regions for which anatomical structures and internal organs were modeled in detail in HBMs (Iwamoto et al., 2002). This was also facilitated by different test series on PMHS thorax to characterize the biofidelity corridors required to assess the biofidelity and accuracy of these newly developed complex HBMs. Test series were conducted on the full intact thorax with various types of impactors to emulate the thoracic response in real world impact scenarios, such as (Cesari & Bouquet, 1990, 1994; J. Forman et al., 2005; Hardy et al., 2001; Kent et al., 2004; Kroell, 1971; Kroell et al., 1974; L'Abbe et al., 1982; Shaw et al., 2004; Yoganandan et al., 1997). Tests were also conducted on the denuded or eviscerated thorax such as (Kent, 2008; Kindig et al., 2010) as well as tissue level tests on ribs to characterize the mechanical and material properties such as (Albert et al., 2017; J. L. Forman et al., 2010; Katzenberger et al., 2020; Kemper et al., 2005, 2007). Sled tests with full body cadavers were also carried out to understand the kinematics and chest deflections sustained under seatbelt and airbag type loads such as (Acosta et al., 2016; J. Forman et al., 2009; Lebarbe, 2005; Lopez-Valdes et al., 2010;

Michaelson et al., 2008; Shaw et al., 2009). Data from such tests was used to validate the various HBMs and establish their biofidelity.

Once the biofidelity of the HBMs was established to be reasonably accurate, researchers strived to develop thoracic injury risk functions (IRFs) and injury assessment strategies that took advantage of the complexity and tissue-level injury prediction ability of the HBMs. Initially, the HBMs were treated as advanced dummies and IRFs developed for chest deflection of ATDs like HIII were directly applied to the evaluation of injury from HBM simulation data. IRFs developed for human PMHS like from (Kent & Patrie, 2005; Laituri et al., 2005) etc. were also directly used with HBMs in some cases, assuming the HBM to be fairly biofidelic (Guleyupoglu, Koya, & Gayzik, 2018). These IRFs were based on single-point chest deflection and as such failed to take advantage of the full capability of the HBMs. With the advent of multi-point chest compression measurement in THOR, it was logical that IRFs based on such multi-point deflections were explored for the HBMs as well. HBMs did provide a more accurate deformation of the entire thorax and ribcage under asymmetrical loading like that from a seatbelt (Shaw et al., 2009) as compared to traditional dummies (Danielson et al., 2015). This led to the development of IRFs like combined deflection criteria D_c for the HUMOS2LAB HBM (Song et al., 2011) and D_c THOR for THUMSv3 (Mendoza-Vazquez et al., 2015). Going a step further, taking advantage of the local strain measurement capability of the HBMs, injury prediction methodology using rib strain based fracture risk was developed by (J. L. Forman et al., 2012) and was applied to the SAFER HBM (Pipkorn et al., 2019) and GHBMC models (Guleyupoglu, Koya, Barnard, et al., 2018).

Even after such advancements, there are still some challenges when using HBMs for thoracic injury prediction in frontal impacts. The various HBMs differ in their internal geometry of the thorax, the level of detail in the FE mesh and also the specific material properties of the

internal organs, as well as how the interactions between the different components of the thorax are modelled. That is why injury risk functions developed and validated using one model may not be applicable to other models and may also yield spurious injury risk predictions. Similarly, applying IRFs developed from PMHS data like (J. L. Forman et al., 2012; Kent & Patrie, 2005; Laituri et al., 2005) directly to HBMs without an appropriate transfer function may give incorrect results based on the level of biofidelity of the HBM. Another factor to consider is the simulations and PMHS test dataset used to develop the IRFs. IRFs are developed by relating the PMHS injury outcomes with the injury metrics (simulation outputs) extracted from HBMs in matched simulations. As such the underlying dataset of PMHS tests has a fundamental role and influence on the subsequent IRF. However, there has been a lack of consistency in these datasets in the attempts for developing IRFs for various HBMs. For example, the dataset used to develop the Dc injury criterion for the HUMOS2LAB is not the same as the dataset used for DcTHOR for THUMSv3, while both are different from the dataset used for the SAFER HBM rib strain IRF validation. Each of these is also dissimilar in terms of the matched pair simulations performed with the particular HBM for IRF development. Also, sufficient information regarding the boundary conditions and setup of simulations may not be available which makes replicating the methods on a new HBM difficult.

Thus, there is a need to develop a framework which standardizes the thoracic IRF development methodology for HBMs. This framework should include the PMHS test dataset to be used for matched pair simulations as well as a detailed guide to setup the boundary and loading conditions for the simulations. The guide should also include information on the specific data needed to be output from the simulations and the process to develop thoracic IRFs from these outputs. Such a framework will allow for tuning IRFs for application to a specific HBM while

providing a means to arrive at comparable thoracic injury risk prediction across various HBMs, despite their differences.

1.2 Objectives

As discussed in the previous section, there is a need to develop a harmonized framework for developing thoracic IRFs for various HBMs, which will drive towards comparable prediction of injury risk across various HBMs, despite the differences in the models. Therefore the overall objective of this thesis will be to develop such a framework for generating injury risk functions for predicting risk of thoracic injury in frontal impacts. The outcome will be a set of detailed guidelines for setting up and performing simulations and developing IRFs, which can be applied to any model to generate model-specific IRF. The entire process will be demonstrated using the THUMSv4.1 50th percentile male occupant model with the explicit solver LS-Dyna environment.

The work in this thesis is mainly broken down into two main tasks:

- Task 1 – PMHS Data and Simulations for IRF Development and Validation
- Task 2 – Injury Risk Functions Development
- Task 3 – Application to alternate Human Body Model
- Task 4 – In-Vehicle Simulations

Each of these tasks represents a chapter of the thesis, with additional chapters providing introduction and conclusions. Chapter 2 (Task 1) mainly focuses on providing detailed guidelines for setting up the boundary and loading conditions for matched pair HBM simulations representing the PMHS tests dataset. This chapter also details the PMHS test dataset used and the final simulation matrix. Chapter 3 (Task 2) focuses on providing detailed guidelines for developing and validating the injury risk functions from the simulation obtained from Task 1. These two chapters

together form the framework for developing thoracic IRFs for various HBMs. Chapter 4 (Task 3) shows the application of the developed framework from tasks 1 and 2 to a different HBM, namely the GHBMC v6.0. Chapter 5 (Task 4) shows the injury risk prediction from both the models in a realistic vehicle environment subjected to 56 kph frontal collision and compares it with field data describing risk from comparable collisions. Finally, Chapter 5 discusses some of the learnings from this work, scope for future work and concludes the thesis.

CHAPTER 2: TASK 1 – PMHS data and simulations for IRF development and validation

2.1 Selection Of Loadcases (PMHS Data)

The literature was surveyed to identify existing PMHS studies on the thorax that could be used to develop model-specific injury risk functions. Since the 1970s, a lot of research has gone into understanding the response and injury tolerance of the human thorax under different types of loading. The following selection criteria were used to select the loadcases for simulating thorax loading:

- The thorax was loaded primarily in the anterior to posterior direction.
- The PMHS used were unembalmed and the entire intact thorax was tested i.e. tests with denuded or eviscerated thorax were discarded.
- PMHS characteristics like sex, age, weight, height, and chest depth were available for each test.
- Injury information in terms of number of rib fractures sustained was known for each test.
- Sufficient information of the experiment setup and loading and boundary conditions was available for reproducing the test in simulation environment.

A literature search with these criteria yielded 16 test series with 19 types of loading conditions.

These were broadly divided into three groups:

1. Impactor Cases – pendulum type impacts to the thorax.
2. Table Top Cases – subjects laying supine on a table.
3. Sled Cases – subjects seated in pseudo-vehicle environments.

Among these 19 loadcases, there were a total of 195 PMHS tests, of which 86 (44%) had 3+ rib fractures. Table 1 gives the details of the selected loadcases. The selected dataset consisted of a wide variety of loading conditions and also a good balance of injurious and non-injurious tests. The PMHS details and injury information for each individual test are given in **Appendix A**.

Table 1 PMHS test series selected for simulation

<i>Type</i>	<i>PMHS Test Series</i>	<i>Loading Condition</i>	<i>No. of PMHS</i>	<i>Total no. of Tests</i>	<i>No. of tests with 3+ rib fractures</i>
Impactor	Kroell 1971, 1974	Rigid hub	38	38	30
	Horsch 1988	Rigid hub	3	3	3
	Yoganandan 1997	Rigid hub	7	7	5
	Hardy 2001	Rigid rod	3	3	3
	Shaw 2004	Rigid steering wheel rim	4	4	2
Table Top	Kent 2004	Rigid hub	15	18	3
		Distributed belt		16	1
		Single diagonal belt		18	2
		Double diagonal belt		15	2
	Forman 2005	Load limited double diagonal belt	3	23	2
	Salzar 2009	Single diagonal belt	3	6	0
	Cesari 1990, 1994	Single diagonal belt	17	17	14
	Kemper 2011	Single diagonal belt	2	2	2
Sled	Shaw 2009	$\Delta V = 40$ kph, 3-point standard belt	8	8	7
	Acosta 2016	$\Delta V = 30$ kph, 3-point 3kN LL belt	5	5	2
		$\Delta V = 30$ kph, 3-point 3kN LL belt Oblique frontal loading direction	3	3	2
	Forman 2006	$\Delta V = 29$ kph, 3-point standard belt	3	3	0
	Forman 2009	$\Delta V = 48$ kph, 3-point 3kN LL belt	3	3	3
	Michaelson 2008	$\Delta V = 48$ kph, 3-point standard belt	3	3	3

2.2 Simulations

2.2.1 HBM Instrumentation

Before setting up the HBM for the selected loadcases, it was instrumented to output a series of measurements which could be considered to form potential metric candidates for the development of injury risk functions. The instrumentation included strain-based and deflection-based outputs. These outputs were evaluated and utilized for the development of candidate metrics for the definition of injury risk functions. The THUMS v4.1 model was setup to output the strains of cortical bone parts of all ribs and sternum, as well as strains of costal cartilage parts (Figure 1 c). The maximum values of the maximum principal strain (MPS) time-histories were stored for each of the individual ribs, sternum and costal cartilage. The model was also setup to output the nodal coordinates of points on the anterior ribcage for measurement of skeletal deformation. 24 nodes were selected to represent the anterior ends of each rib and 5 nodes were selected on the sternum representing – 1) jugular notch 2) manubrium base 3) Mid-sternum 4) xiphisternal joint and 5) xiphoid process as shown in Figure 1 b. Local coordinate systems were modelled on each vertebral body from T1 to T12 according to SAE J211 sign convention as shown in Figure 1 a. Nodal outputs of the skeletal measurement points in global coordinates were transformed into deflection in the selected vertebral local coordinate systems in post-processing. All the nodes for measurement and forming local coordinate systems were selected from existing nodes in the HBM and no new nodes/elements were added to the HBM. This instrumented THUMS v4.1 model was then used in setting up the simulations for the development of injury risk functions.

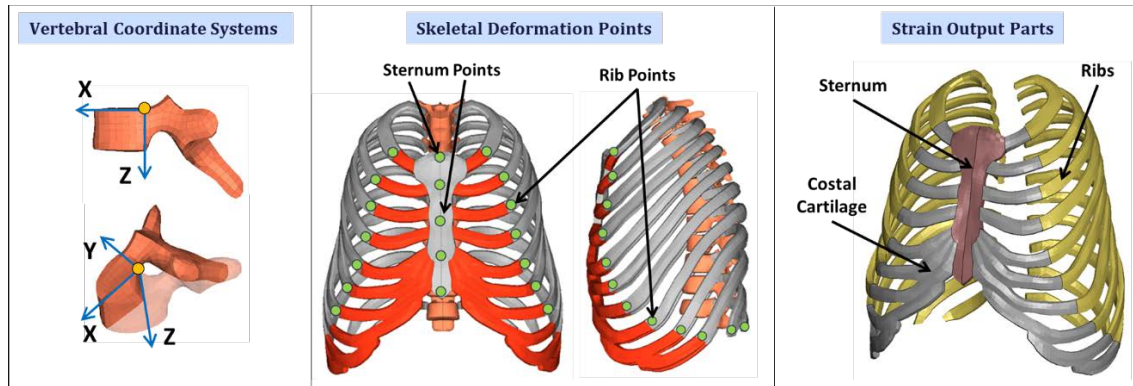


Figure 1 HBM Instrumentation - a) Local coordinate systems on vertebrae T1 - T12 b) skeletal deflection points c) parts for output of strain

2.2.2 Simulations For IRF Development

Impactor Cases

Introduction

From the selected loadcases (Section 2.1), five were classified as being Impactor type loadcases. These were typically characterized by pendulum type impacts to the thorax of a PMHS in an upright sitting posture. These type of loadcases were used to characterize the human thoracic responses under blunt force trauma. Table 2 shows the selected impactor test series.

Table 2 Impactor type PMHS test series

Type	PMHS Test Series	Loading Condition	No. of PMHS	Total no. of Tests	No. of tests with 3+ rib fractures
Impactor	Kroell 1971, 1974	Rigid hub	38	38	30
	Horsch 1988	Rigid hub	3	3	3
	Yoganandan 1997	Rigid hub	7	7	5
	Hardy 2001	Rigid rod	3	3	3
	Shaw 2004	Rigid steering wheel rim	4	4	2

The sections below describe the process of setting up each impactor case in finite element simulation environment. Before simulations setup in these conditions can be used for injury risk function development, it should be ensured that the PMHS responses are relatively well captured by the HBM for each case i.e. the HBM response is relatively biofidelic in the selected cases. First, the biofidelity of THUMS v4.1 for the impactor cases was examined by evaluating the response in a single exemplar simulation for each loadcase (representing the “average” or typical input condition). Following the initial biofidelity evaluation, matched-pair test specific simulations were performed to expand the simulation dataset for IRF development, and to develop IRFs via regressing the HBM responses against the matched PMHS injuries.

FE Setup

Kroell 1971, 1974

From 1971 to 1974, Kroell et al. conducted a series of tests with an objective to provide improved quantification of injury tolerance and thoracic mechanical response (force-time, deflection-time, and force deflection relationships) for blunt sternal impact to the human cadaver (Kroell, 1971; Kroell et al., 1974). In total, 38 tests were conducted on 38 unembalmed PMHS (ranging in age from 19-81 years, in weight from 37.2-94.8 kg, with 8 females and 30 males) with blunt impacts using a horizontal, propelled striker mass. The impactor was an unpadded wooden hub with 152mm diameter and was centered in the mid-sagittal plane at the level of fourth inter-costal space. The impactor mass varied from 1.6-23.6 kg and the initial impact velocities ranged from 4.3-13.8 m/s with the smaller masses associated with higher velocities. PMHS chest response in terms of force-deflection curves (and corridors) and injury findings in terms of ribcage fractures are available for each test.

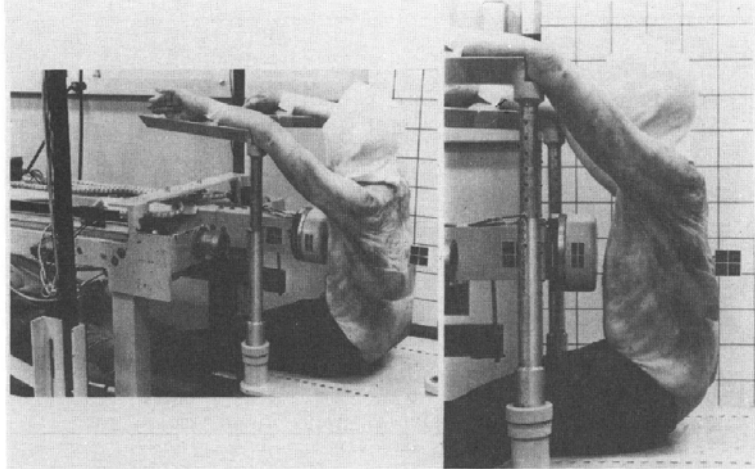


Figure 2 Pretest experimental setup from (Kroell et al., 1974)

The THUMS v4.1 model validation catalogue uses the Kroell test series as one of the thorax validation cases of the model (Shigeta et al., 2009). This setup is publicly available from Toyota. The posture of THUMS v4.1 in this validation case can be considered as a reference to position any other HBM. As shown in **Figure 2**, in the tests, the subject is seated upright on a rigid flat table with arms raised above the line of impact but not constrained. The THUMS v4.1 validation skeletal posture is as shown in **Figure 3**.

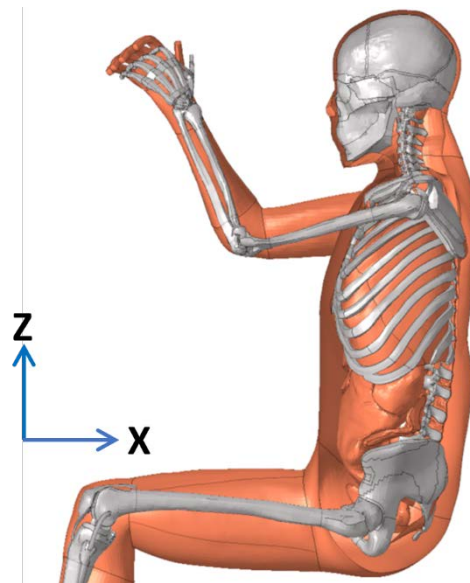


Figure 3 THUMS v4.1 M50 model posture for Kroell 1974 thorax validation case.

To model this setup with any other HBM would require more information with respect to skeletal posture, than what was specified in the reference literature. However, different HBMs may differ in specific bony geometry and features. Thus, instead of specific nodes/elements, several anatomical landmarks were selected to define the skeletal posture. All positioning simulations were performed by rigid body movements of bones and the soft tissue was kept deformable to get a smooth transition of the FE mesh as well as a more natural movement of the joints.

The reference literature did not provide any metric to quantify the PMHS posture and orientation. However, it does indicate that the tests were performed with the surrogates seated in an upright posture on a rigid flat surface. Therefore, this study suggests approximate angles between anatomical landmarks which can be used for orienting and positioning any HBM into the upright sitting posture. First, the model was oriented such that the pelvis was approximately in an upright sitting orientation. Next, the upper legs were positioned by moving the femurs such that the angle made by joining the H-point (femoral head center) and the center of the most lateral point of the femoral condyle with the vertical is approximately 90 deg (Figure 4).

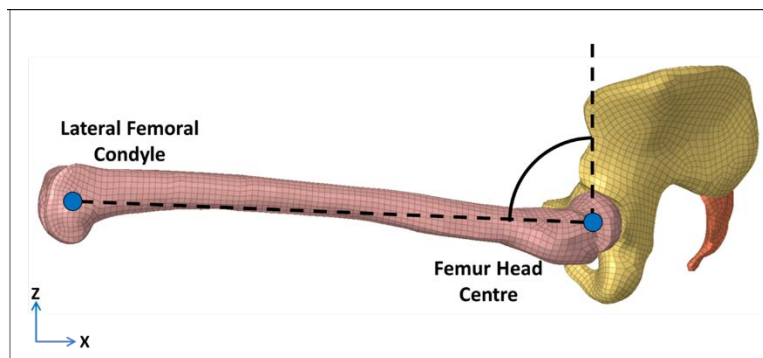


Figure 4 Upper leg (femurs) orientation with reference angle

Next, the upper body was positioned such that the line joining the T1 and L5 (vertebral body centers of gravity) formed approximately a right angle with the horizontal in the XZ plane as shown in Figure 5.

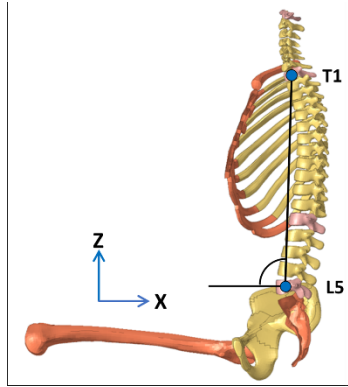


Figure 5 Torso orientation with reference angle

In all positioning simulations, the model was constrained to only move in the sagittal plane (i.e., XZ plane shown in Figure 5). The arms were then positioned by moving the humerus such that the upper arms and torso formed approximately a right angle in the XZ plane (as shown in **Figure 3**). The impactor was modelled as a rigid 152 mm diameter cylinder with 12 mm radius chamfer. The reference literature did not specify the exact length of the impactor. So, it was modelled to be 80 mm in length, long enough to avoid situations of model soft tissue wrapping around it after impact. The rigid material used the density and elastic modulus (for contact handling only) properties of steel. As required, additional nodal mass was added to nodes, to bring the total mass of the impactor equal to that used in tests. The rigid flat seat was modelled with a flat surface of shell elements using the same material characteristics as the pendulum. The flat seat is positioned just below the upper thighs and buttocks of the HBM, however gravity settling on the seat is not essential for this loadcase. The impactor was centered at the mid-sagittal plane and aligned with the fourth inter-costal space in the tests. The impactor setup from Toyota for the THUMS v4.1 model validation was used in this study. It was constrained to move only in the X translational motion, and all other degrees of freedom were fixed. The rigid seat was fixed in space. The impactor was given an initial velocity in the X direction. Gravity was applied in the negative

Z direction. No external constraints were applied to the HBM. Friction coefficient for the contact between the impactor and the HBM, and between the seat and the HBM was defined as 0.2. The final simulation setup is shown in **Figure 6 b**.

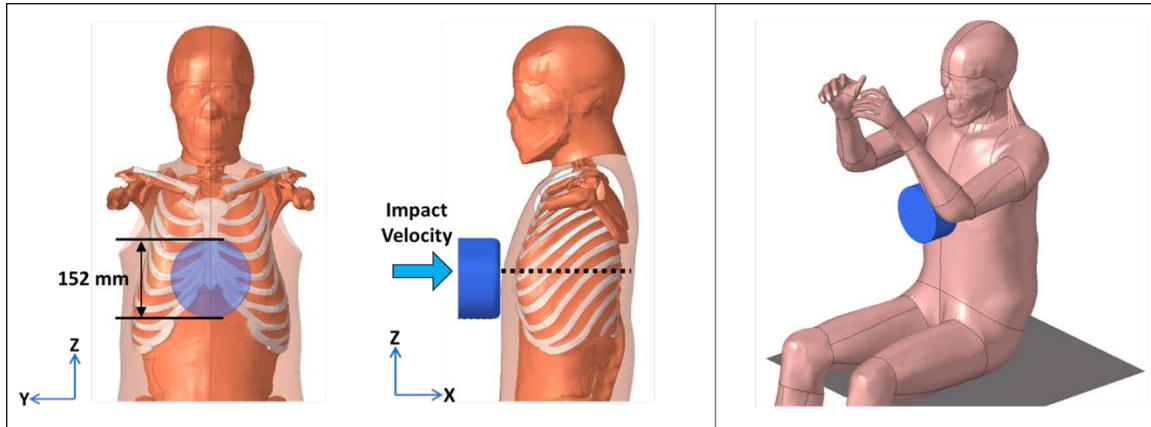


Figure 6 a) Impactor dimensions and position b) Final FE Setup

Horsch 1988

In 1988, Horsch et al. conducted blunt frontal impact tests on 3 unembalmed male PMHS following the same protocol of Kroell et al. 1974 (Horsch, 1988). However, these tests were performed with a low impactor mass of 4.25 kg and a higher initial velocity of 13.4 m/s. The PMHS ranged from 58-69 years in age and 65-72 kg in weight. Same test setup and initial, loading and boundary conditions as of Kroell 1974 was used. PMHS chest response in terms of force-deflection curves and injury findings in terms of ribcage fractures are available for each test.

As this test series followed the same protocol as Kroell 1974, the same HBM posture and position from the previous loadcase could be used. The HBM was positioned and postured following the same procedure as that described for the Kroell case above. The impactor mass was adjusted to 4.25 kg by changing the additional mass added at the nodes. If the impactor mass exceeded 4.25 kg even after the additional nodal mass was set to zero, the mass was adjusted by

modifying the density of the rigid impactor. The impactor was given an initial velocity of 13.4 m/s in the X direction. Gravity was applied in the Z direction. The final setup is as shown in the Figure 7.

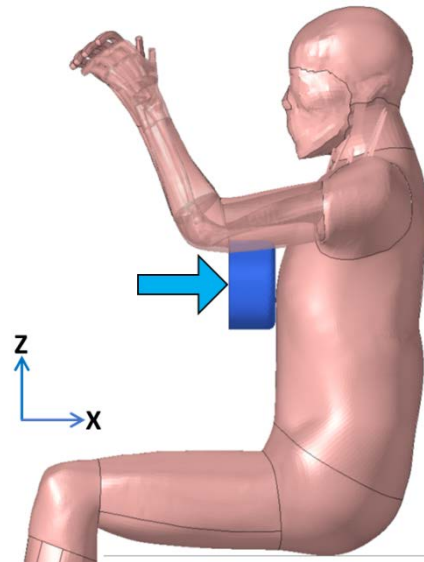


Figure 7 Final simulation setup for Horsch 1988

Yoganandan 1997

Yoganandan et al. performed a series of blunt impact tests on 7 unembalmed male human cadavers to characterize the biomechanical response of the human thoraco-abdominal region (Yoganandan et al., 1997). The PMHS ranged in age from 62-68 years and in weight from 56-91 kg. Dynamic loading was applied in a 15 deg oblique direction to the right anterior thorax using a pendulum impactor similar to that of Kroell 1974 tests. The weight of the impactor was 23.5 kg, and the impact velocity was 4.3 m/s. Deformation time histories along the line of impact, impact force time histories and injury findings in terms of ribcage fractures are available for each test.

For this test series, the starting position and posture of the PMHS was similar to that of Kroell 1974 tests. Thus, the HBM posture obtained in the Kroell 1974 setup could be used for this

loadcase. In the tests, the torso was rotated from right to left by 15 deg such that the loading contact occurred on the right antero-lateral thorax. To achieve this in the FE model, the impactor was rotated by 15 deg around the Z axis passing through the HBM posterior mid-line as shown in Figure 8a. The impactor vertical level was kept same at the fourth intercostal space as that of Kroell 1974. The impactor mass was adjusted to 23.5 kg by using the same procedure as defined in Kroell 1974 and Horsch 1988 cases. The impactor was constrained to only translate along its axis of symmetry with an initial velocity of 4.3 m/s. The final setup is shown in the Figure 8b.

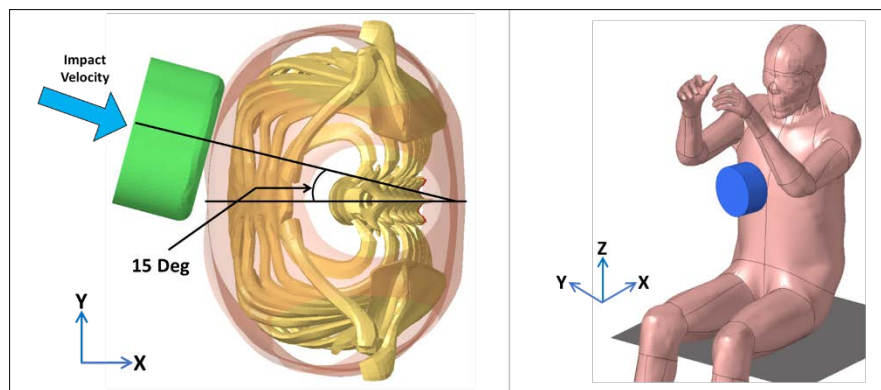


Figure 8 a) Orientation of impactor and impact velocity b) Final simulation setup

Hardy 2001

Hardy et al. conducted a series of tests with various types of impactors to characterize the biomechanical impact response of the human abdomen to frontal impact loading (Hardy et al., 2001). Three types of loading conditions were used: rigid-bar impacts, seatbelt loading and close-proximity airbag deployments. This test series primarily focused on abdominal loading rather than thoracic loading. However, tests were conducted at the lower thorax region (T11 level) with the rigid-bar which could be used for thoracic loading scenario. Hence, out of the total 33 tests on 20 PMHS, only 3 tests with rigid-bar, free back, lower thorax loading were selected for this study. The selected tests PMHS, two of which were male, ranged from 64-74 years of age, and from 61-

75 kg. The cadavers were impacted by a 25 mm diameter rigid bar attached to a ballistic pendulum, resulting in a total impactor mass of 48 kg. The rigid bar made an initial contact with the epigastric region, approximately at the T11 level, with an initial velocity ranging from 6-9 m/s. The PMHS were sat upright with a free back configuration for the selected 3 tests as shown in **Figure 9**. The force-deflection response and injury findings in terms of ribcage fractures are available for each test.

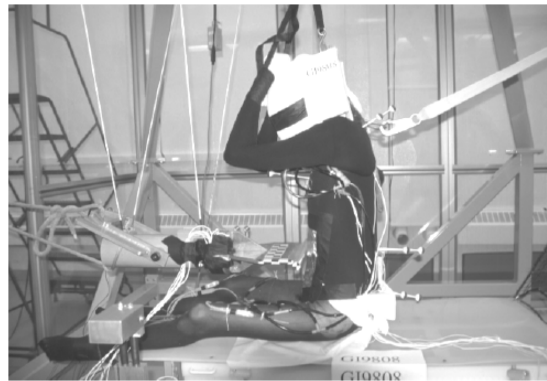


Figure 9 Free-back, rigid-bar experimental setup from (Hardy et al., 2001)

The experimental setup for the free-back, rigid-bar impact was similar to Kroell 1974 case, with the subject sitting upright on a flat rigid seat with arms raised (**Figure 9**). Hence, the same HBM posture and position as defined for Kroell 1974 case was used for this loadcase. The rigid bar was modelled as a 25 mm diameter cylindrical pipe, long enough to cover the entire chest breadth of the HBM. The bar was defined as a rigid material using the same characteristics as in the previous tests. Additional nodal mass was added to bring the total impactor mass to 48 kg (similar to how it was defined for Kroell 1974 impactor mass). The bar was aligned horizontally at the T11 level (as shown in **Figure 10a**) and was constrained to only translate in the X direction. The bar was given an initial velocity of 6 m/s in the X fore-aft direction. Friction coefficient for

the contact between the impactor and the HBM, and between the seat and the HBM is defined as 0.2. Final model setup is shown in **Figure 10b**.

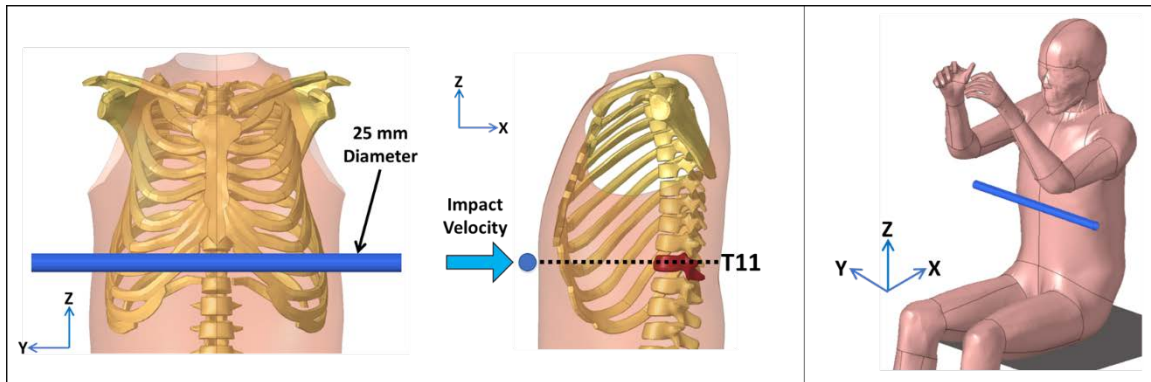


Figure 10 a) Rigid bar position and impact direction b) Final simulation setup

Shaw 2004

Shaw et al. tested 4 male PMHS in a test condition designed to approximate the lower thorax / upper abdomen impacting a steering wheel rim in a frontal crash (Shaw et al., 2004). A rigid surrogate wheel rim, oriented at 45 deg and ballasted to 64 kg impacted the subject's torso at T12 level with an initial velocity of 4 m/s. The subjects were seated upright and the subject's spine was rigidly mounted to a vertical fixture. The PMHS ranged in age from 40-66 years and in weight from 43-69 kg. The force-penetration response and injury findings in terms of ribcage fractures are available for each test. Experimental setup is shown in **Figure 11**.

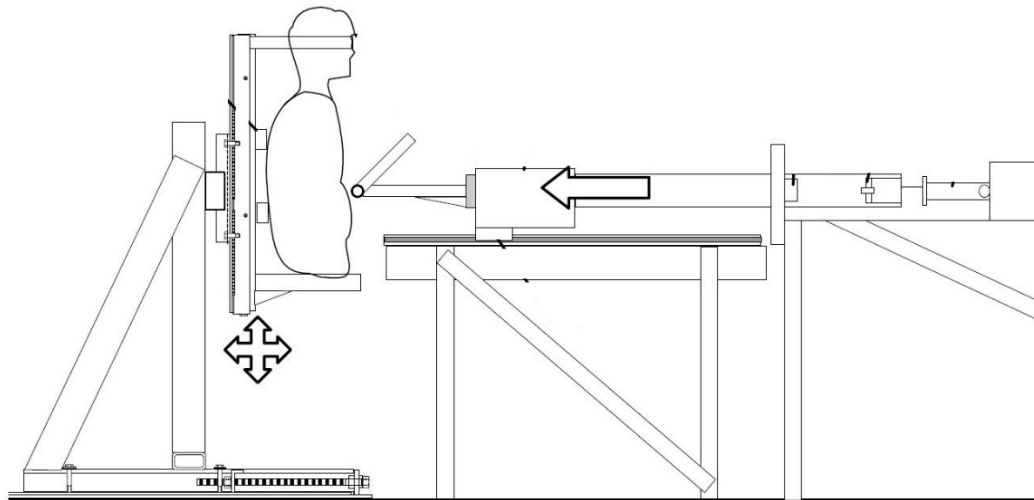


Figure 11 Experimental setup for (Shaw et al., 2004)

As the subjects were in the upright posture for these tests, again the initial position and posture of the HBM was taken from the Kroell 1974 case. In the tests, the cadaver spine was rigidly fixed to the vertical fixture by screwing aluminum blocks into T6, T8, T10, T12 and L4 vertebrae as shown in **Figure 12**. The pelvis was also fixed rigidly to prevent rearward movement. This boundary condition was modelled in FE by constraining the pelvis and spinal column nodes in all degrees of freedom. This fixed the pelvis and spinal column in space, similar to the vertical fixture used in the tests.

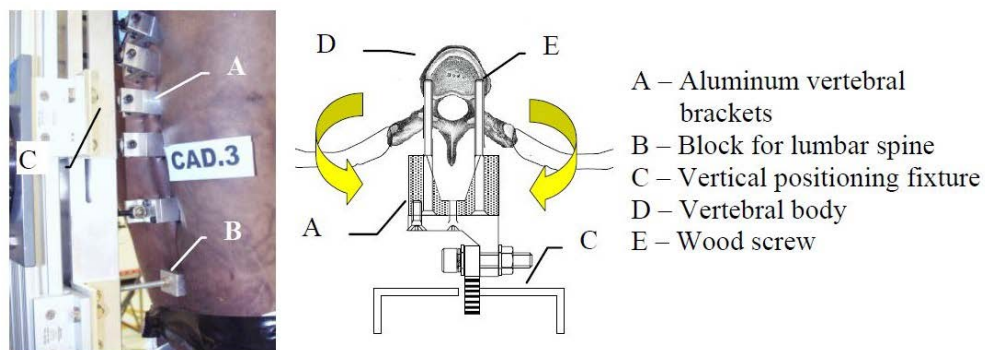


Figure 12 PMHS spinal mount and fixture used in (Shaw et al., 2004)

The rigid steering wheel rim was modelled with minor diameter of 25 mm as specified in the tests. The surrogate steering rim in the tests was based on a standard steering wheel, however the major diameter is not specified. Hence, the rim was assumed to have an outer diameter of 380 mm based on a standard 15 inch steering wheel. The rim material model was the same as described in previous tests. The total mass of the rim was modified to be 64 kg by using additional nodal mass as required. The rim was centered at the mid-sagittal plane and positioned at an angle of 45 deg such that its leading edge was approximately at the T12 level, as shown in the **Figure 13a**. The rim was constrained to only translate in the fore-aft direction and was given an initial velocity of 4 m/s. The coefficient of friction between the rim and thorax was defined to be 0.2. The upper and lower extremities of the subjects were amputated in the tests. For simplicity, the long bones of the upper and lower extremities were constrained to be fixed in space in the original Kroell 1974 case orientation. The upper and lower extremities parts were excluded from the contact defined between the steering wheel rim and HBM. The final simulation setup is shown in **Figure 13b**.

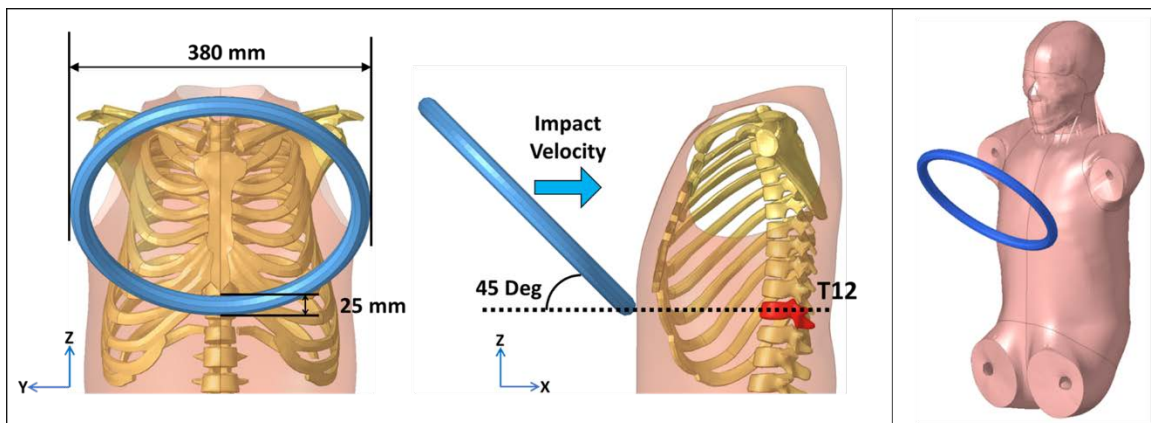


Figure 13 a) Steering wheel rim position and impact direction b) Final simulation setup

HBM Biofidelity

After the model setup, the biofidelity of the HBM in the given loadcase was verified with the experimental data. Although IRFs can, in certain circumstances, be developed for models with limited biofidelity, lack of biofidelity may prevent the development of a robust IRF if the model does not capture some fundamental PMHS behavior. Therefore, it is advisable to check and, if necessary, improve the biofidelity of the model before developing any IRF.

Kroell 1971, 1974

The corridors of impact force vs chest deflection given in the reference literature (Kroell, 1971; Kroell et al., 1974) for 50th percentile males were used for verifying the biofidelity of the THUMS v4.1 model. The impact force was measured as the contact force between the impactor and HBM thorax. The chest deflection was measured as the difference in the X-displacement of impactor face and a node on the posterior thoracic surface in line with the center of the impactor face (Figure 14 a). The results are as shown in the Figure 14 b. The THUMS v4.1 model was found to be reasonably biofidelic under this loadcase.

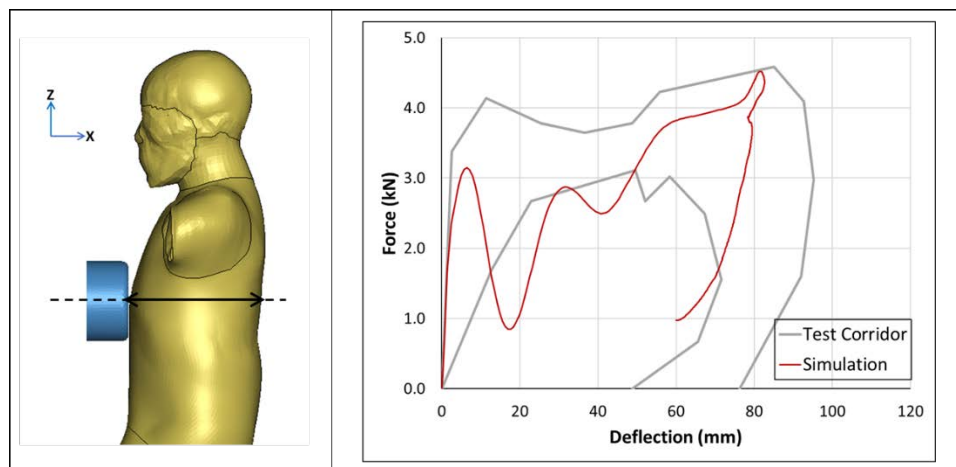


Figure 14 a) Chest deflection measurement b) Comparison of THUMS thoracic response with PMHS corridor for Kroell 1974

Horsch 1988

The HBM biofidelity in this loadcase was evaluated using the PMHS impact force vs chest compression data from the individual tests. The simulation impact force was measured as the contact force between the impactor and thorax surface, while the chest compression was calculated as the difference in the X-displacement of impactor face and a node on the posterior thoracic surface in line with the center of the impactor face, similar to Kroell 1974 (as shown in Figure 14a). The chest compression was then normalized by the initial chest depth to compare with the PMHS test responses. The force v normalized deflection comparison is shown in Figure 15. The THUMS v4.1 model was found to be reasonably biofidelic under this loadcase.

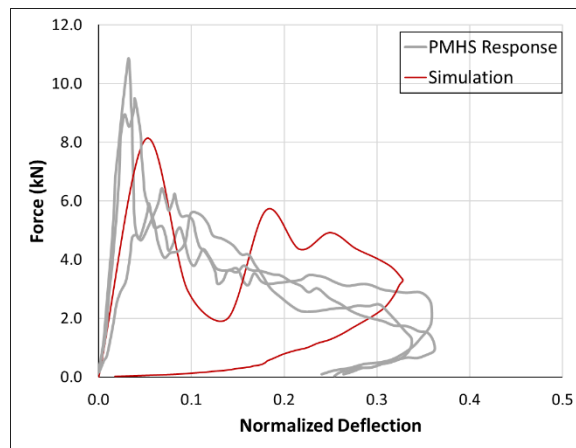


Figure 15 Force v normalized chest deflection comparison for Horsch 1988

Yoganandan 1997

The HBM biofidelity in this loadcase was evaluated using the normalized force-deformation corridors available from the PMHS tests. The deformation was calculated as the chest compression along the line of impact as shown in Figure 16 a. This deformation time history was normalized by the initial chest depth of the HBM along the line of impact. The force was measured

from the contact force between the impactor and thorax. The results are shown in Figure 16b. The THUMS v4.1 model was found to be reasonably biofidelic in this impact loadcase.

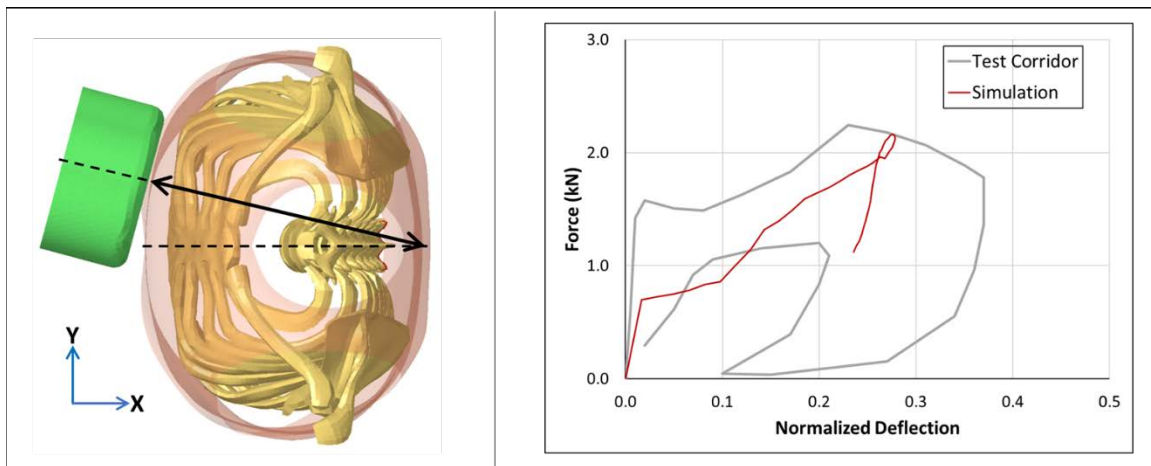


Figure 16 a) Chest deflection measurement b) Force v normalized deflection comparison for Yoganandan 1997

Hardy 2001

The HBM biofidelity was evaluated for this loadcase by comparing the force-penetration response with the data available from the tests. The force is measured as the contact force between the bar and the HBM thorax. The penetration is measured as the displacement of the bar, after the initiation of contact with the thorax, along the impact direction. The results are shown in the Figure 17. The THUMS v4.1 model was found to be reasonably biofidelic in this impact loadcase.

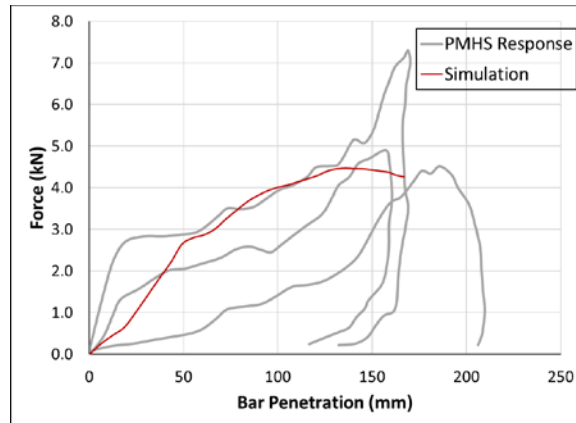


Figure 17 Force v bar penetration comparison for Hardy 2001

Shaw 2004

The HBM biofidelity in this loadcase was evaluated by comparing the impact force vs normalized torso deflection response with the data available from the tests. The impact force is measured as the total contact force between the steering wheel rim and the HBM torso. The deflection is measured as the compression along the line of impact (as shown in Figure 18a) and is normalized by the pre-impact HBM torso depth. The results are shown in Figure 18b. The THUMS v4.1 model was found to be reasonably biofidelic in this impact loadcase.

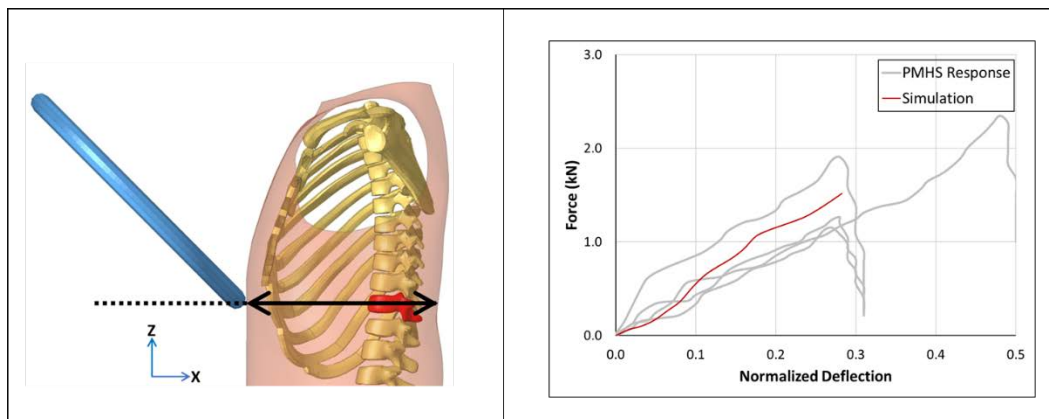


Figure 18 a) Chest deflection measurement b) Force v normalized deflection comparison for Shaw 2004

Test Specific Simulations

To maximize the dataset for injury risk function development and to capture the PMHS size variability, test-specific simulations are setup corresponding to each individual test by modifying the loading conditions, targeting the test inputs applied to the PMHS. For the impactor cases, a scaling law is applied to the mass of the impactor hitting the HBM, without making any changes to the initial velocity. The objective of this type of scaling is to expose the HBM to an impact that can be comparable to the impact received by the PMHS in the matched-pair test, and to induce comparable chest compression and injury severity between the HBM and the PMHS. In this scaling, geometrical similarity, identical density and stiffness of the thorax is assumed between the PMHS and the HBM, same as equal-stress equal-velocity scaling (Mertz, 1984). The impactor mass is scaled such that the initial momentum of the impactor relative to the total body mass of the subject is equal for the HBM and matched-pair PMHS test. The scaled impactor mass is given by the Equation 1:

$$m_{scaled} = m_{test} \times \frac{M_{HBM}}{M_{PMHS}} \quad (1)$$

Where m_{scaled} is the matched-pair simulation impactor mass, m_{test} is impactor mass in matched-pair test, M_{HBM} is the HBM total body mass and M_{PMHS} is the matched-pair PMHS total body mass. The test and scaled impactor masses for simulations with THUMS v4.1 are given in **Appendix B**. This exercise increases the impactor simulation dataset to 55 total matched-pair simulations.

Table-Top Cases

Introduction

From the selected loadcases (Section 2.1), eight were classified as being Table-top type loadcases. These were typically characterized by the PMHS laying supine on a flat table or supported in the supine position and loading applied to the anterior aspect of the thorax. **Table 3** shows selected Table-top loadcases.

Table 3 Table-top type PMHS test series

<i>Type</i>	<i>PMHS Test Series</i>	<i>Loading Condition</i>	<i>No. of PMHS</i>	<i>Total no. of Tests</i>	<i>No. of tests with 3+ rib fractures</i>
Table Top	Kent 2004	Rigid hub	15	18	3
		Distributed belt		16	1
		Single diagonal belt		18	2
		Double diagonal belt		15	2
	Forman 2005	Load limited double diagonal belt	3	23	2
	Salzar 2009	Single diagonal belt	3	6	0
	Cesari 1990, 1994	Single diagonal belt	17	17	14
	Kemper 2011	Single diagonal belt	2	2	2

The sections below describe the process of setting up each table-top case in finite element simulation environment. Before simulations setup in these conditions can be used for injury risk function development, it should be ensured that the PMHS responses are relatively well captured by the HBM for each case i.e. the HBM response is relatively biofidelic in the selected cases. First, the biofidelity of THUMS v4.1 for the table-top cases was examined by evaluating the response in a single exemplar simulation for each load case (representing the “average” or typical input condition). Following the initial biofidelity evaluation, matched-pair test specific simulations were

performed to expand the simulation dataset for IRF development, and to develop IRFs via regressing the HBM responses against the matched PMHS injuries.

FE Setup

Kent 2004

Kent et al. conducted a series of tests on 15 PMHS to produce thoracic response corridors using four loading conditions on the anterior thorax – single and diagonal belt, distributed loading and hub loading (Kent et al., 2004). This study quantified the force-deflection response of the same thorax to different loading conditions using dynamic, non-impact loading. The subjects were laid supine on a flat rigid table and the anterior aspect of the thorax was dynamically loaded. Multiple tests were performed on a single subject using all the four loading conditions, with the final test being of injurious severity. The subjects ranged in age from 54-85 years, in weight from 45-112 kg and 8 out of the 15 were females. The thorax was loaded by imposing prescribed displacement (to the hub, or to the belt ends for single, double diagonal and distributed belts) at a target rate of 1 m/s. The hub was 152 mm in diameter to emulate Kroell 1974 loading, the diagonal belts were 50 mm wide and made of sail cloth to minimize belt elongation, and for distributed loading a 203 mm wide belt made of sail cloth was used. The experimental setup was as shown in **Figure 19**. The thoracic force-deflection response corridors as well as injury findings in terms of ribcage fractures are available for each test.

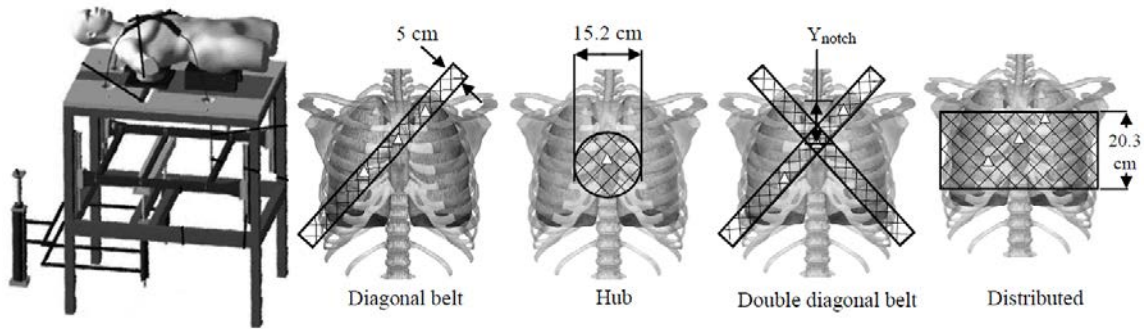


Figure 19 Experimental setup and different loading conditions (Kent et al., 2004)

- *HBM Posture on Table*

For all the loading conditions, the subjects were laid supine on a flat rigid table. Hence, as a first step in modelling the simulation setup, the HBM was settled supine on a flat table under gravity loading. The flat rigid table was modelled as a fully constrained shell surface with rigid material with steel mechanical properties. The dimensions given in Appendix of Kent 2004 paper (shown here in Figure 20 a) were used as a reference to model the table and position the HBM over it. Before the gravity settling, the HBM was aligned at the centerline of the table. Contact between the HBM and table was defined with a friction coefficient of 0.2. The HBM was then simulated to settle on the table under gravitational acceleration in the vertical direction. The simulation was run until full settling of the torso back. To speed up this process and run the simulation for shorter duration, a small downward initial velocity of 0.1 m/s may be applied to the HBM. The settled HBM posture is shown in Figure 20 b. It may happen that the HBM head does not contact the table by the time the torso settles due to the stiffness of the neck. If this happens, a rigid plate of the same material as that of the table could be modelled after the gravity simulation, to support the head in the actual loadcase simulations. This gravity settled position/posture of the HBM is then used in the final loadcase simulations.

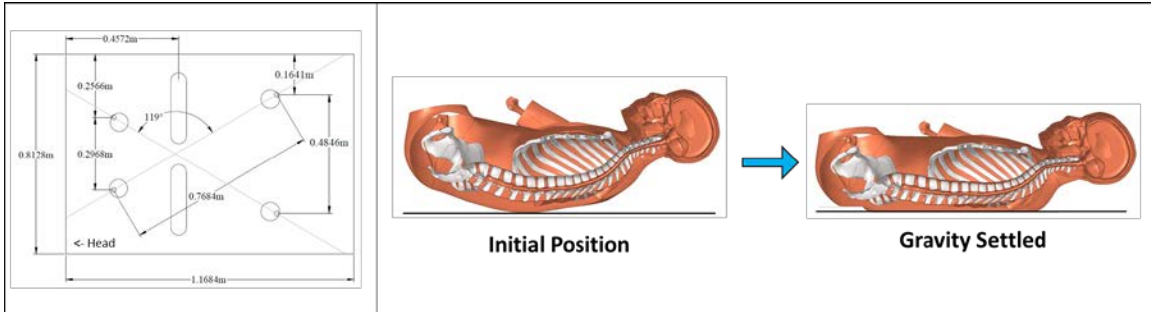


Figure 20 a) Table dimensions from Kent 2004 b) Gravity settling and final HBM settled posture

- *Hub Loading Condition*

The hub load was applied with a 152mm diameter steel circular plate intended to mimic the loading surface described by Kroell 1974 (Kent et al., 2004). Hence, the same hub impactor that was used in the Kroell 1974 impactor loadcase was used for this loadcase. The center of the hub was located at the intersection of the mid-sagittal plane and approximately the fourth intercostal space as shown in the Figure 21 b. The hub was constrained to translate only in the Z direction and given a prescribed displacement time history (shown in Figure 21 a) as input. The coefficient of friction for the contact between the hub and HBM thorax; and the table and HBM was defined to be 0.2.

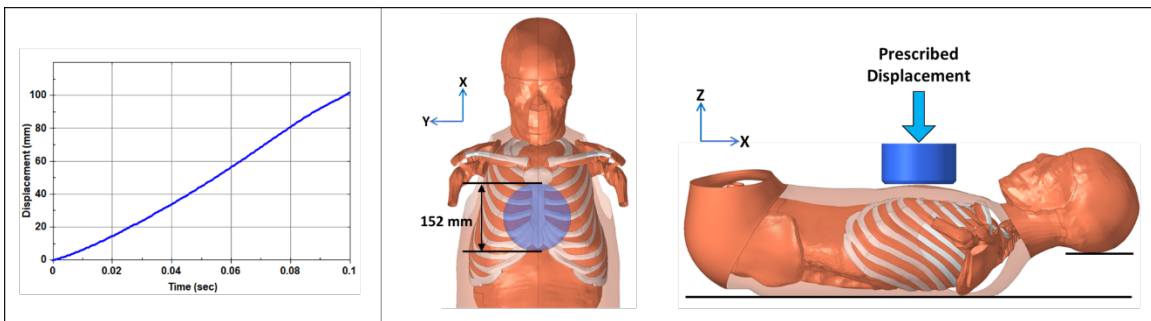


Figure 21 a) Prescribed displacement time history b) Hub impactor position and simulation setup

- *Single Diagonal Belt Loading Condition*

In the single belt loading tests, a 50mm wide diagonal belt passed over the left shoulder of the subject and crossed the anterior thorax approximately 30 deg from the sagittal plane. The belt

engaged the PMHS mid clavicle, crossed the midline approximately mid-sternally and exited the body laterally at approximately ninth rib (Kent et al., 2004). The belt ends passed through holes in the table and passed over a pulley located 95 mm below the table, connecting to the hydraulic master-slave cylinder generating the input pulse (Kent et al., 2004). To represent this setup in simulation, firstly slirings were defined at the location of the pulleys. The table and pulley setup used in the tests is shown in **Figure 20a**. If required, the user may adjust the anchor locations to fit the human body model, so that the belt reasonably matches the targets given in the reference literature. The belt was then routed over the HBM diagonally from top right to bottom left slirings as shown in the Figure 22 a. Belt part in contact with the HBM torso was modelled as 2D shell with 1mm thickness and 50mm total width, and the belt ends were modelled as 1D seatbelt elements. The belt end nodes were constrained to only translate in the Z direction.

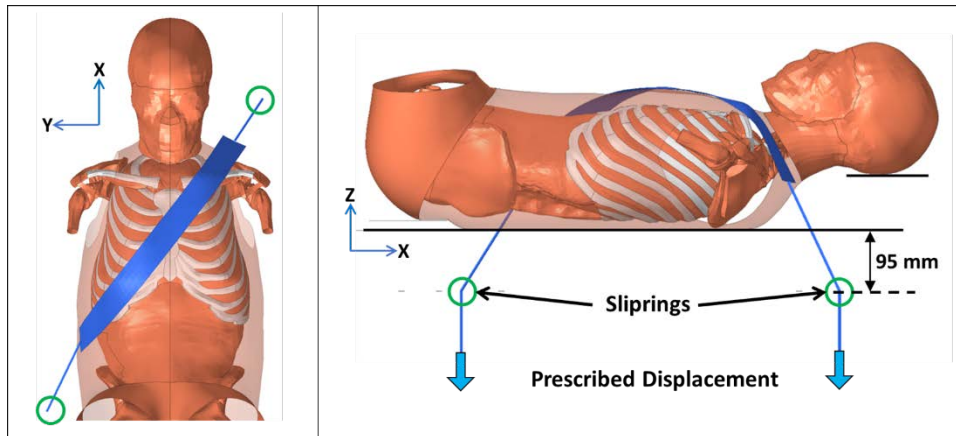


Figure 22 a) Diagonal belt routing over HBM b) Simulation setup

The 2D part of the belt was modelled as *Mat_Fabric and 1D part was modelled as *Mat_Seatbelt in LS-Dyna. The material card for the fabric material and loading curve for the seatbelt material are given in Figure 23. The coefficient of friction for the contact between the belt and the HBM torso was defined to be 0.3 and between the table and the HBM was defined to be 0.2. The same prescribed displacement time history from hub condition (Figure 21 a) was applied as input

loading to the belt end nodes (as shown in Figure 22 b).

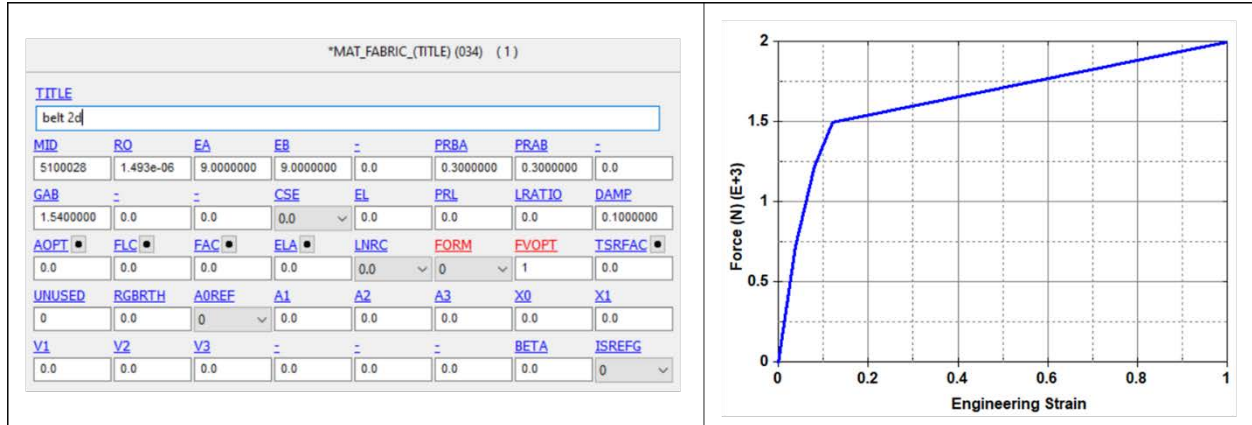


Figure 23 a) Fabric material card for 2D belt material b) Loading curve for 1D belt material

- *Double Diagonal Belt Loading Condition*

In the tests, the double diagonal belt condition involved a second diagonal belt oriented symmetrically to the diagonal belt described in the single belt condition (Kent et al., 2004). This was modelled in the simulation by starting with the previously modelled single belt condition setup and including a duplicate of the entire belt + slinging assembly, mirrored about the mid-sagittal plane. Contact between the second belt and HBM thorax with a coefficient of friction of 0.3 was also added. No contact was defined between the two belts. The same prescribed displacement time history from hub condition (Figure 21 a) is applied as input loading to both the belt end nodes (as shown in Figure 24).

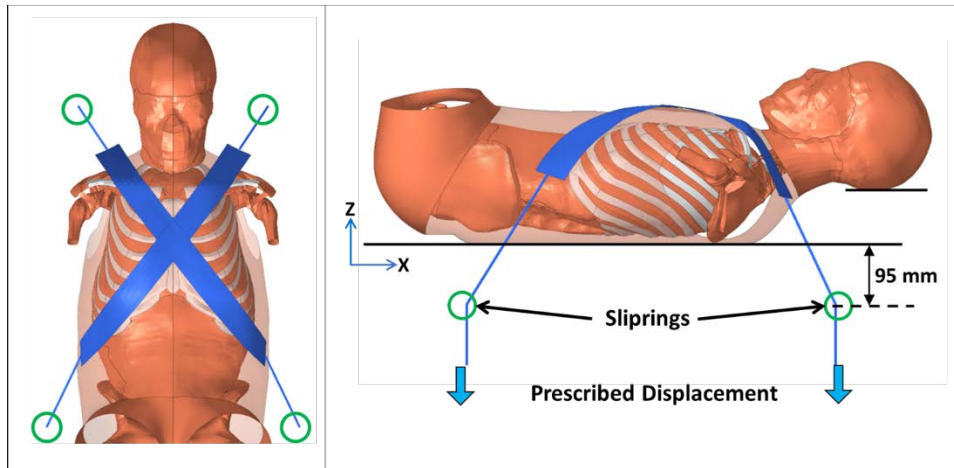


Figure 24 a) Double diagonal belt routing b) Double diagonal belt simulation setup

- *Distributed Loading Condition*

In the distributed loading condition tests, a 203mm wide belt made of the same sail cloth as the diagonal belts, loaded the area approximately between the second and seventh ribs (Kent et al., 2004). The belt ends passed through holes in the table and passed over a pulley located 95 mm below the table, same as that of the diagonal belt loading conditions. In this case, the pulleys were located at the sides of the table as shown in the Figure 25 a. The belt was then routed from slipring to slipring, with the part in contact with the torso modelled as 2D shell elements with 1mm thickness and total width of 203mm, and the belt ends as 1D seatbelt elements. The belt end nodes were constrained to only translate in the Z direction. The material properties of the 2D part were the same as that of the 2D part and those of the 1D part were the same as 1D part of the diagonal belt respectively. The coefficient of friction for the contact between the belt and the HBM torso was defined to be 0.3 and between the table and the HBM was defined to be 0.2. The same prescribed displacement time history from hub condition (Figure 21 a) is applied as input loading to the belt end nodes (as shown in Figure 25).

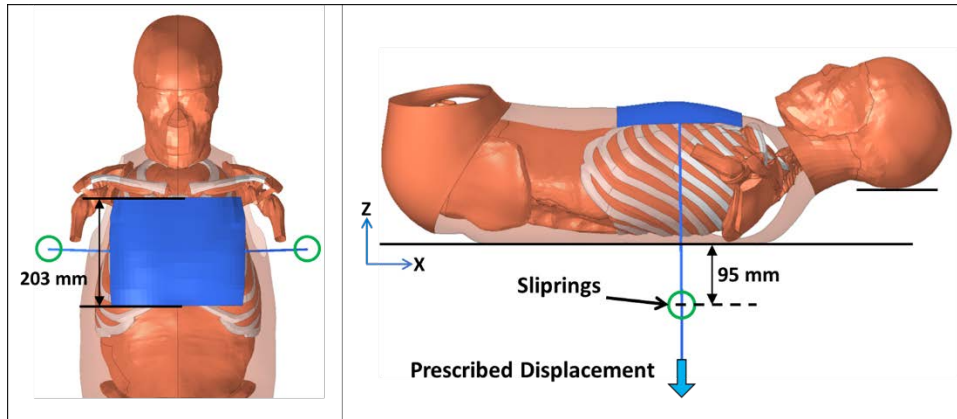


Figure 25 a) Distributed belt routing b) Distributed loading condition simulation setup

Forman 2005

Forman et al. conducted a series of tests on three PMHS using a double diagonal belt table-top configuration to evaluate the thoracic force-deflection response when a force-limited, second shoulder belt is added to a 3-point belt system (J. Forman et al., 2005). The subjects were positioned supine on a flat, rigid surface in a manner identical to that described by Kent et al. (Kent et al., 2004). In each test, custom force-limiters made of aluminum sheets were installed in series with the loading cables on both superior and inferior ends of the second shoulder belt passing over the right shoulder. These force-limiters were constructed to absorb energy by tearing at a constant force. Multiple tests were performed on each PMHS by varying the force-limit from 85 N to 800 N and also with no force limit, upto 20% chest deflection (non-injurious). Lastly a no limit injurious test with 40% chest deflection was performed on each subject. The thorax was loaded by applying prescribed displacement to the belt ends at a rate of 1 m/s. The subjects ranged in age from 38-67 years old, in weight from 49.9-94.8 kg and all of them were females. The experimental

setup is as shown in the **Figure 26**. The thoracic force-deflection responses as well as injury findings in terms of ribcage fractures are available for each test.

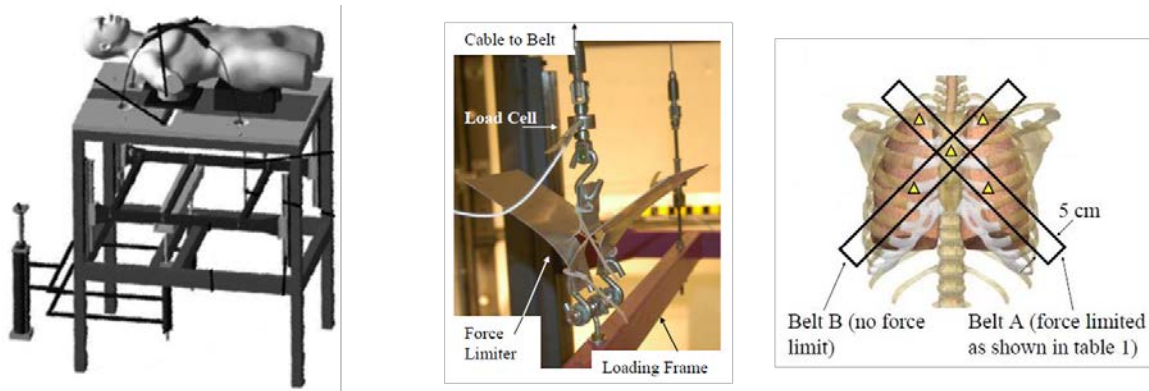


Figure 26 a) Experimental setup for Forman 2005 b) Custom force-limiters c) Belt orientation over subject torso

The test setup for this test series was identical to the double diagonal belt configuration of Kent 2004 tests. Hence, the simulation setup of Kent 2004 double diagonal belt condition was used for this loadcase. The only modification to the Kent 2004 setup was the addition of force-limiters on both ends of the belt in contact with the right clavicle. The force-limiter was modelled using a discrete spring element in series with the 1D belt elements as shown in the Figure 27. The force limit was defined by force-deflection curve of the spring element as shown in the Figure 27 and was modified as per the required force-limit level. The loading and boundary conditions remained the same as that of the Kent 2004 simulation setup.

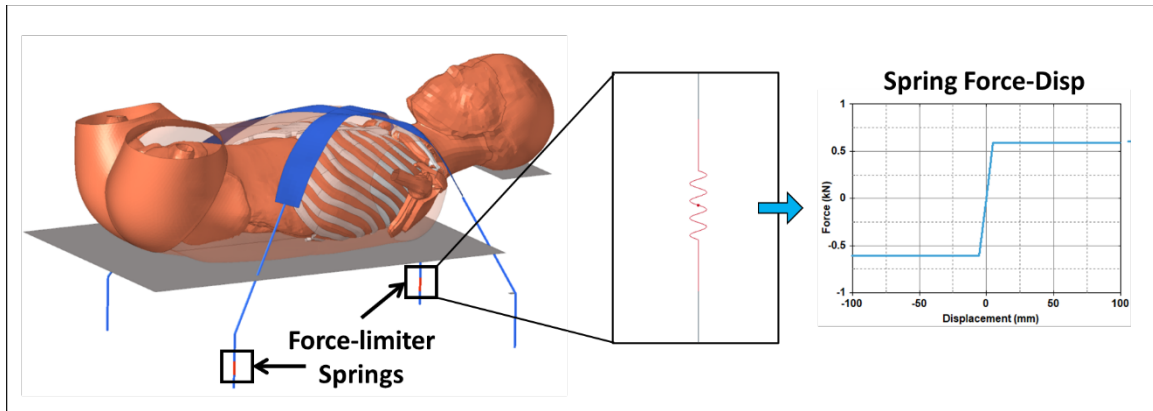


Figure 27 Simulation setup for Forman 2005 case with Force-Displacement curve for spring force-limiters

Salzar 2009

Salzar et al. conducted a series of tests on three PMHS using a single diagonal belt configuration to characterize the thoracic force-deflection response. This data was used to build a 7-parameter thoracic structural model mathematically analogous to a viscous material model (Salzar et al., 2009). The PMHS were mounted supine to a stationary apparatus that supported the spine and shoulders. The distal humeri of the subjects were held via cables which were force-limited to 250 N using the same type of force-limiters as Forman et al. (J. Forman et al., 2005). Two tests were performed on each subject with a ramp-hold displacement loading applied to the belt ends at a rate of 0.5 m/s and 1 m/s up to 20% chest deflection (non-injurious loading). The experimental setup and the spine fixture are shown in the Figure 28. The subjects were all male and ranged in age from 31-62 years old and in weight from 68-90 kg. The thoracic force-deflection responses as well as injury findings in terms of ribcage fractures are available for each test.

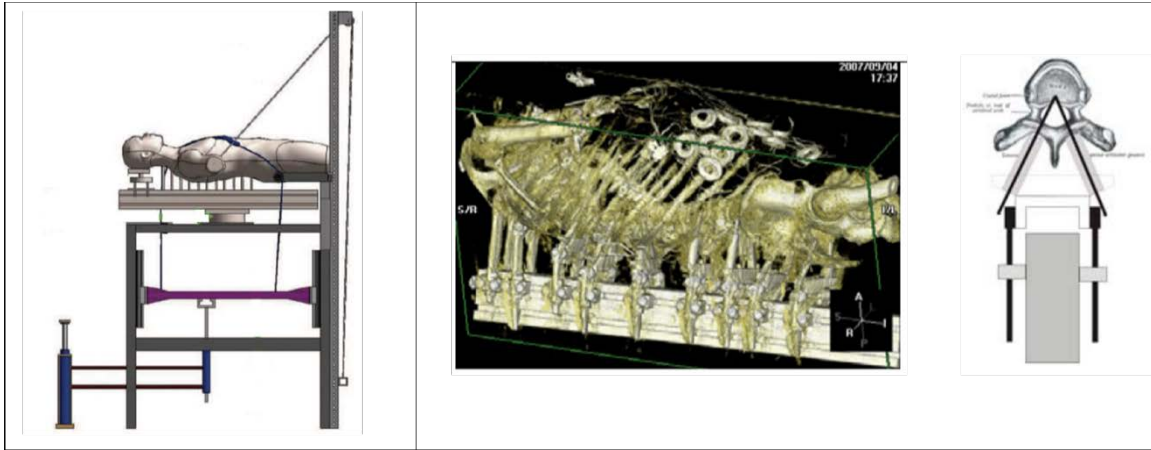


Figure 28a) Experimental setup and b) Spine fixture for Salzar 2009

To emulate the spine fixture from the tests, all the vertebrae and pelvis were constrained rigidly to the table surface. The belt anchor points were modelled as slings like Kent 2004 single diagonal belt condition. The belt was routed over the torso such that it crosses the midline at the mid-sternum at approximately 30 deg from the sagittal plane (as described in the tests (Salzar et al., 2009)). The belt was modelled as 2D shell elements and the end cables as 1D seatbelt elements. The belt dimensions and material properties were the same as that of the Kent 2004 single diagonal belt condition. The cables used for holding the humeri in tests were modelled in FE as 1D seatbelt elements of the same material as 1D part of the diagonal belt. The 250 N force-limiter used in the tests was modelled as a spring element as shown in **Figure 29**. The friction coefficient for the contact between the belt and the HBM torso is defined to be 0.3. The prescribed displacement at a target rate of 1 m/s was applied as input loading to the belt end nodes (as shown in Figure 29).

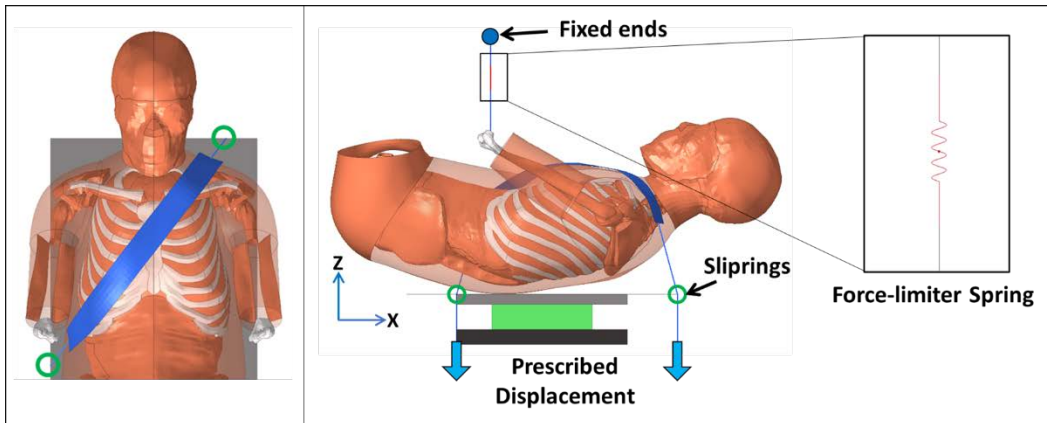


Figure 29 a) Belt orientation and b) Simulation setup for Salzar 2009

Kemper 2011

Kemper et al. performed a series of table top tests with single diagonal belt on two PMHS (one male and one female) to quantify the biomechanical response of the human thorax during dynamic shoulder belt loading representative of that seen in a severe automotive collision (Kemper et al., 2011). The thorax of each PMHS was placed on a spine support fixture designed to allow free motion at the costovertebral joints as well as raise the thorax above the flat table, which could otherwise constrain the deformation and motion of the posterior region of the ribcage. The thorax of each PMHS was then loaded in the single diagonal belt configuration using prescribed displacement at a rate of 1.0 m/s. The PMHS ranged in age from 65-69 years old and in weight from 50.9-76.8 kg. The experimental setup and spine fixture are shown in Figure 30. The thoracic force-deflection responses as well as injury findings in terms of ribcage fractures are available for each test.

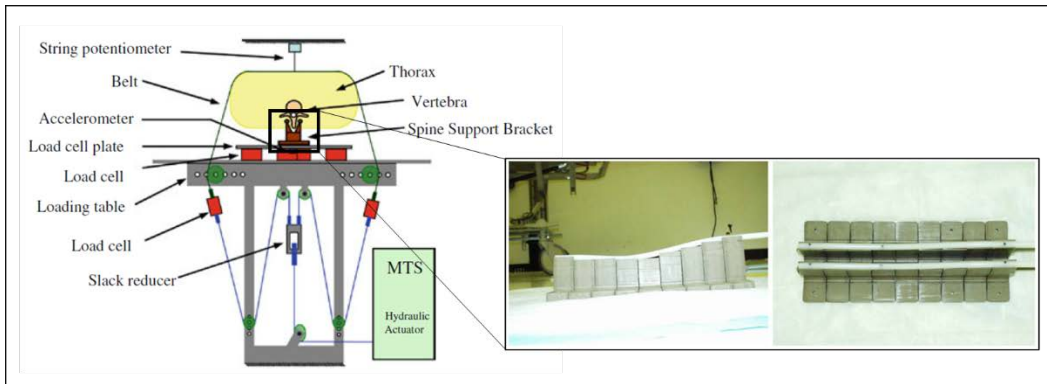


Figure 30 Experimental setup and spine fixture for Kemper 2011

The table top setup used in these tests was similar to the one used in Salzar 2009, in terms of spine fixture and single diagonal belt loading. Hence, for simplicity, the same setup from Salzar 2009 was used for these tests. However, the only difference was that Kemper et al. did not constrain the humeri of the test subjects in any way. Hence, the cables holding the distal humeri (from Salzar 2009 case) were removed from the simulation setup for Kemper 2011 (this) case. Prescribed displacement at a target rate of 1 m/s was applied to the belt ends. The final simulation setup with the THUMS v4.1 model is shown in Figure 31.

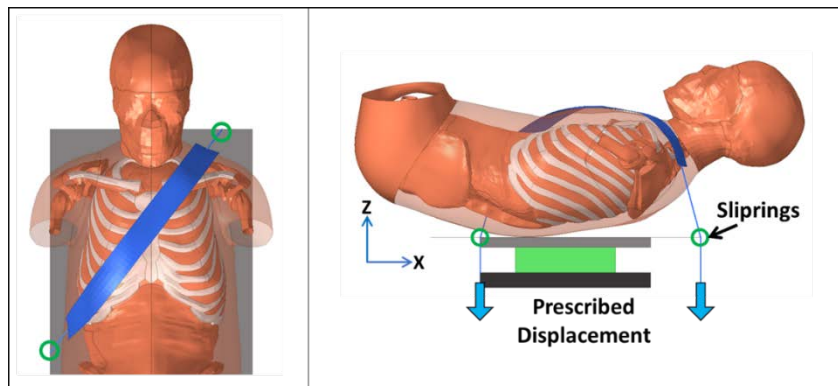


Figure 31 Belt orientation and simulation setup for Kemper 2011

Cesari 1990,1994

Cesari et al. performed a series of table top tests on seventeen PMHS to understand the deformation of the human thorax when loaded by a diagonal seatbelt (Cesari & Bouquet, 1990,

1994). Each subject was laid supine on a rigid flat table and a generic seatbelt strap was placed across the torso in a geometrical layout similar to that of a car driver wearing a shoulder belt. The belt ends were pulled dynamically by the impulse of a dynamic impactor as shown in **Figure 32**. The PMHS (five female and twelve male) ranged in age from 17-86 years old and in weight from 41-92.5 kg. The maximum deflection on 11 points on the anterior thoracic surface and injury findings in terms of ribcage fractures are available for each test.

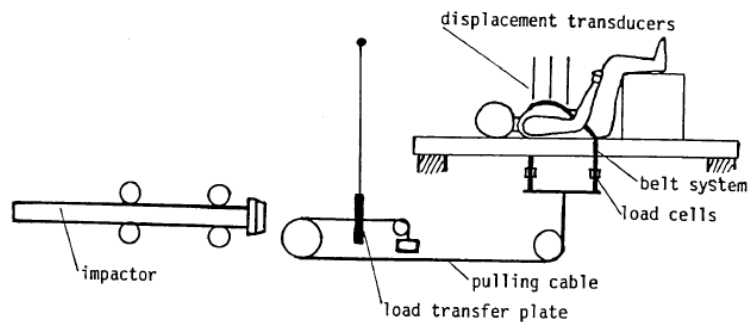


Figure 32 Experimental setup for Cesari 1990,1994.

The test setup for this loadcase had the subjects resting supine on a flat rigid table under gravity. The posture and position of the PMHS in the tests is not described in detail in the literature. However, the FE setup for this loadcase is available for the THUMS v4.1 model from Toyota and was used in this study for simplicity. The simulation setup of Kent 2004 single diagonal belt condition is a good approximation of this test setup and may be used for other HBMs. The loading condition is a prescribed velocity time history applied to the belt ends in Z direction. The velocity time history and final simulation setup are shown in Figure 33. The coefficient of friction for the contact between the belt and the HBM torso is defined to be 0.3 and between the table and the HBM is defined to be 0.2.

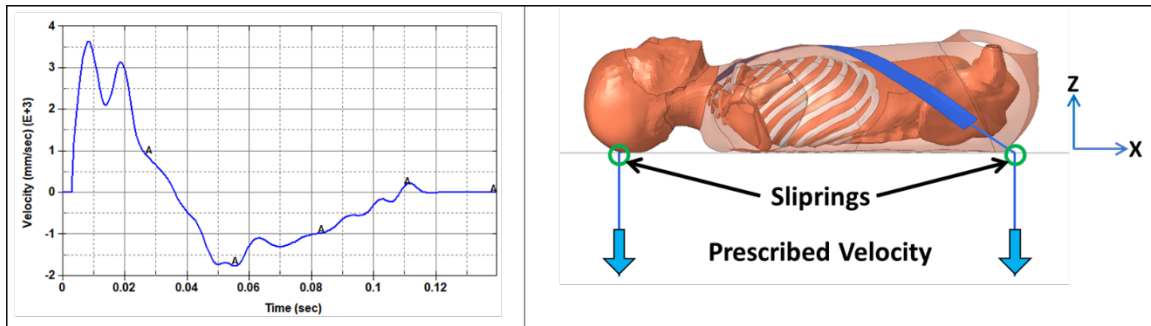


Figure 33 a) Prescribed velocity time history and b) Simulation setup for Cesari 1990,1994

HBM Biofidelity

Kent 2004

In the tests, the thoracic response was characterized using the deflection at the midline of the sternum and the reaction force calculated between the posterior thorax and the table. Kent et al. developed corridors on the posterior force vs percentage chest deflection, normalized to a 45-year-old 50th percentile male. These corridors are available for each of the four loading conditions up to 20% chest deflection. The HBM biofidelity was evaluated by comparing the force vs normalized chest deflection response in each condition with the corridors proposed by Kent et al. The chest deflection was measured by the change in length between the nodes on anterior thorax and posterior thorax on the midline as shown in the Figure 34. This deflection was normalized by the initial distance between the nodes. The force was measured as the contact force between the thorax and the table. The results for each loading condition are shown in Figure 35.

The THUMS v4.1 model response was found to be somewhat stiffer than the PMHS average corridor in all the four loading conditions. However, the difference between the model and the corridor was relatively small – small enough that we have some confidence that it would

not substantially affect the kinematics of the model in whole-body use cases, or the fundamental nature of the interaction with a restraint system. Perhaps more importantly, the model seems to be capturing the sensitivity to differences in loading condition correctly. The model response consistently falls above the PMHS corridors by about the same amount. This means that the relationship between loading method and force-deflection response is the same for the model as it is for the PMHS. This is more important than the individual differences, because if the model were not sensitive in the right way, it would limit its utility in assessing the effects of different types of restraint conditions. As a result of the subtle nature of the differences, as well as the correct sensitivity that the model exhibits, it was acceptable to accommodate the small difference in biofidelity by tuning the IRF specifically for this model.

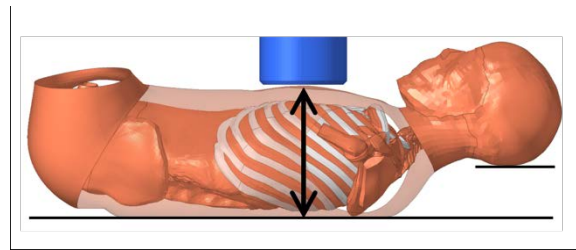


Figure 34 Chest deflection measurement for Kent 2004 (hub loading example)

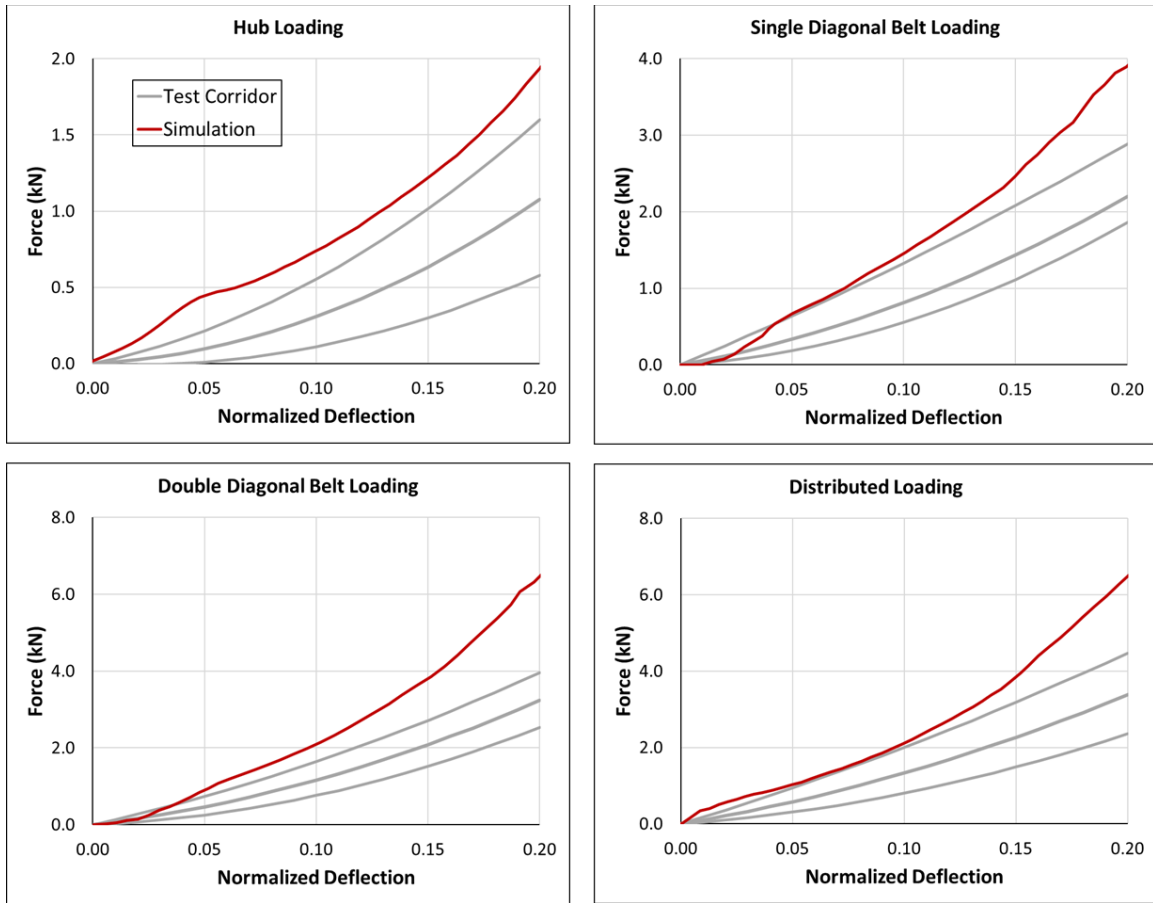


Figure 35 Force v normalized deflection comparison for Kent 2004 (clockwise) a) hub b) single diagonal belt c) distributed and d) double diagonal belt loading condition

Forman 2005

The HBM biofidelity is evaluated by comparing the force vs normalized chest deflection response with the response from the tests for the 600N force limit level. The chest deflection was measured in the same way as for Kent 2004 cases (Figure 34). The deflection was normalized by the initial distance between the nodes. The force was measured as the contact force between the thorax and the table. The results for the 600 N force-limit level are shown in Figure 36. As with the Kent et al. load cases described above, the THUMS v4.1 model response was found to be consistently stiffer than the PMHS by a small amount.

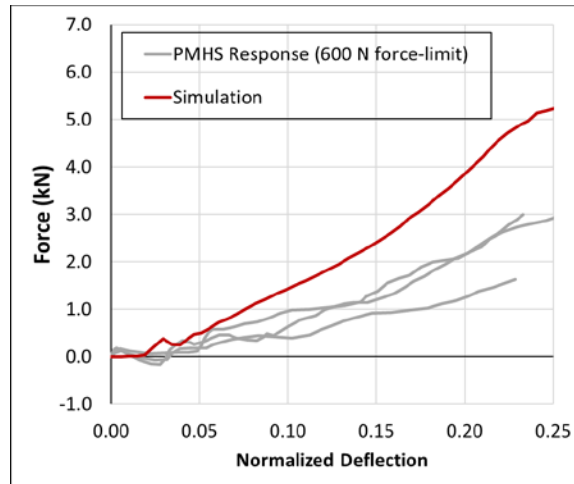


Figure 36 Force v normalized deflection comparison for Forman 2005 600 N force-limit condition. Salzar 2009

The HBM biofidelity for this loadcase was evaluated by comparing the reaction force versus the normalized chest deflection response from the simulations with the response curves from the tests. The reaction force was measured as the total force at the section defined in the deformable loadcell. The chest deflection was measured by the change in length between the nodes on the anterior and posterior of the thorax at the T8 level as shown in the Figure 37a. The absolute deflection is then normalized by the original length that is the chest depth. Results are shown in Figure 37b. The THUMS v4.1 model was found to fall within the range of the PMHS responses, however the chest deflections applied in this load case were substantially lower than the other table-top cases described above (approx. 8% deflection vs. up to 25% deflection). Given the force-displacement trajectory shown in Figure 37b, it is likely that the model response would prove to be stiffer than the PMHS at higher deflections, consistent with the observations above

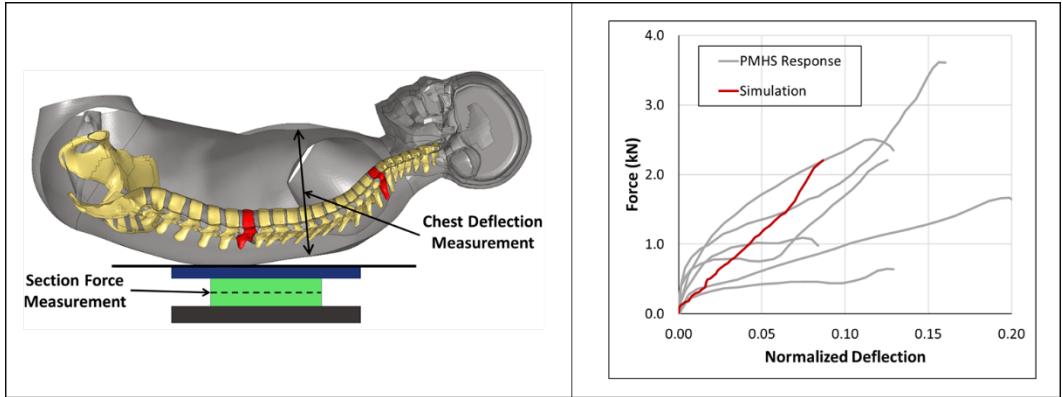


Figure 37 a) Chest deflection and force measurement b) Force v normalized chest deflection comparison for Salzar 2009

Kemper 2011

The HBM biofidelity for this loadcase is evaluated by comparing the reaction force versus the normalized chest deflection response from the simulations with the response curves from the tests. The method for measuring chest deflection and the posterior force was the same as for Salzar 2009 case. The results are shown in Figure 38. Consistent with the observations in the above loadcases, the THUMS v4.1 response was found to be stiffer than the PMHS response.

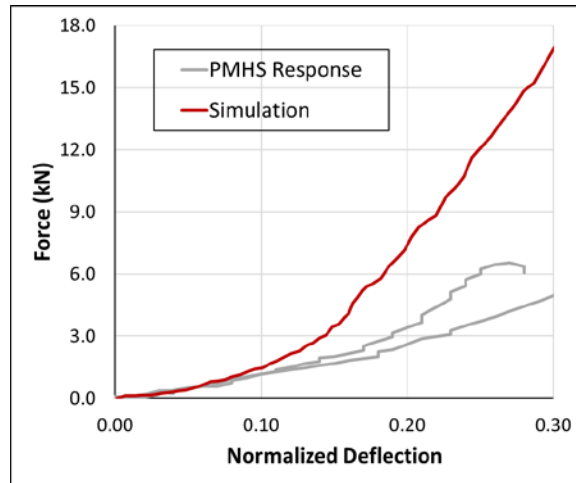


Figure 38 Force v normalized deflection comparison for Kemper 2011

Cesari 1990,1994

The HBM biofidelity was evaluated by comparing the deflection time history of 8 points on the anterior thoracic surface with the deflection corridors from the tests. The corridors were defined as a range for the maximum deflection of each point. Nodes were selected on the anterior thoracic surface corresponding to the points (as shown in Figure 39) and the deflection time history was measured as the Z displacement of these nodes. The results for the THUMS v4.1 model are shown in Figure 39. The model responses tended to fall within the PMHS ranges, suggesting that when loading is applied by a shoulder belt with a specified displacement at the mid-sternum, the distribution of displacements at other locations on the chest is consistent with the pattern of displacement observed in PMHS.

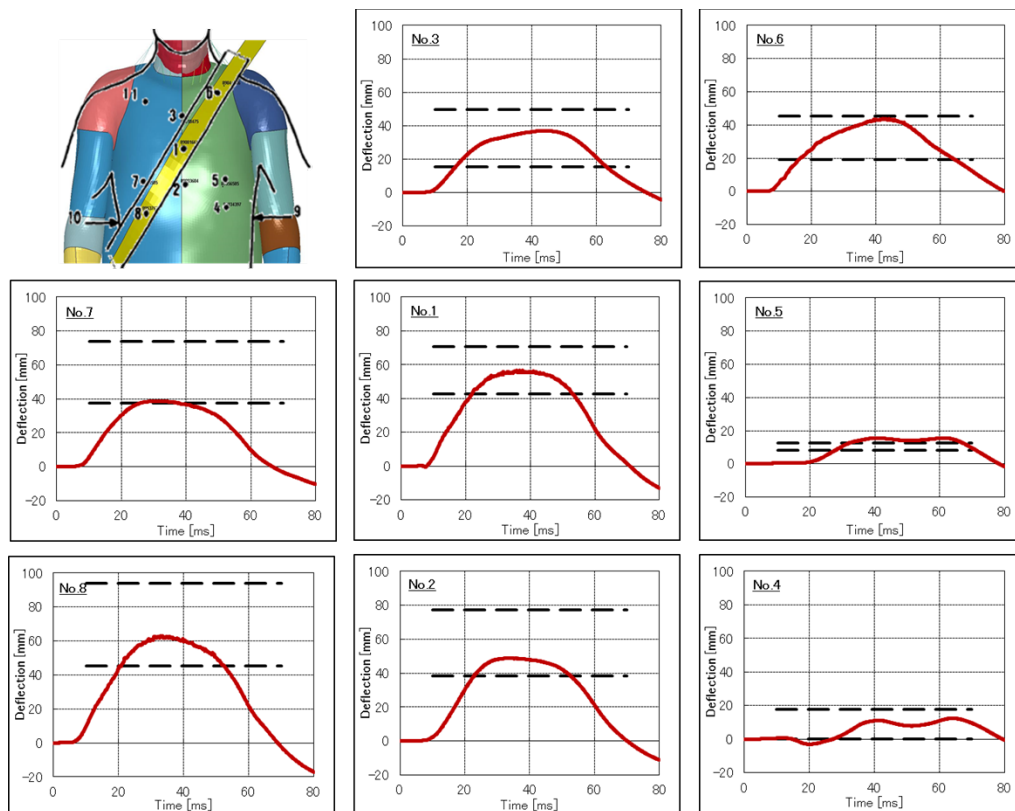


Figure 39 Deflection time histories of torso points and comparison with PMHS range for maximum deflections for Cesari 1990, 1994

Test Specific Simulations

Like the impactor loadcases, test-specific simulations were setup corresponding to each individual test by modifying the loading conditions, targeting the test inputs applied to the PMHS. The loading input in all the table-top cases was in the form of a prescribed displacement of the loader (hub or belts). These prescribed displacement time histories were available for each individual test and were normalized (in magnitude) using the chest depth of the particular PMHS used in the test. These normalized displacement time histories were then rescaled using the chest depth of the HBM (e.g. 230mm for THUMS v4.1) before using as input for the matched-pair simulations. The objective of this type of scaling was to expose the HBM to a loading that was comparable to the loading received by the PMHS in the matched-pair test, and to induce comparable chest compression and injury severity between the HBM and the PMHS. The normalized displacement time histories for each table-top test are given **Appendix D**. This exercise increased the table-top simulation dataset to 115 matched-pair simulations.

2.2.3 Simulations For IRF Validation

Sled Cases

Introduction

From the selected loadcases (Section 2.1), six were classified as being Sled type loadcases. These were typically characterized by the PMHS restrained in a pseudo-vehicle environment and subjected to a frontal impact crash pulse. **Table 4** shows the selected sled type PMHS test series.

Table 4 Sled type PMHS test series

<i>Type</i>	<i>PMHS Test Series</i>	<i>Loading Condition</i>	<i>No. of PMHS</i>	<i>Total no. of Tests</i>	<i>No. of tests with 3+ rib fx</i>
Sled	Gold Standard 1	$\Delta V = 40$ kph, 3-point standard belt	8	8	7
	Gold Standard 2	$\Delta V = 30$ kph, 3-point 3kN LL belt	5	5	2
	Gold Standard 3	$\Delta V = 30$ kph, 3-point 3kN LL belt Oblique frontal loading direction	3	3	2
	Low Speed Front	$\Delta V = 29$ kph, 3-point standard belt	3	3	0
	Rear Seat (Forman 2009)	$\Delta V = 48$ kph, 3-point 3kN LL belt	3	3	3
	Rear Seat (Michaelson 2008)	$\Delta V = 48$ kph, 3-point standard belt	3	3	3

The following sections describe the simulation setup of the six sled loadcases. Comparison of the THUMS v4.1 kinematics with PMHS data from the test series (based on select anatomical landmarks) for each sled condition is also described in this section. In the sled condition, load transfer does not occur directly from an impactor to the HBM thorax like in the case of impactor or table-top conditions. Transfer of forces from the impact crash pulse to the HBM is dependent on the interaction of the HBM with the restraint systems and the sled environment. Hence it may not be possible to get matched-pair test-specific sled simulations without morphing/modifying the HBM itself and violating the objective of this study. Thus, only one simulation representing each sled loadcase was performed with the THUMS v4.1.

FE Setup and HBM Kinematics

Gold Standard Sled Cases

A generic environment with horizontal steel sheet as seat, knees constrained by rigid fixation and having 3-point seatbelt as restraint was developed at the University of Virginia to provide a reasonable approximation of real-world frontal impact crash loading of a belted occupant

while providing repeatable and reproducible test conditions that yielded torso response data suitable for analysis (Acosta et al., 2016; Pipkorn et al., 2019; Shaw et al., 2009). This sled configuration is commonly known as the Gold Standard Sled and depending on the crash pulse and restraint type, tests are classified as Gold Standard 1, 2 or 3 cases. The Gold Standard 1 configuration consists of a standard 3-point seatbelt (non-force limited) and a 40 km/h full frontal impact crash pulse (Shaw et al., 2009). Shaw et al. 2009 performed a series of tests with eight male PMHS (ranged in age from 37-76 years old and in weight from 64-88 kg) in this configuration. The Gold Standard 2 configuration consists of a 3 kN force-limited shoulder belt and a 30 km/h full frontal impact crash pulse (Acosta et al., 2016). Acosta et al. 2016 performed a series of tests on five male PMHS (ranging in age from 59-74 years old and in weight from 68-70 kg) in this configuration. The Gold Standard 3 configuration consists of the same 3 kN force-limited shoulder belt, but with a 30 km/h 30-degree near-side oblique frontal impact crash pulse (Acosta et al., 2016). Acosta et al. 2016 performed a series of tests on three male PMHS (ranging in age from 66-69 years old and in weight from 64-76 kg) in this configuration. The experimental setup and crash pulses are shown in Figure 40. The occupant kinematics of select anatomical locations (Head COG, T1, T8, L2 and pelvis), chest deflections, shoulder belt forces and injury information in terms of ribcage fractures are available for each test.

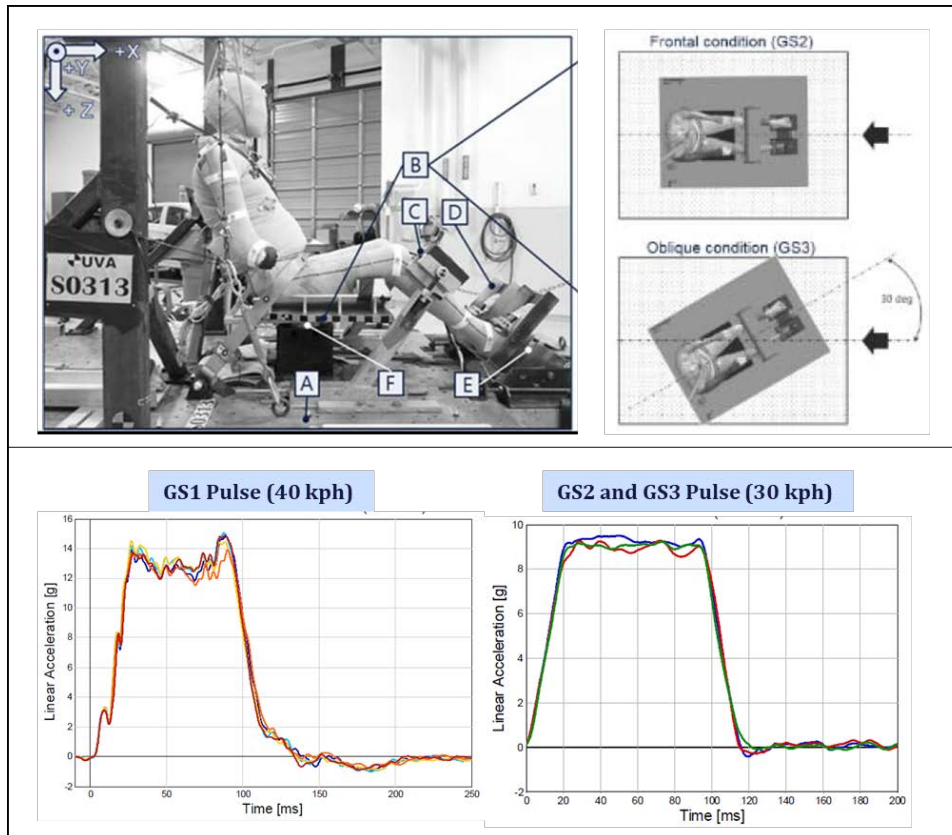


Figure 40 a) Gold Standard sled experiment setup and b) Gold standard impact crash pulses

The sled setup was modelled using the information given in the reference literature (Acosta et al., 2016; Shaw et al., 2009). All the components of the sled were modelled with rigid steel material except the belt restraint system. The shoulder belt force-limiters for GS2 and GS3 were modelled as discrete retractor elements with force v/s pull-out characteristics. The THUMS v4.1 model was settled into the sled seat under gravity using pre-simulation. The knee fixture was then adjusted over the knees of the HBM. The seatbelt was routed over the HBM torso and lap considering the reference measurements given in the literature. The final position and posture of the THUMS v4.1 model is shown in the Figure 41 along with comparison with the PMHS position measurements in Table 5. The belt position over the ribcage is shown in Figure 42 along with comparison with

PMHS measurements. The rigid sled was constrained to only translate in the direction of the impact and the crash pulse was applied to the rigid floor as a prescribed acceleration.

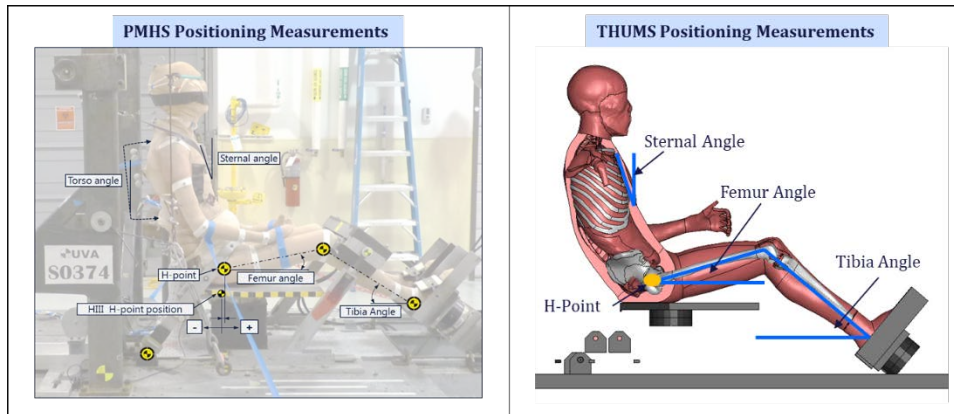


Figure 41 THUMS v4.1 position and posture in Gold Standard sled setup

Table 5 Comparison of PMHS and THUMS v4.1 posture in Gold Standard sled setup

<i>Name</i>	<i>PMHS Avg</i>	<i>THUMS v4.1</i>
Sternal Angle (deg)	22.5	19.5
Femur Angle (deg)	9.7	10.4
Tibia Angle (deg)	37.1	37.6

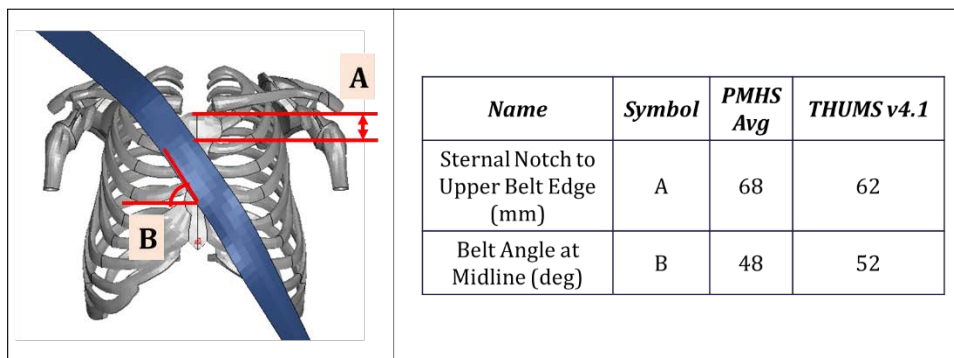


Figure 42 Belt position over torso for THUMS v4.1 in Gold Standard Setup and comparison with PMHS position

- *Gold Standard 1*

The final model setup and boundary conditions for GS1 case are shown in Figure 43. The simulation was run with the GS1 crash pulse and occupant kinematics were compared between the HBM and PMHS using displacement time histories of select anatomical locations in the mid-sagittal plane relative to the sled. The upper shoulder belt forces from simulation were also compared with the tests to ensure that the HBM was subjected to a loading that was comparable to the loading received by the PMHS in the tests. The kinematics and upper shoulder belt forces comparison is shown in Figure 44.

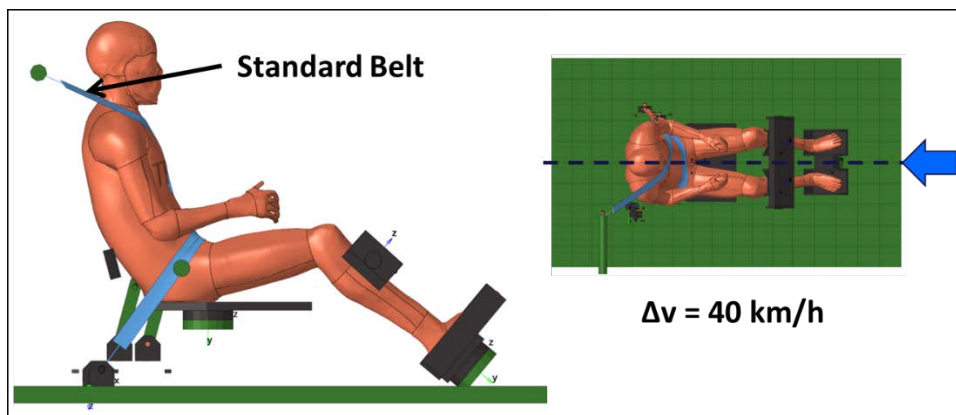


Figure 43 Gold Standard 1 sled setup with THUMS v4.1

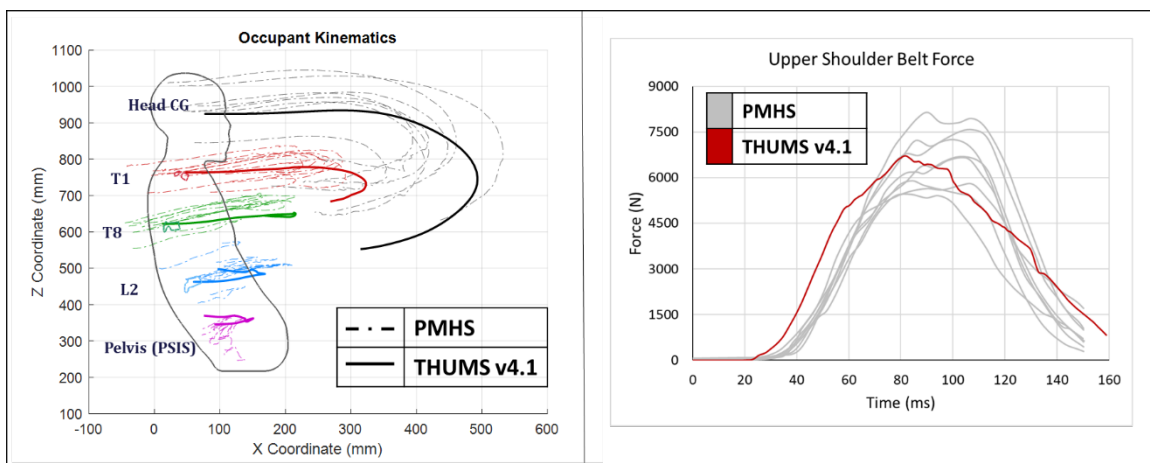


Figure 44 Occupant kinematics and upper shoulder belt forces comparison for GS1

- *Gold Standard 2*

The final model setup and boundary conditions for GS2 case are shown in Figure 45. The simulation was run with the GS2 crash pulse and occupant kinematics were compared between the HBM and PMHS using displacement time histories of select anatomical locations in the mid-sagittal plane relative to the sled. Upper shoulder belt forces from simulation were also compared with the tests to ensure that the HBM was subjected to a loading that was comparable to the loading received by the PMHS in the tests. The kinematics and upper shoulder belt forces comparison is shown in Figure 46.

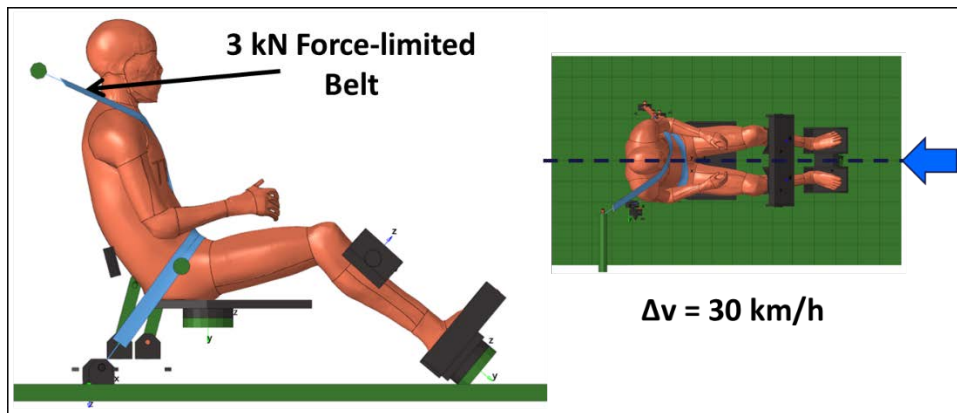


Figure 45 Gold Standard 2 setup with THUMS v4.1

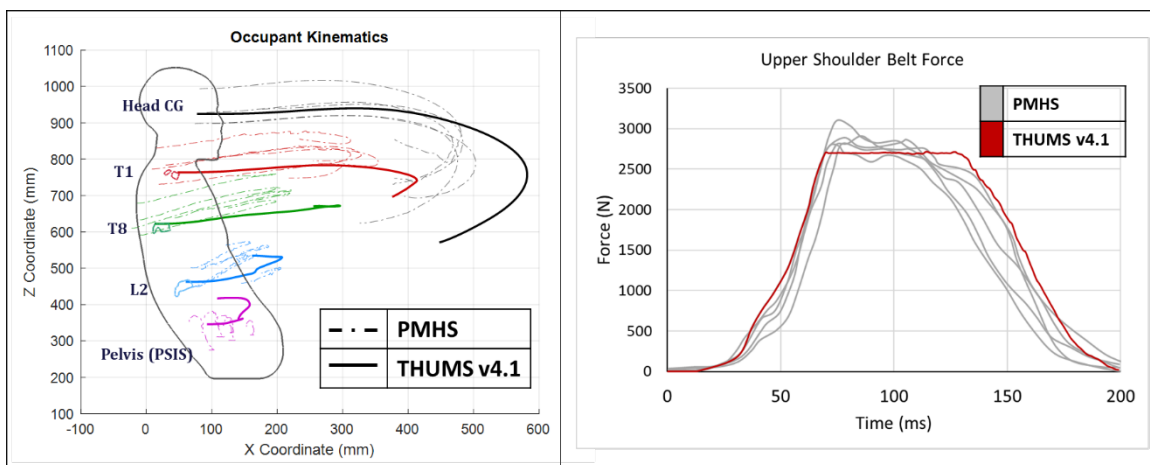


Figure 46 Occupant kinematics and upper shoulder belt forces comparison for GS2

- *Gold Standard 3*

The final model setup and boundary conditions for GS3 case are shown in Figure 47. The simulation was run with the GS3 crash pulse and occupant kinematics were compared between the HBM and PMHS using displacement time histories of select anatomical locations in the mid-sagittal and axial plane relative to the sled. Upper shoulder belt forces from simulation were also compared with the tests to ensure that the HBM was subjected to a loading that is comparable to the loading received by the PMHS in the tests. The kinematics and upper shoulder belt forces comparison is shown in Figure 48.

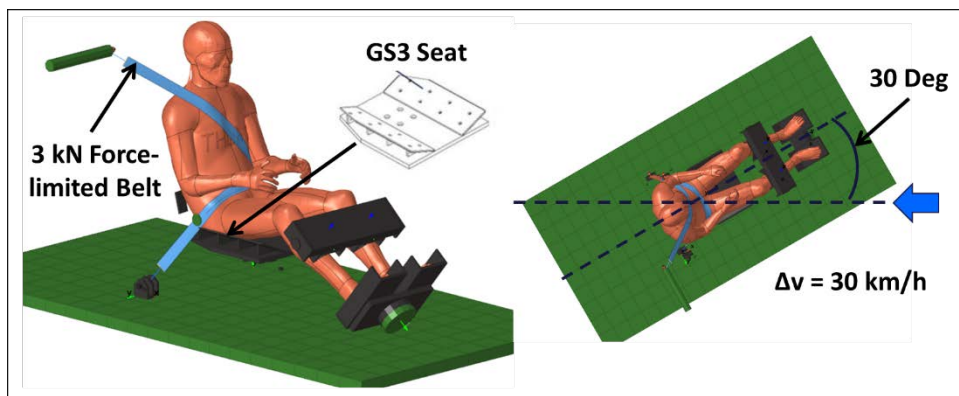


Figure 47 Gold Standard 3 sled setup with THUMS v4.1

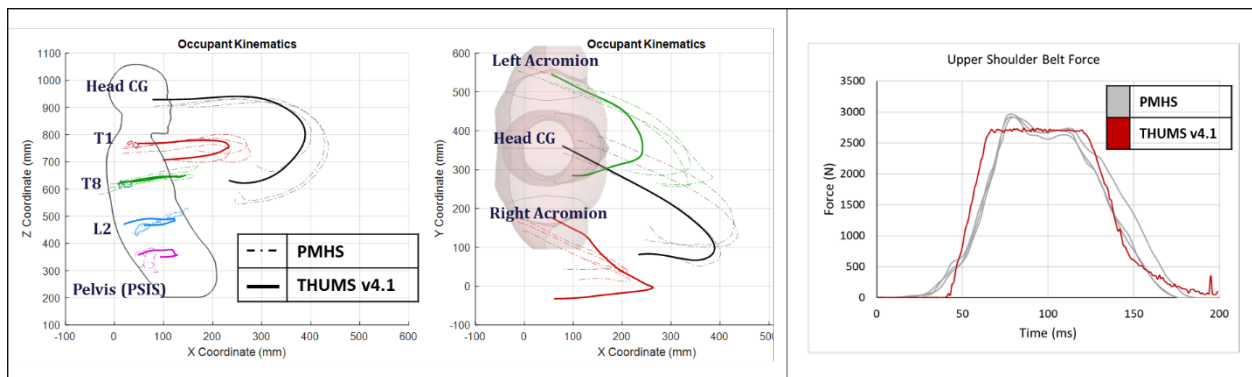


Figure 48 Occupant kinematics and upper shoulder belt forces comparison for GS3

Rear Seat Sled Cases

Michaelson et al. performed a series of sled tests to develop a baseline response for rear seated PMHS in frontal crashes (Michaelson et al., 2008). Sled tests were performed in a sled buck representing the rear seat compartment of a mid-size sedan. The PMHS were positioned in the right-rear passenger seat, restrained by a standard 3-point seatbelt and subjected to a frontal impact crash pulse of 48 km/h delta-v. The PMHS ranged in age from 51-57 years old, in weight from 55-109 kg, and two of the three were males. Forman et al. expanded this study by further testing three male PMHS with a 3-point belt system equipped with a dual-stage force-limiting and pretensioning retractor in the same rear seat sled environment (J. Forman et al., 2009). The PMHS in this study ranged in age from 67-72 years old and in weight from 67-72 kg. Occupant kinematics of select anatomical locations, chest deflections and injury information in terms of ribcage fractures was available for each test of both the sled test series. Experimental sled setup and the impact crash pulse are shown in Figure 49.

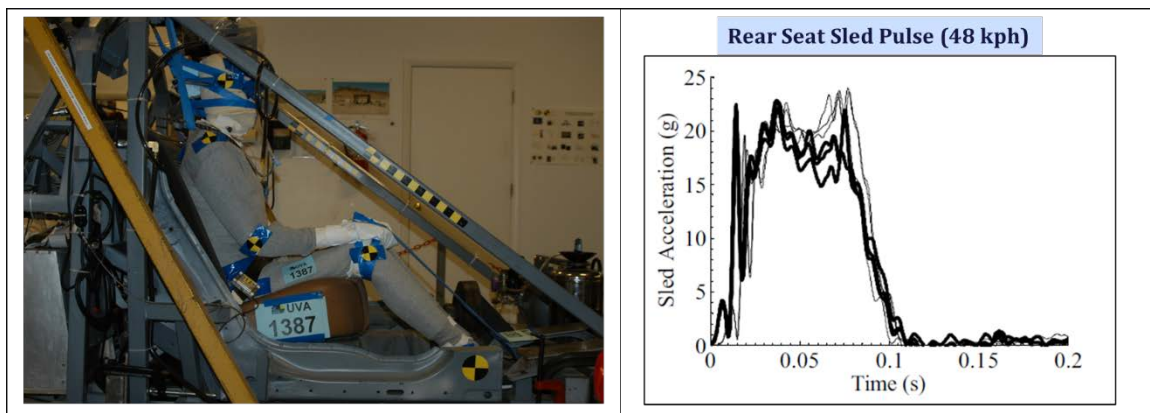


Figure 49 a) Experiment setup and b) Impact crash pulse for Rear Seat Sled cases

The sled and seat assembly were modelled from a mid-size sedan, same as that of the physical tests. The sled structure material was modelled as rigid steel and constrained to translate only in the direction of the frontal impact. The seat consisted of a rear bench seat cushion and seatback,

modelled as foam materials, and reinforced with steel beams (same as physical seats). The rear seat sled assembly in simulation environment is shown in Figure 50.

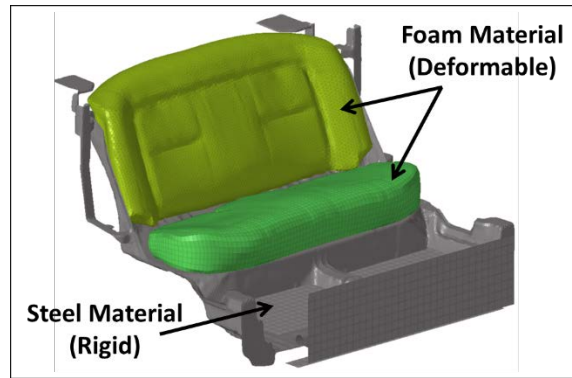


Figure 50 Rear seat sled assembly in simulation environment

The HBM was positioned on the right passenger side of the seat and settled into the seat and cushion using a gravity pre-simulation. The final position and posture of the THUMS v4.1 model in the sled is shown in Figure 51 along with comparison with PMHS position measurements.

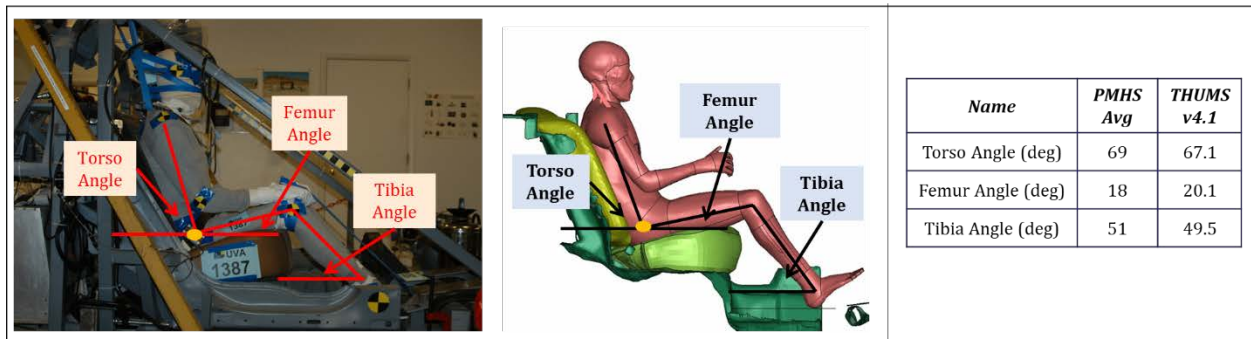


Figure 51 a) THUMS v4.1 position and posture in the Rear Seat sled b) Comparison with the PMHS position measurements

The seatbelt was then routed over the HBM torso and its final position over the ribcage along with comparison with PMHS position measurements is shown in Figure 52.

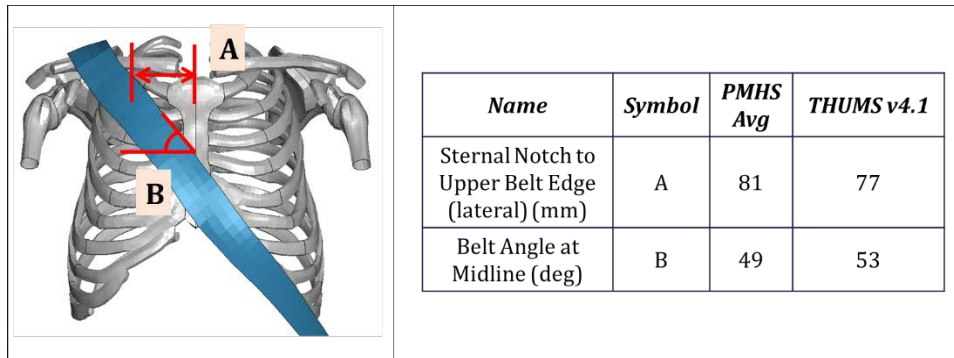


Figure 52 Belt position over torso for THUMS v4.1 in Rear seat sled Setup and comparison with PMHS position

Both the standard (Michaelson et al., 2008) and the pretensioned force-limited (FL+PT) (J. Forman et al., 2009) restraint systems included a rear deck mounted retractor. The standard belt was not pretensioned or force limited. The FL+PT was pretensioned at the retractor, and included a progressive, two-stage force-limiter designed to yield at an initial limit of 3 kN upto a defined belt payout, at which point the yield force limit increased to 4 kN. The pretensioner was fired at 12 ms after initiation of impact. This FL+PT retractor was modelled in the simulation environment using discrete retractor and pretensioner elements with defined retractor force v/s belt payout curve as given in the reference literature (J. Forman et al., 2009) as shown in Figure 53. The final model setup is shown in Figure 53.

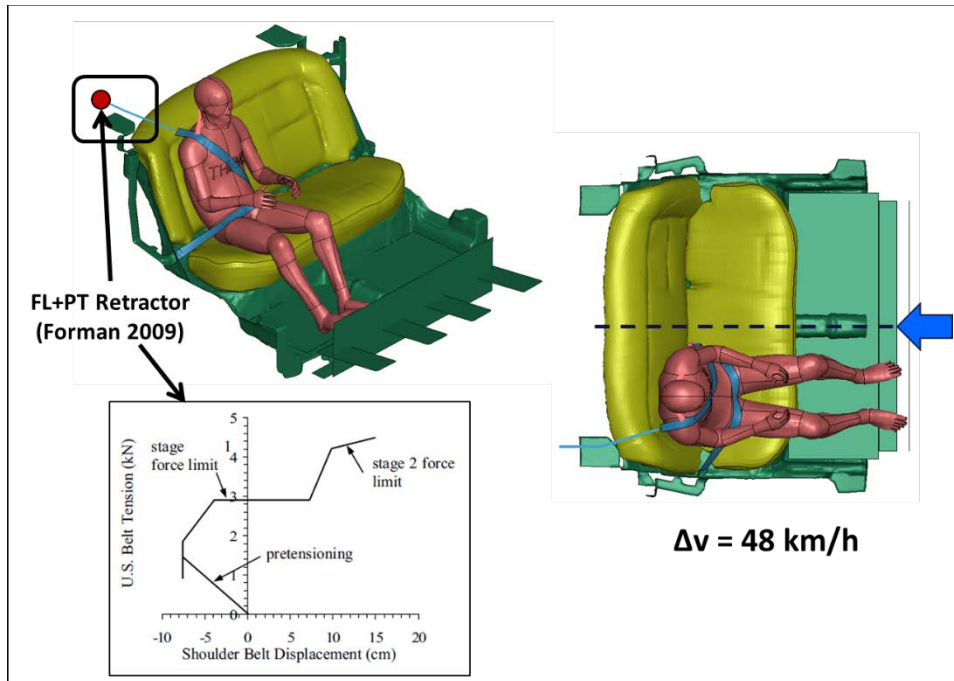


Figure 53 Rear seat sled setup with THUMS v4.1 and Force v Belt payout curve for FL+PT cases (Forman 2009)

- *Michaelson 2008*

For Michaelson 2008 (standard belt condition), the pretensioning and force-limiting characteristics of the retractor element were turned off in the simulation. It was observed that the THUMS v4.1 model undergoes submarining (defined as the slip of the lap belt over the anterior-superior iliac spines of the pelvis) in this case at 94 ms from the start of the initial impact pulse. Submarining was also in all of PMHS tested in this sled and restraint configuration (Michaelson et al., 2008). Upper shoulder belt forces from simulation were compared with the tests to ensure that the HBM is subjected to a loading that is comparable to the loading received by the PMHS in the tests and is shown in Figure 54.

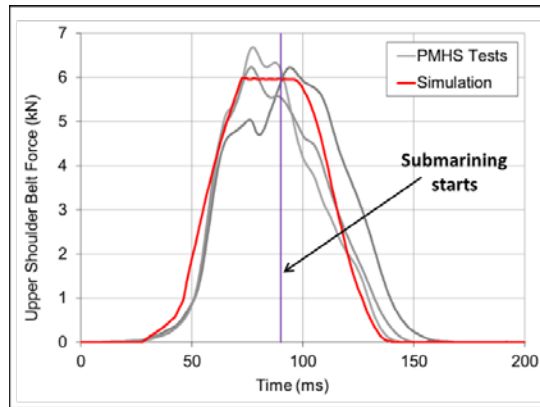


Figure 54 Upper shoulder belt force comparison for Michaelson 2008

As the upper shoulder belt forces were comparable between the simulations and the PMHS tests, this simulation setup was used for thoracic injury prediction despite the THUMS v4.1 model submarining. The results from this sled case simulation (up to the time of start of submarining) were used in the injury risk function development.

- *Forman 2009*

For Forman 2009 (FL+PT belt condition), the pretensioning and force-limiting characteristics of the retractor element were enabled. The pretensioner was fired at 12 ms after the time of the initiation of the impact pulse. The upper shoulder belt forces were consistent between the simulation and the experiment results as shown in Figure 55.

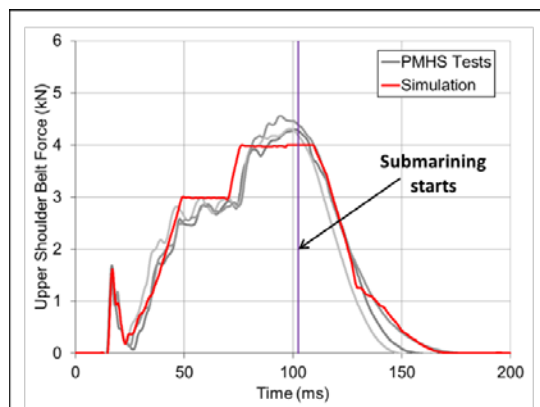


Figure 55 Upper shoulder belt force comparison for Forman 2009

It was observed that the THUMS v4.1 model submarined in this sled simulation case at 102 ms after the start of the impact pulse. Submarining was defined as the slip of the lap belt over the anterior-superior iliac spines (ASIS) of the pelvis. Submarining was observed in one out of the three PMHS tested in this sled and restraint configuration (J. Forman et al., 2009). As the upper shoulder belt forces were comparable between the simulations and the PMHS tests, this simulation setup was used for thoracic injury prediction despite the THUMS v4.1 model submarining. The results from this sled case simulation (up to the time of start of submarining) were used in the injury risk function development.

Low-Speed Frontal Sled Cases

Forman et al. performed a series of sled tests to investigate the thoracic deformation, kinematics and injury responses of belted PMHS in low-speed frontal crashes (J. Forman et al., 2006). Three male PMHS were tested in a sled environment simulating an occupant seated in the right front passenger seat of a mid-sized sedan. The PMHS were restrained using a 3-point standard i.e., not force-limited seatbelt and the sled was subjected to an impact crash pulse of 29 km/h delta-v. The PMHS ranged in age from 39-49 years old and in weight from 58.1-79.4 kg. Occupant kinematics of select anatomical locations, chest deflections and injury information in terms of ribcage fractures was available for each test. Experimental sled setup and impact crash pulse are shown in Figure 56.

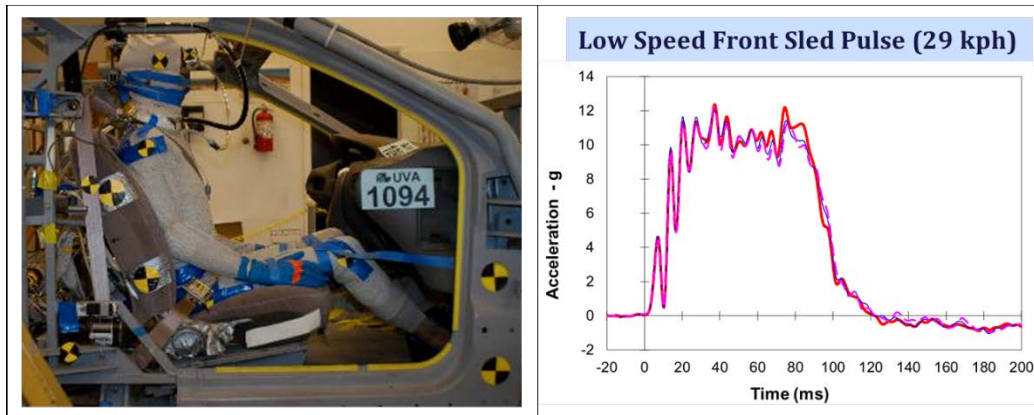


Figure 56 a) Experiment setup and b) Impact crash pulse for low-speed frontal sled tests

All the PMHS tests were performed with a buck derived from a mid-sized sedan. A sled of the passenger compartment derived from an FE model of a generic mid-sized sedan, available from NHTSA, was used to model these tests. Apart from the right front passenger seat, center console and dashboard, all the rest of the sled was rigidized and constrained to move only in the direction of impact. The deceleration pulse from the tests was applied to this sled. The full vehicle and derived sled model are shown in **Figure 57**.

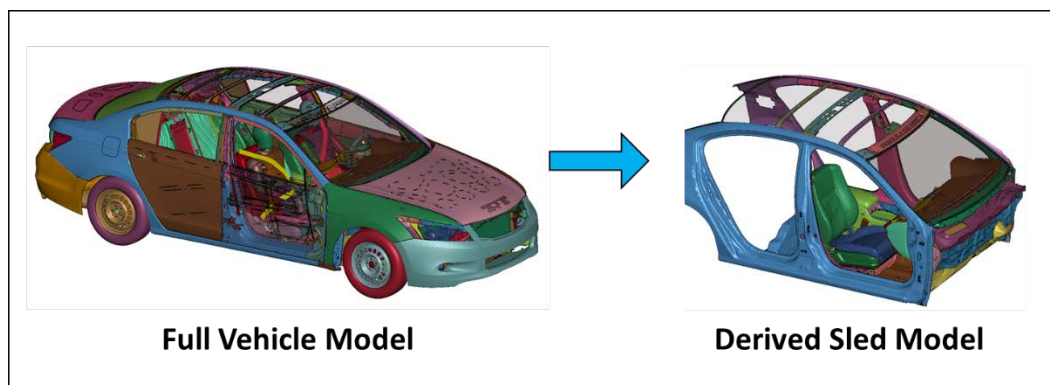


Figure 57 Sled model used for Low Speed Frontal Sled simulations.

The HBM was positioned on the right passenger seat and settled into the seat and cushion using a gravity pre-simulation. The final position and posture of the THUMS v4.1 model in the sled is shown in **Figure 58** along with comparison with PMHS position measurements.

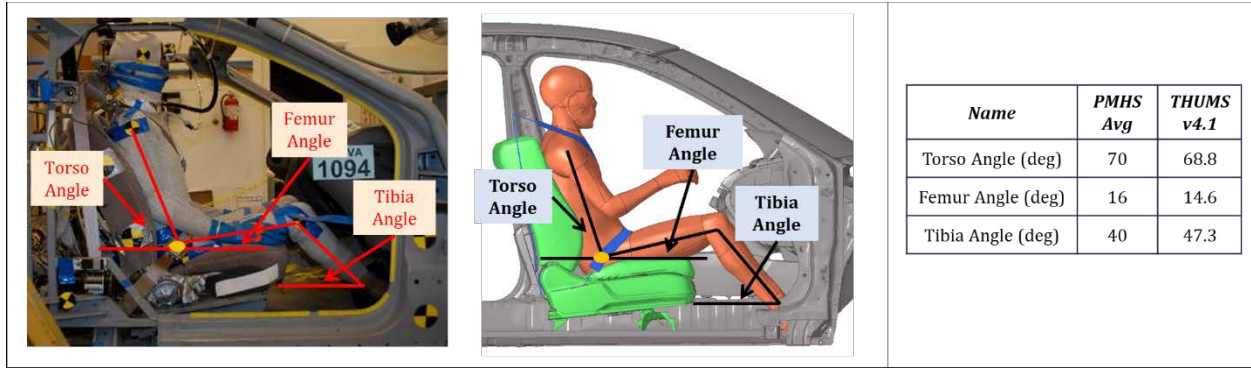


Figure 58 a) THUMS v4.1 position and posture in the Low Speed Frontal sled b) Comparison with the PMHS position measurements

The seatbelt was then routed over the HBM torso and its final position over the ribcage along with comparison with PMHS position measurements is shown in **Figure 59**.

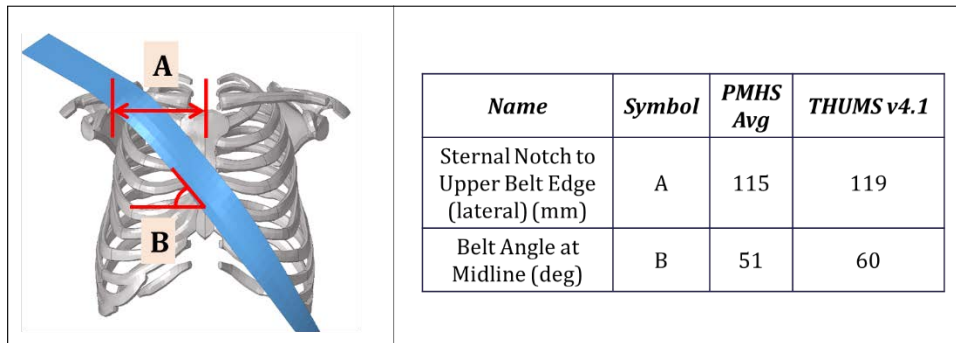


Figure 59 Belt position over torso for THUMS v4.1 in Low speed frontal sled Setup and comparison with PMHS position

Final model setup is shown in figure. Upper shoulder belt forces from simulation were compared with the tests to ensure that the HBM is subjected to a loading that is comparable to the loading received by the PMHS in the tests and is shown in **Figure 60**. The shoulder belt forces were found to be comparable between the tests and the simulation and the simulation setup was used for thoracic injury prediction with the THUMS v4.1 model.

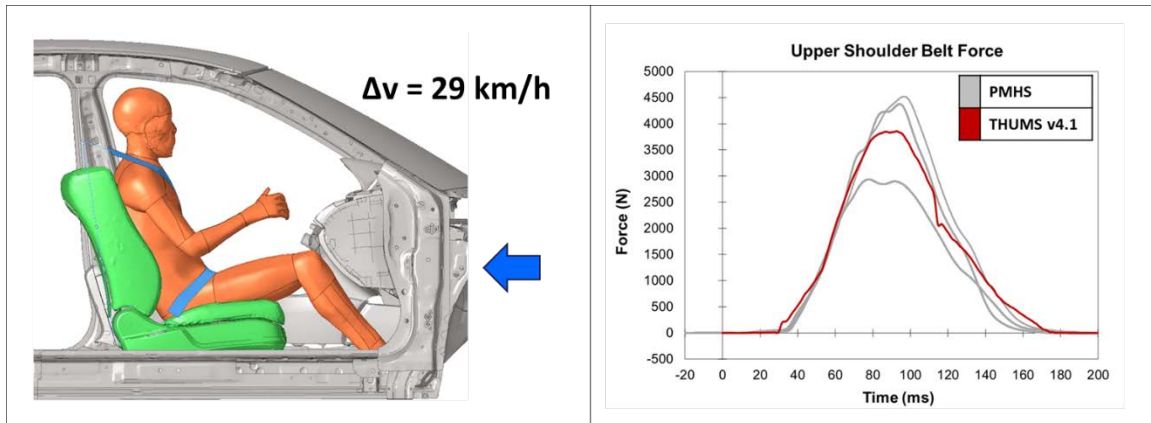


Figure 60 a) Final simulation setup for Low speed frontal sled case with THUMSv4.1 b) Upper shoulder belt forces comparison.

2.3 Summary

In this chapter, the selection and simulation of 19 load cases (consisting of 170 impactor and table-top tests, and 25 sled tests) used for the development of a frontal impact IRF for thoracic injury prediction for the THUMS v4.1 HBM is described. THUMS v4.1 was observed to exhibit reasonable biofidelity in all loadcases, giving confidence that it is likely to interact with a vehicle safety restraint system in a realistic manner. The THUMS V4.1 was observed to be slightly stiffer than PMHS-based corridors in the table-top cases. However, this difference was consistent, indicating that the THUMS chest is sensitive to changes in loading application in a manner that is consistent with PMHS. Test-specific simulations were also performed for the impactor and table-top load cases, modifying the input conditions to better match each of the individual PMHS tests. These test-specific simulations will serve as the basis for the thoracic IRF development described in the following chapter.

CHAPTER 3: TASK 2 – Injury Risk Functions Development

3.1 Strategy

As described in **Section 2.2.2**, 170 test specific simulations of impactor and table-top cases were performed for developing injury risk functions. For each of these simulations, the injury information in terms of rib fractures sustained in the corresponding PMHS test was available from the reference literatures. The Abbreviated Injury Scale defines any occurrence of three or more rib fractures (unilateral or bilateral) to be representative of AIS3+ rib cage injury (**AAAM, 2008**). This injury level has been used to develop thoracic injury risk functions for the THOR ATD (**Poplin et al., 2017**). Previous studies have also considered an occurrence of seven or more rib fractures in PMHS tests to be representative of AIS3+ rib cage injury (**Kent & Patrie, 2005; Laituri et al., 2005**). Hence, these two levels of injury were selected for developing thoracic injury risk functions in this study. For each of the 170 reference tests used in this study, the rib fracture information was converted into binary outcomes for the two levels (3+ and 7+ rib fractures) and is given in **Appendix A**.

The HBM was instrumented (as described in **Section 2.2.1**) to output a series of measurements which could be considered to form potential metric candidates for the development of injury risk functions. The instrumentation included strain-based and deflection-based outputs. The deflection-based outputs (**Figure 1 b**) gave information about the global compression or change in shape of the ribcage at different locations (like rib ends or mid-sternum). The strain outputs (**Figure 1 c**) gave information regarding the local strains developed in the ribs for each test. Given the availability of these two different types of injury metrics from HBMs, two types of

injury risk functions were developed – Deflection Based (described in **Section 3.2**) and Strain Based (described in **Section 3.3**). For each type, the 170 simulations of impactor and table-top cases were used to develop the IRF and the sled case simulations were used for the validation of the IRF. PMHS age from each test was also considered as a covariate while developing the IRFs.

3.2 Deflection Based IRF

3.2.1 Development of Injury Risk Curves

The instrumentation of HBM (as described in **Section 2.2.1**) enabled the calculation of deflection time histories of different rib anterior ends and points on sternum in different local vertebral coordinate systems. This facilitated the use of combined deflection metrics of multiple points on the rib cage as well as single point metrics for developing injury risk functions. In this study the following deflection metrics were considered as injury predictors:

1. Mid-sternum Deflection w.r.t T8 –

This metric was defined as the absolute maximum X deflection of the mid-sternum point (D in **Figure 61**) with respect to the T8 vertebral coordinate system.

2. DC –

The combined deflection DC proposed by (Song et al., 2011) and is calculated as

$$DC = D(t) + Cf.[(dD - Lc) + |(dD - Lc)|]$$

Where $D(t)$ is the time history of the X deflection of mid-sternum node w.r.t T8, $dD = LR(t) - LL(t)$ (time histories of X deflections of Rib 7 ends w.r.t T12), Cf is the contribution factor and Lc is the characteristic length. The values of Cf = 0.15 and

Lc=24 mm proposed by Song et al 2011 were used in this study. The points LR and LL are as shown in **Figure 61**.

3. Cmax –

Cmax was defined as the absolute maximum X deflection out of the four deflection measurement locations of UR, UL, LR and LL as shown in **Figure 61**. This metric was proposed for THOR M50 ATD by (Poplin et al., 2017).

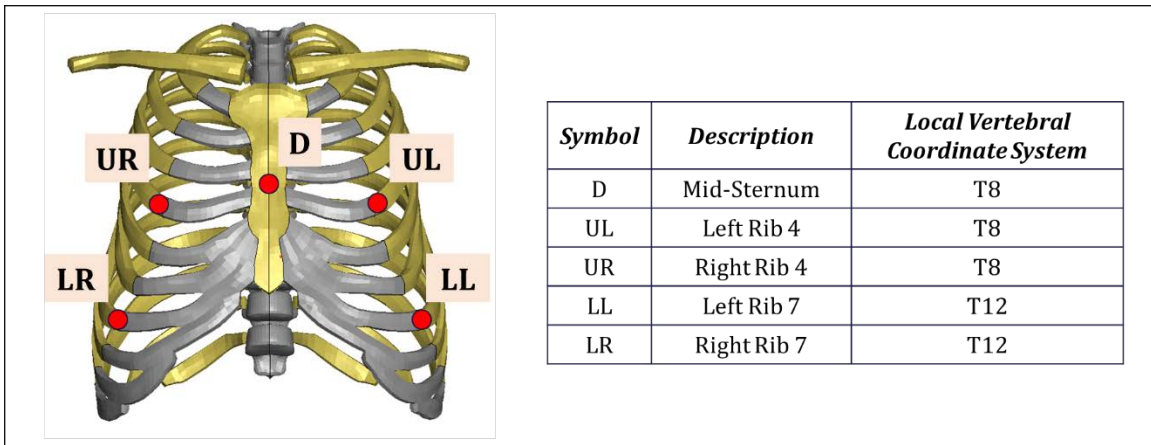


Figure 61 Measurement locations for deflection-based injury metrics

Alongwith the above metrics, age of the PMHS was also considered as a covariate when developing the injury risk functions.

The dataset of impactor and table-top cases used in this study contained some cases where multiple tests were performed on the same PMHS (eg. Salzar 2009 Single Belt, Forman 2005 Double Belt). Kent 2004 cases also had same cadavers tested under different loading conditions. Hence it was necessary to use an approach which captured this while developing the injury risk functions. In this study, Generalized Estimating Equations (GEE) models were used as they account for clustering of data and seek to model a population average based on a specified correlation structure. The tests (and the corresponding paired simulations) were grouped together

in clusters based on the PMHS used i.e. multiple tests performed on a specific PMHS formed a cluster irrespective of type of test. The ‘geepack’ package in R Statistical Software was used to analyze the data and form GEE models of the selected metrics with an ‘exchangeable’ correlation structure. The final form of the injury risk formula is similar to the logistic regression formula:

$$\text{Probability of Injury} = \frac{1}{1 + e^{-q}}$$

$$q = \alpha + \sum_i \beta_i X_i$$

Where, α is the intercept, X_i are the model predictors and β_i are the coefficients associated with each predictor. The QIC (Quasi-likelihood under the Independence model Criterion) statistic, which is analogous to AIC statistic, was used to compare GEE models for model selection. The lower the QIC value, the better the model. Models were developed for both the 3+ and 7+ rib fracture risk injury levels.

3.2.2 Results

The developed GEE models for all metrics alongwith the model coefficients and p-values are given in **Table 6** (for 3+ rib fracture injury level) and **Table 7** (for 7+ rib fracture injury level). The QIC values and Area under the Receiver Operating Characteristic curve (AUROC) values for each model are also given in the same tables.

Table 6 Deflection Model Coefficients for 3+ rib fracture risk injury levels

Model	Variable	Coefficient	p-value	QIC	AUROC
Mid-Sternum	Intercept	-7.6531	2.26E-6	168	0.87
	Mid-Sternum	0.1432	2.51E-11		
	Age	0.0467	0.0115		
DC	Intercept	-6.1679	0.00063	189	0.84
	DC	0.1193	1.4E-6		
	Age	0.0344	0.07947		
Cmax	Intercept	-1.8033	0.094	211	0.71
	Cmax	0.0741	3.7E-6		
	Age	-0.0153	0.339		

Table 7 Deflection Model Coefficients for 7+ rib fracture risk injury levels

Model	Variable	Coefficient	p-value	QIC	AUROC
Mid-Sternum	Intercept	-7.3842	8.7E-7	154	0.84
	Mid-Sternum	0.1206	2.6E-6		
	Age	0.0343	0.0083		
DC	Intercept	-6.2426	3.0E-6	164	0.8
	DC	0.1030	3.2E-6		
	Age	0.0262	0.044		
Cmax	Intercept	-3.7076	0.00077	184	0.76
	Cmax	0.0902	1.3E-6		
	Age	0.0051	0.7332		

Age of the PMHS was found to not be a significant covariate in the models for DC and Cmax for the 3+ rib fractures injury level and for the Cmax at the 7+ rib fractures injury level. The Mid-sternum deflection models had the lowest QIC and the highest AUROC for both the injury levels.

Age was also a significant covariate in the Mid-sternum deflection models. Thus, despite its simplicity, the Mid-sternum deflection metric model was found to be the best predictor of thoracic injury. The injury risk curves for this model at 3+ and 7+ rib fractures injury level are shown in **Figure 62** and **Figure 63** respectively.

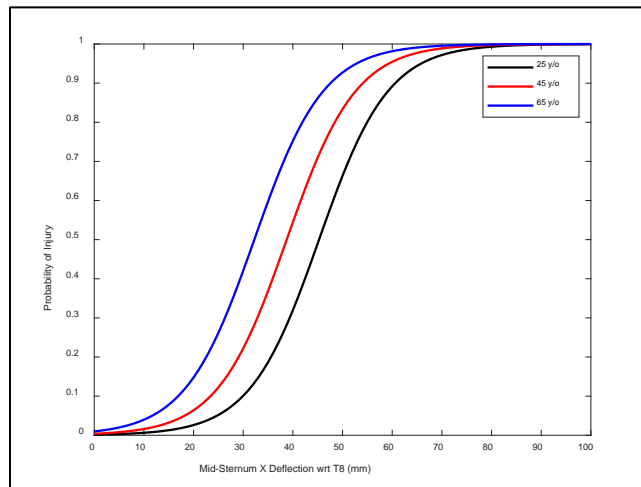


Figure 62 Mid-Sternum deflection metric injury risk curves for 3+ rib fractures injury level

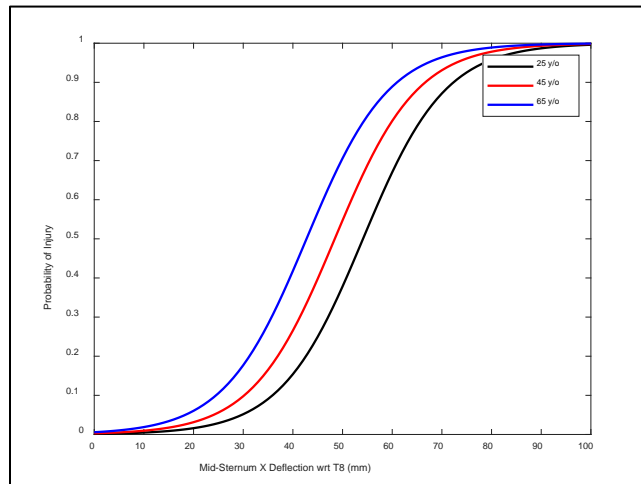


Figure 63 Mid-Sternum deflection metric injury risk curves for 7+ rib fractures injury level

3.2.3 Validation with Sled Cases

The sled loadcases described in **Section 2.2.3** were used to check the predictive ability of the injury risk functions developed from the impactor and table-top case simulations. The Mid-sternum models (developed in the previous section) were used to predict the risk of thoracic injury in the sled simulations. Injury risk was predicted for each individual sled test using the age of the corresponding PMHS used in the test, and the mid-sternum deflection from the simulation corresponding to the loadcase. The individual predicted risks of injury for each sled test are given in **Appendix C**.

To check the predictive ability of the injury risk models, a visualization technique known as Reliability Diagrams was used. These diagrams are a qualitative depiction of the Hosmer-Lemeshow test and are useful in visualizing the calibration of a prediction model and its tendency for under or overestimation of injury. **Figure 64** shows an exemplary Reliability Diagram with highlighted important regions. Following example shows how points on this diagram are calculated:

Example: Suppose a particular test series had 3 tests performed with 2 of them being injurious and 1 non-injurious. Then the Mean Observed value will be $2/3 = 0.667$, which will be the Y coordinate on the reliability diagram. For the 3 simulations corresponding to these tests, the predicted risk of injury hypothetically maybe 0.4, 0.8 and 0.3 respectively. Then the Mean Predicted value will be $AVERAGE(0.4, 0.8, 0.3) = 0.5$, which will be the X coordinate on the reliability diagram. Thus, this example test series corresponds to the point (0.5, 0.667) on the Reliability Diagram (marked as “Example Loadcase” in **Figure 64**).

A perfect prediction point will lie on the diagonal line from (0,0) to (1,1), the upper triangular region above this diagonal is the region of under prediction and the lower triangular region is region of over prediction.

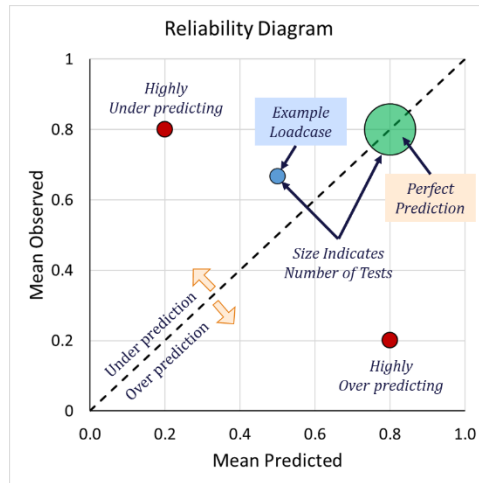


Figure 64 Example Reliability Diagram

Such reliability diagrams were plotted for all the loadcases (impactor, table-top and sled) for both injury levels of 3+ and 7+ rib fractures using the mid-sternum deflection models and are shown in **Figure 65**.

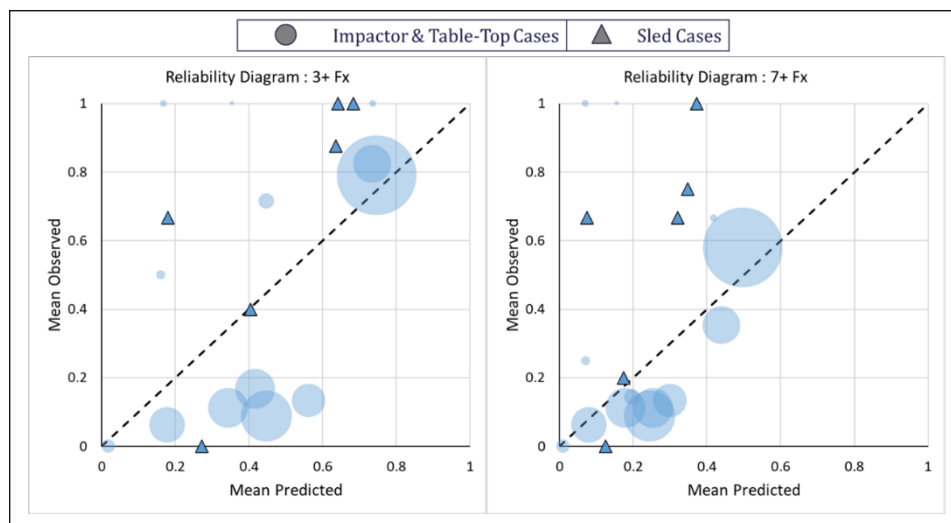


Figure 65 Reliability diagrams for Mid-Sternum deflection models. (diameter of the circle indicates the sample size present in that particular loadcase)

The impactor and table-top loadcases fell approximately at the diagonal without any inherent bias for under or over prediction. This is expected as the injury risk models were developed using this data. The prediction for sled loadcases also appeared to be unbiased for the 3+ injury risk levels. However, for the 7+ injury risk level, the model was observed to be biased towards underprediction. Further, AUROC values were also calculated for all the sled tests combined, which were 0.81 and 0.78 for 3+ and 7+ rib fracture levels respectively.

3.2.4 Conclusion

Despite its simplicity, the absolute maximum mid-sternum X deflection with respect to T8 vertebral coordinate system was found to be the best deflection-based injury metric for THUMS v4.1 HBM in this study (IRF model coefficients shown in the table below). Age was also a significant covariate and was included in the injury risk function. The 3+ rib fracture injury risk curve developed from the set of impactor and table-top simulations, gave reasonable predictions of thoracic injury when applied to the sled loadcases (though the 7+ rib fracture IRF tended towards underprediction).

Model	Variable	Coefficient
3+ Rib Fractures	Intercept	-7.6531
	Mid-Sternum Deflection	0.1432
	Age	0.0467
7+ Rib Fractures	Intercept	-7.3842
	Mid-Sternum Deflection	0.1206
	Age	0.0343

Note that these particular results apply to this particular human body model. There is no guarantee that mid-sternum chest deflection would be an adequate predictor for other HBMs, with different construction, anatomy, stiffness, and interaction between the thoracic components. This, coupled with the 7+ underprediction observed here, suggests that it is still wise to explore other types of measures (e.g., strain-based measures) to improve the likelihood of identifying measures that may provide robust prediction across different models and loading conditions. In the sections below strain-based injury prediction method is developed which is tuned for the THUMS V4.1, to complement and compare against the deflection-based IRF developed above.

3.3 Strain Based IRF

3.3.1 Probabilistic Rib Fracture Risk Prediction Framework

Forman et al. 2012 developed a probabilistic framework for translating injury risk for an individual rib calculated from a fracture risk function (e.g. developed using survival analysis) to a risk of sustaining a certain number of rib fractures in HBM simulations (J. L. Forman et al., 2012). The framework included an age adjusted rib cortical bone strain based injury risk function developed from dynamic test data from twelve human subjects (Kemper et al., 2005, 2007) and was presented as an empirical cumulative distribution function. In a recent study, Larsson et al. 2021 developed age-dependent rib strain-based fracture risk function from data from material coupon testing performed on rib cortical bone samples from 61 PMHSs (Katzenberger et al., 2020; Larsson et al., 2021). This study also updated the probabilistic framework from Forman 2012 with the newly developed fracture risk functions.

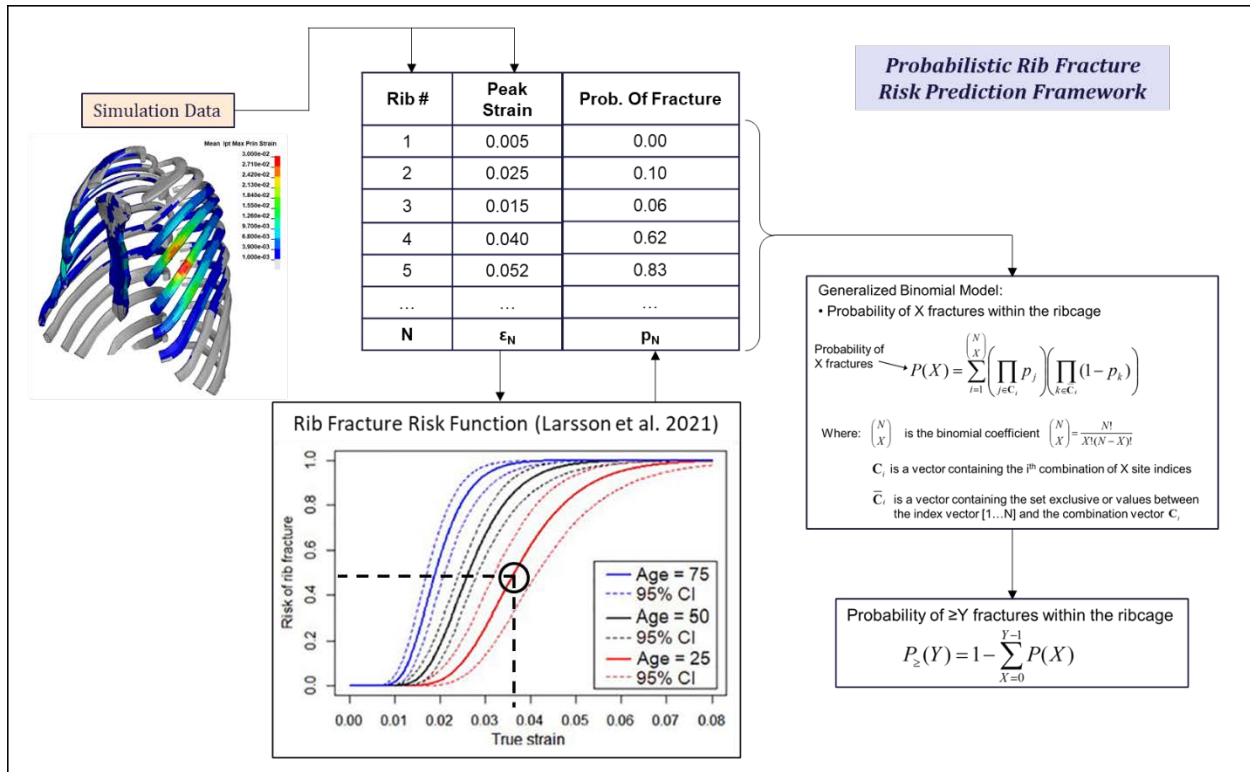


Figure 66 Flowchart outlining the probabilistic rib fracture risk prediction framework from Forman 2012 with fracture risk function from Larsson 2021.

Figure 66 shows a flowchart outlining the probabilistic framework method. First step of the process is to extract and sort the strain data output from simulations. In the current study, the rib strains for THUMS v4.1 for each of the 170 simulations of impactor and table-top cases were extracted and sorted using the following method:

1. From the instrumentation described in **Section 2.2.1**, Maximum Principal Strain output for each element of each of the 24 ribs for the entire time history of the simulation was collected.
2. For each rib, the strain data was further processed to find the 95th percentile peak MPS across all elements of the rib and across the entire time history of the simulation. This strain value was called MPS95 for the particular rib.
3. Step 2 resulted in a vector of 24 MPS95 values, corresponding to the 24 ribs.

The next step in the framework is to pass each of these 24 strain values to the fracture risk function (from Larsson et al. 2021), to predict the probability of each rib fracturing. This results in a vector of 24 probabilities of fracture (corresponding to each rib). This vector is then further processed using a Generalized Binomial model to calculate the risk of sustaining multiple rib fractures, given the probabilities of individual ribs fracturing (J. L. Forman et al., 2012). In the current study, this process was used to calculate the risk of 3+ and 7+ rib fractures for THUMS v4.1 in each of the simulations.

3.3.2 Optimization of Rib Fracture Risk Curve for HBM

The underlying rib fracture risk function from Larsson et al. 2021, which is used in the probabilistic framework, was developed using data obtained from performing tests on human rib cortical bone specimens. Application of this function directly to HBMs may not yield good results due to factors such as material properties of the FE ribs, the anatomical geometry, FE connections between different parts of the ribcage as well as the FE mesh size and density used in the HBM. Hence, it was necessary to calibrate the rib fracture risk function for the HBM (THUMS v4.1 in the current case) such that it gives good results in predicting multiple rib fractures using the probabilistic framework.

Larsson et al. 2021 have developed rib fracture risk functions using survival analysis with three probability distributions – lognormal, log-logistic and Weibull. The final recommended risk function in that study was with the lognormal distribution (Larsson et al., 2021). However, all the three types of equations were considered as potential fracture risk functions for calibrating to the THUMS v4.1 model. The three parametric equations are given in **Figure 67**.

$$\begin{aligned} \text{Weibull risk (strain, AGE)} &= 1 - \exp\left(-\left(\frac{\text{strain}}{\exp(\beta_0 + \beta_1 \cdot \text{AGE})}\right)^\alpha\right) \\ \text{Log - normal risk (strain, AGE)} &= \frac{1}{2} + \frac{1}{2} \operatorname{erf}\left[\frac{\ln(\text{strain}) - (\beta_0 + \beta_1 \cdot \text{AGE})}{\sqrt{2} \cdot \alpha}\right] \\ \text{Log - logistic risk (strain, AGE)} &= 1 - \frac{1}{1 + \left(\frac{\text{strain}}{\exp(\beta_0 + \beta_1 \cdot \text{AGE})}\right)^\alpha} \end{aligned}$$

Figure 67 Equations for fracture risk functions used in Larsson et al 2021.

The data from 170 test-specific simulations of impactor and table-top cases was used to calibrate each of the potential fracture risk functions separately. While calibrating, the “ α ” parameter in the equation was kept constant (to the value given by Larsson et al 2021) to preserve the curve shape. The parameters “ β_0 ” and “ β_1 ” in the equations were varied for calibration. For each iteration of a set of “ β_0 ” and “ β_1 ” values, the following steps were implemented:

1. For each of the 170 impactor and table-top simulations, the rib MPS95 vector (described in **Section 3.3.1, step 3**) and Age of the corresponding test PMHS, was used to calculate the risk of sustaining 3+ and 7+ rib fractures using the probabilistic framework (described in **Section 3.3.1**).
2. With the calculated probability of injury from Step 1, the Negative Log-Likelihood was calculated for each simulation using the below equation:

$$\text{Negative LogLikelihood(NLL)} = -((Y \times \log P) + ((1 - Y) \times \log (1 - P)))$$

Where, Y is the binary value for injury, 1=injury and 0=non-injury, P is the calculated probability of injury from Step 1.

The NLL values were separately calculated for 3+ and 7+ rib fractures injury level for each simulation.

3. The NLL values of individual simulations were then summed over the entire dataset of 170 simulations. This was called the Sum Negative Log-Likelihood or SNLL. The SNLL values were separately calculated for the 3+ and 7+ rib fractures injury level and were named SNLL_3 and SNLL_7 respectively.
4. The SNLL_3 and SNLL_7 values were added together to form the combined sum SNLL_Comb.

The aim of the calibration was to find a set of “ β_0 ” and “ β_1 ” parameters which minimized the SNLL values which is analogous to the Maximum Likelihood Estimation method. Two optimizations were performed –

- a) **Combined Optimization** = minimizing the SNLL_Comb value, resulting in one calibrated equation which is applicable to both 3+ and 7+ rib fractures injury levels.
- b) **Independent Optimization** = minimizing SNLL_3 and SNLL_7 separately, resulting in two calibrated equations, separately applicable to 3+ and 7+ rib fractures injury level.

All optimizations were performed using the Surrogate Optimization routine from the Global Optimization Toolbox in MATLAB R2021a.

The whole optimization process resulted in a set of rib fracture risk functions (set of optimized β_0 and β_1 values) calibrated to be used with the THUMS v4.1 model in the probabilistic rib fracture risk prediction framework.

3.3.3 Results

The optimization procedure outlined in the previous section was applied to all the three probability distribution equations – log-normal, log-logistic and Weibull. The optimized

parameters and SNLL values for Combined Optimization and Independent Optimization for 3+ and 7+ rib fractures injury levels are given in **Table 8**, **Table 9** and **Table 10** respectively.

Table 8 Parameters calibrated for THUMS v4.1 using Combined Optimization

	β_0 (optimized)	β_1 (optimized)	α (from Larsson 2021)	SNLL_Comb
Log-normal	-3.6358	-0.0147	0.3026	349.9
Log-logistic	-3.724	-0.0134	5.6986	311.9
Weibull	-3.3696	-0.016	3.3562	305.9

Table 9 Parameters calibrated for THUMS v4.1 using Independent Optimization for 3+ rib fractures injury level

	β_0 (optimized)	β_1 (optimized)	α (from Larsson 2021)	SNLL_3
Log-normal	-3.6063	-0.0123	0.3026	122.5
Log-logistic	-3.9138	-0.0078	5.6986	118.9
Weibull	-3.0665	-0.0179	3.3562	115.5

Table 10 Parameters calibrated for THUMS v4.1 using Independent Optimization for 7+ rib fractures injury level

	β_0 (optimized)	β_1 (optimized)	α (from Larsson 2021)	SNLL_7
Log-normal	-3.8084	-0.0158	0.3026	151.6
Log-logistic	-4.3031	-0.0069	5.6986	151.1
Weibull	-3.72	-0.0135	3.3562	140.6

The Weibull Distribution equation had the lowest SNLL values in all the cases, for combined optimization (one equation for both injury levels) as well as independent optimizations (separate functions for 3+ and 7+ rib fractures injury levels). Hence, this equation with the optimized parameters was selected to be used with the THUMS v4.1 model in the probabilistic rib fracture prediction framework. **Figure 68** shows the comparison of original fracture risk curves from Larsson et al. 2021 and the calibrated curves for THUMS v4.1 for the age of 45 years old. The need to calibrate the original functions for application to an HBM is highlighted by the differences between the calibrated curves for THUMS v4.1 and the original curves. Direct application of fracture risk functions from Larsson et al. 2021 would have resulted in an underestimation of injury risk in the simulations with THUMS v4.1 model.

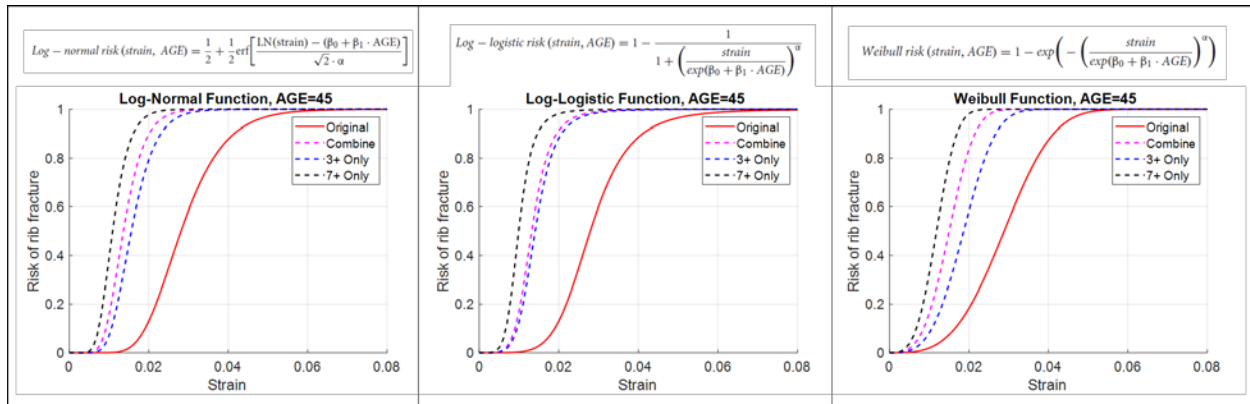


Figure 68 Comparison of original fracture risk curves from Larsson et al. 2021 (red) and calibrated fracture risk curves (dotted black, pink, blue) for THUMS v4.1 model for age of 45 years old

3.3.4 Validation with Sled Cases

Similar to the Deflection IRF, the sled cases were used to check the predictive ability of the rib fracture risk function optimized in the previous section. Injury risk was predicted for each

individual sled test using the age of the corresponding PMHS used in the test, and the vector of 24 MPS95 rib strain values (as described in **Section 3.3.1, step 3**) from the simulation corresponding to the loadcase. The individual predicted risks of injury for each sled test are given in **Appendix E**. Reliability diagrams (described in **Section 3.2.3**) were used to visualize the performance of the Weibull equations obtained from combined optimization as well as independent optimization for the 3+ and 7+ rib fractures injury levels. **Figure 69** and **Figure 70** show the reliability diagrams with the results from combined and independently optimized Weibull fracture risk functions respectively. **Figure 71** shows the results of both combined and independent optimizations overlaid on the same reliability diagram. The data points from the independently optimized fracture risk functions are clustered closer to the diagonal as compared to the data points from combined optimized risk function in **Figure 71**. This shows that the independently optimized functions perform better at predicting the respective injury level (3+ or 7+ rib fractures) than the combined optimized function. Further, AUROC was calculated for the impactor and table-top cases, the sled cases and all together, and are given in **Table 11**. The SNLL_Comb (305.9) is higher than the sum of SNLL_3 and SNLL_7 ($115.5+140.6 = 256.1$), suggesting that the independently optimized equations provide a better likelihood estimation. Considering all these factors, the independently optimized Weibull equations were finalized for the THUMS v4.1 model.

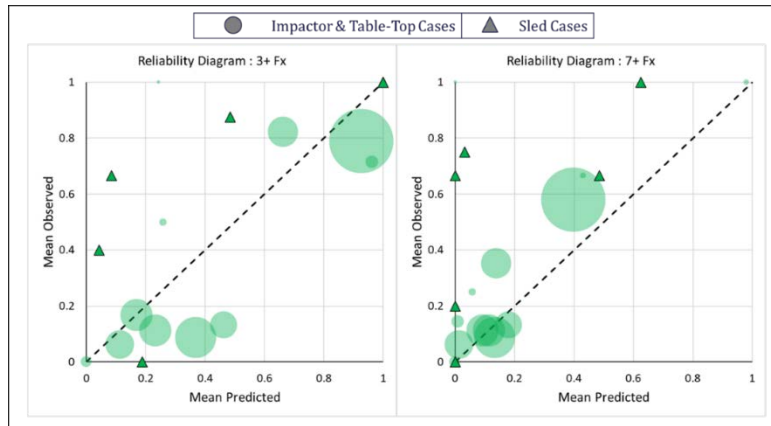


Figure 69 Reliability diagrams for 3+ and 7+ rib fractures injury levels with Combined Optimized Weibull fracture risk function for strain based probabilistic framework

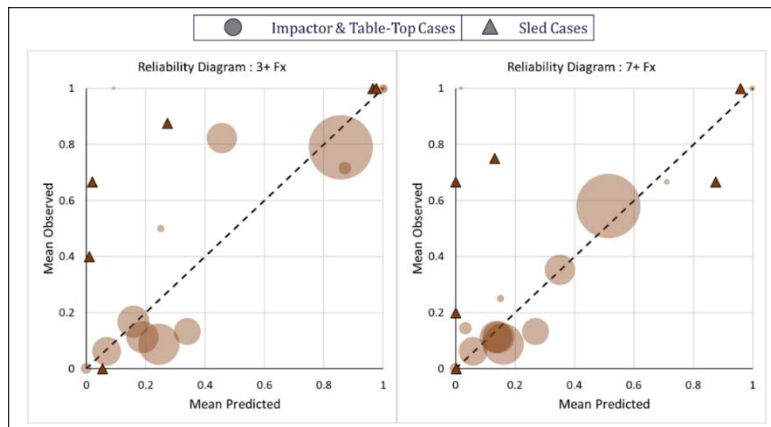


Figure 70 Reliability diagrams for 3+ and 7+ rib fractures injury levels with Independently Optimized Weibull fracture risk functions for strain based probabilistic framework

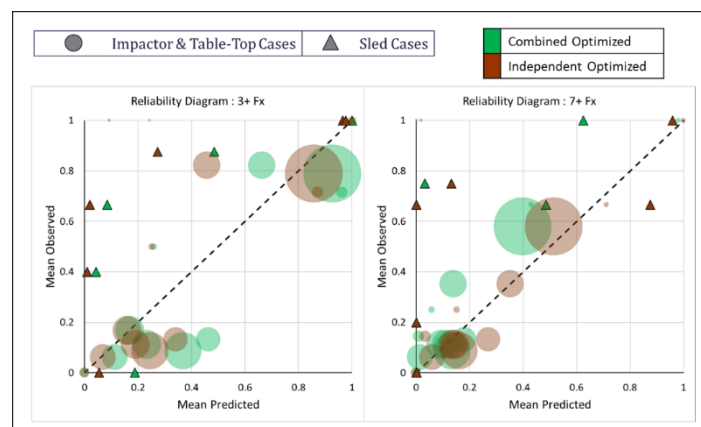


Figure 71 Comparison of Reliability diagrams with combined optimized and independently optimized Weibull fracture risk functions for strain based probabilistic framework

Table 11 AUROC values for combined and independently optimized weibull fracture risk functions for strain based probabilistic framework

<i>AUROC – Impactor and Table-Top Cases</i>		
	3+ Rib fractures injury level	7+ Rib fractures injury level
Combined Optimized IRF	0.912	0.895
Independently Optimized IRFs	0.915	0.897
<i>AUROC – Sled Cases</i>		
	3+ Rib fractures injury level	7+ Rib fractures injury level
Combined Optimized IRF	0.831	0.750
Independently Optimized IRFs	0.818	0.763
<i>AUROC – All Cases</i>		
	3+ Rib fractures injury level	7+ Rib fractures injury level
Combined Optimized IRF	0.892	0.862
Independently Optimized IRFs	0.894	0.866

3.3.5 Conclusion

The underlying fracture risk function for the strain-based probabilistic rib fracture risk prediction framework was calibrated for the THUMS v4.1 model using the optimization process described in **Section 3.3.2**. Three types of probability distribution functions from Larsson et al. 2021, namely lognormal, loglogistic and Weibull, were used in the optimization. Risk functions were optimized in two ways – a) Combined optimization: one risk function for both 3+ and 7+ rib

fractures injury level and b) Independent optimization: two separate risk functions for the 3+ and 7+ rib fractures injury level. From the likelihood estimation (SNLL values), AUROC values for the simulations and validation with sled cases (reliability diagrams), described in **Sections 3.3.3 and 3.3.4**, it was found that the independently optimized fracture risk functions with the Weibull equations were the best predictors of thoracic injury using the strain-based probabilistic rib fracture prediction framework with the THUMS v4.1 model. The finalized coefficients of the Weibull equation for THUMS v4.1 are given in **Table 12**.

Table 12 Finalized parameters for the Weibull fracture risk functions to be used in the strain-based probabilistic rib fracture prediction framework with the THUMS v4.1 model

	β_0	β_1	α
3+ Rib fractures injury level	-3.0665	-0.0179	3.3562
7+ Rib fractures injury level	-3.72	-0.0135	3.3562

$$Weibull\ risk\ (strain, AGE) = 1 - \exp\left(-\left(\frac{strain}{\exp(\beta_0 + \beta_1 \cdot AGE)}\right)^\alpha\right)$$

3.4 Summary

The results from this chapter suggest that the mid-sternum deflection and more complex strain-based methods offer comparable potential as injury risk predictors when applied to the THUMS v4.1 model in the specific frontal impact loadcases described above. Both methods exhibit age-dependency, which is to be expected. Both methods also exhibit similar AUROC's (indicating correlation between the metric and the outcome) and similar predictive ability within this dataset. However, as noted before, this does not necessarily mean that both methods would be similarly predictive for other HBMs, or in other load cases. In the following chapter (Chapter 4),

the robustness of these potential methods is compared by applying to a different human body model. Finally, Chapter 5 also compares the predictions derived from these two methods in a loading environment of increased complexity more representative of an in-vehicle application scenario, with loading applied by both a seatbelt and an airbag.

CHAPTER 4: Task 3 – Application to Alternate Human Body

Model

One of the main objectives of this study was that the methodology and guidelines developed for generating thoracic IRFs should include a reasonable amount of detail such that they could be applied to any other human body model. The processes described in the previous chapters were then applied to the GHBMC v6.0 model to demonstrate that the framework may be applied to other HBMs, and to compare the robustness of mid-sternum deflection vs. strain-based measures when applied to a different HBM. Chapters 2 and 3 above were used as instructions to set up simulations with the GHBMC v6.0 model in a manner comparable to the THUMS v4.1.

The model was set up to perform the 170 test-specific simulations described in Chapter 2 as well as the 13 different biofidelity simulations. The test-specific simulations were then processed to evaluate the rib fracture prediction ability of sternal deflection and rib strain measured on the GHBMC v6.0. Where a statistically significant relationship was observed, these data were then used to develop GHBMC-specific IRFs using the methodology described in Chapter 3. The goal of this task was two-fold: 1) to refine the instructions above by applying to a second model (and adding more specificity where needed); and 2) to demonstrate that this framework may be applied to generate model-specific IRFs in a comparable manner across different HBMs. This exercise was successful in identifying specific points of refinement for the instructions above like descriptions of the simulation setups, data outputs, and methods for analysis, with a goal of enabling application to other HBMs in the future.

4.1 Deflection Based IRF

After evaluating the results, the deflection-based IRF derived for the GHBMC (**Figure 72**) exhibited some characteristics that called into question its suitability as a predictor with this model. One of the odd results of the deflection-based IRF was that chest deflection was not a significant predictor of 3+ rib fractures and age was a not significant predictor of any level of injury in the model. Moreover, the shape of the function did not follow the expected IRF form, and instead had a “flat” shape with a noticeable risk at zero deflection, and less than 100% risk at very high deflection. Therefore, a deflection-based IRF is not recommended for use with the GHBMC at this time. It is important to mention that this is not necessarily indicative of any limitation in the GHBMC model itself. It may be reflective of the challenges of generalizing injury prediction with chest deflection measurement. The internal deflection of a model’s ribcage is likely to depend on the specific geometry and construction of that model. In the THUMS, single-point measurement of mid-sternal deflection happened to be a good predictor of injury. In other models, with different geometries and constructions, other types of deflection measurement (e.g., multi-point deflection) may predict injury better than mid-sternal deflection. Instead of seeking to develop the best deflection-based metric for each model, it is likely more efficient to focus on other measures that can be shown to provide more reliable prediction across models (for example, the strain-based metrics described below).

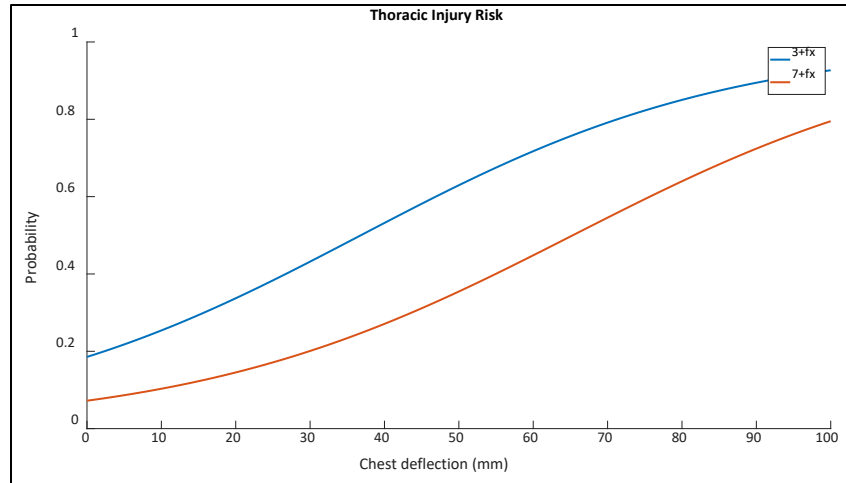


Figure 72 Mid-sternum deflection based thoracic IRF for the GHBMC v6.0 model

4.2 Strain Based IRF

As with the THUMS analysis in Chapter 3, the local rib-strain IRF was also calibrated for use with the GHBMC model, based on the strains observed in its ribs. The strain-based individual rib fracture probability function from (Larsson et al., 2021) was calibrated to maximize prediction likelihood using a Weibull distribution and the combined optimization methodology described in section 3.3. The parameters for the optimized fracture risk curve for the GHBMC model are given in **Table 13**. For the GHBMC, the calibrated fracture probability functions turned out to be closer to the original Larsson 2021 curves (**Figure 73**). In other words, the optimal strain-based IRF for the GHBMC turned out to be closer to the original rib ultimate strain distributions that were derived from local rib bone material property tests, as described by Larsson (2021). In contrast, the tuned strain-based IRF for THUMS resulted in a curve substantially to the left of the original Larsson (2021) curve, meaning that THUMS needs less strain than GHBMC to arrive at a comparable level of injury risk prediction. In other words, THUMS tends to systematically experience less rib strain than GHBMC, and a different local IRF is needed to arrive at comparable injury prediction

between the two models. This difference may be due to difference in model construction (such as mesh density), the mechanics of deformation of the ribcage, or other unforeseen factors. Regardless of the cause, these results highlight the utility of this framework, providing guidelines to tune local IRF for application to specific HBMs to arrive at comparable injury prediction.

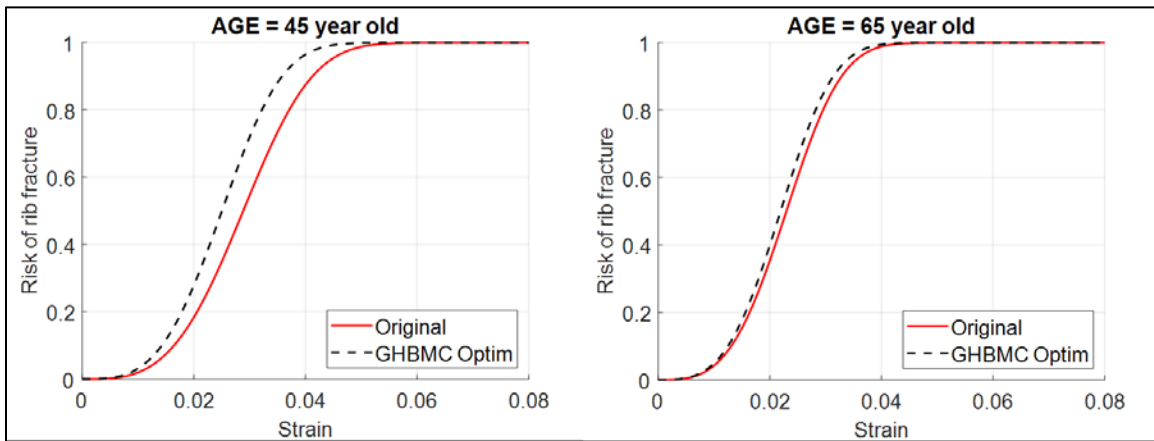


Figure 73 Tuned rib strain IRF for the GHBMC v6.0 model (red) and original strain IRF from Larsson et al 2021 (black dashed)

Table 13 Strain IRF parameters (Weibull distribution) tuned for the GHBMC v6.0

	β_0	β_1	α
Combined optimization for 3+ and 7+ fractures	-3.27987	-0.00663	3.3562

4.3 Summary

In this chapter, the framework for generating thoracic IRFs for HBMS developed using the THUMS v4.1 model was applied to a different model, namely the GHBMC v6.0. This exercise helped in identifying refinements and improving the description of the simulation setups, data outputs and methods for analysis in the framework. For the THUMS v4.1 model, both the strain-

based and the mid-sternum deflection based IRF method resulted in comparable predictive ability. In contrast, mid-sternum deflection was not found to be a suitable predictor with the GHBM. The strain-based method, however, did provide suitable prediction with the GHBM, with a local failure curve closer to the cortical bone ultimate strain data described in the literature. The following chapter compares the injury predictions from the two HBMs, with IRFs derived using the current framework, in a loading environment of increased complexity more representative of an in-vehicle application scenario, with loading applied by both a seatbelt and an airbag.

CHAPTER 5: Task 4 – In-Vehicle Simulation

In this task, the thoracic injury risk functions developed in previous chapters were exercised by applying to simulations with the THUMS v4.1 and GHBMC v6.0 in exemplar simulations in a realistic vehicle environment.

5.1 Simulation Setup

5.1.1 Vehicle Environment and Loadcase

After the development of the thoracic injury risk functions, it was desired to demonstrate the application of these IRFs (to the two HBMs) in a crash simulation with a vehicle environment. For this purpose, a mid-size sedan (2014 Honda Accord) vehicle model available from NHTSA was used as the vehicle environment (Singh et al., 2018). This vehicle model includes advanced restraint systems of curtain airbag, driver airbag and pretensioner force-limited seatbelt. The NCAP 56 kph frontal impact loadcase was selected for simulation. The vehicle simulation setup is shown in Figure 74. These full vehicle simulations were performed first with the THOR M50 dummy in the driver position, to reduce the computational time. The full vehicle kinematics were derived from selected reference nodes in terms of nodal accelerations to capture the entire 3D motion (translation + rotational) of the vehicle in these simulations.

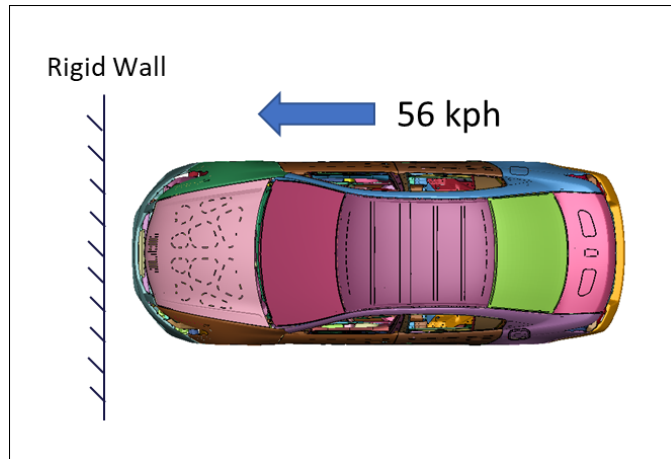


Figure 74 Loadcase selected for in-vehicle simulations

A sled model was developed by reducing the vehicle model to only the passenger cabin. The body-in-white (BIW) and vehicle exteriors like door panels etc. were converted to rigid material. All the interiors of the vehicle were retained in the sled model and were kept of deformable material. The sled model with rigid and deformable parts is shown in Figure 75.

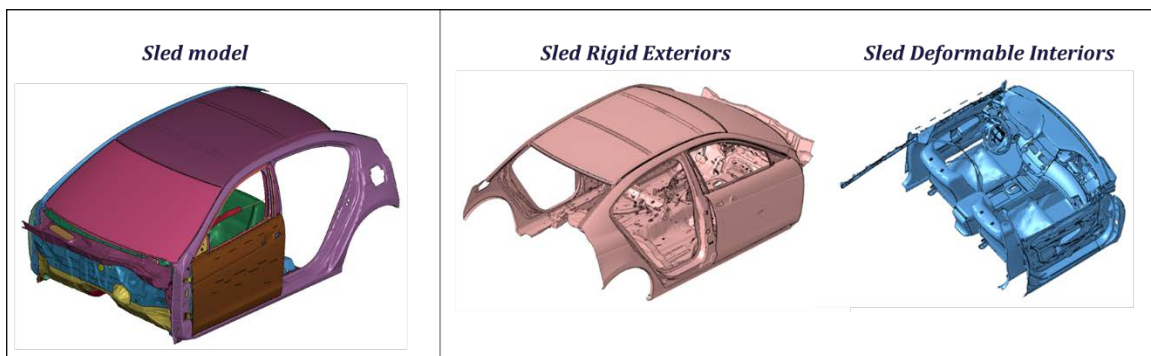


Figure 75 Reduced sled model with rigid exteriors and deformable interiors

The kinematics (nodal accelerations) derived from the full vehicle simulations were input as prescribed motion to the same reference points in the sled model to achieve the same vehicle kinematics (Figure 76). The sled model (with the full vehicle kinematics) was used for simulations with the human body models to reduce the complexity and computational time of the simulations.

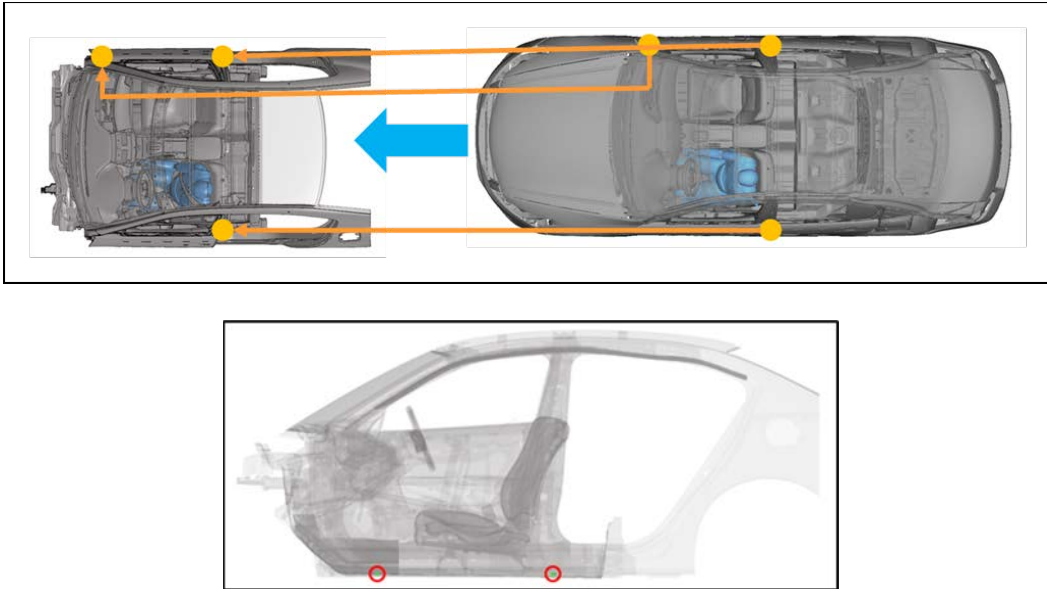


Figure 76 Transfer of kinematics from full vehicle simulation to sled model: Top view (top), side view (bottom)

5.1.2 HBM Position and Posture in Vehicle

Both the HBMs, THUMS v4.1 and GHBMC v6.0 were positioned and seated in the sled model using the THOR M50 position/posture in the full vehicle as reference (Singh et al., 2018). The positioning was carried out in three different steps. First, HBMs were positioned to match the location of the THOR H- point, based on how the THOR model is positioned in NHTSA’s publicly released 2014 Honda Accord simulation suite (with integrated THOR model; <https://www.nhtsa.gov/crash-simulation-vehicle-models>). Next, the legs were positioned to remove any penetration from the feet and the carpet. Finally, the outer skin of the model from step 2 was converted into rigid, and the body was moved to the final position through prescribed motion to deform the seat cushion to conform to the model. The seatbelt was then routed separately for each model to fit the torso and lap. The positioned HBMs are as shown in Figure 77. Both the HBMs were instrumented to output the predictors of thoracic injury as described in the previous chapters.

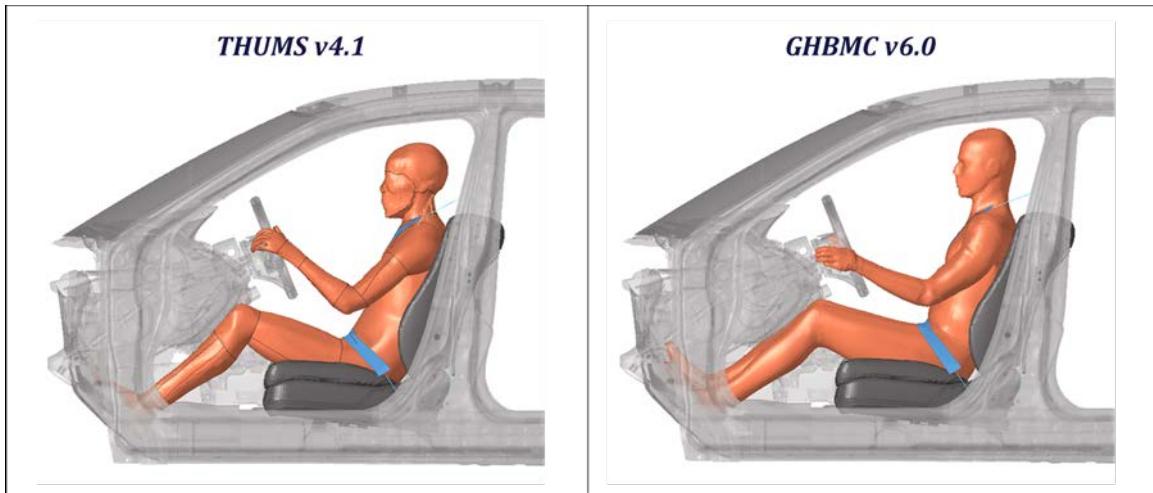


Figure 77 HBMs positioned and seated in the sled model

5.2 Results

Simulations with both the human body models ran to completion with normal termination (total runtime of 140ms). The risk of sustaining 3+ and 7+ rib fractures was calculated using the IRFs developed in chapters 3 (for the THUMS v4.1) and 4 (for the GHBMC v6.0). As the thoracic IRFs were age-dependent, risk of injury was calculated for three age groups, namely, 25, 45 and 65 years old. Injury risks calculated for the THUMS v4.1 model with the Deflection IRF and Strain IRF are given in Table 14 and Table 15 respectively.

Table 14 Injury risk for THUMS v4.1 using Deflection IRF

Age	Risk of 3+ Rib Fx	Risk of 7+ Rib Fx
25 y/o	13.3 %	6.6 %
45 y/o	28.1 %	12.4 %
65 y/o	49.9 %	21.9 %

Table 15 Injury risk for THUMS v4.1 using Strain IRF

Age	Risk of 3+ Rib Fx	Risk of 7+ Rib Fx
25 y/o	9.7E-2 %	<0.01 %
45 y/o	2.4 %	0.1 %
65 y/o	27.9 %	4.99 %

Only the Strain IRF was valid for the GHBMC model. Hence, the injury risks calculated for the GHBMC v6.0 model with Strain IRF are given in Table 16.

Table 16 Injury risk for GHBMC v6.0 using Strain IRF

Age	Risk of 3+ Rib Fx	Risk of 7+ Rib Fx
25 y/o	0.8 %	<0.01 %
45 y/o	2.7 %	<0.01 %
65 y/o	7.8 %	<0.01 %

To contextualize these results, the expected risk of AIS3+ thoracic injury was calculated based on the analyses of field data from belted occupants in frontal collisions. Forman et al. 2019 (J. Forman et al., 2019) described regression models for AIS 3+ rib fracture injury for belted occupants in frontal collisions (in NASS-CDS), controlling for ΔV , vehicle model year, sex, age, stature, and BMI. That analysis was subsequently followed up with an expanded study also including recently available data from CISS. From the regression models of those two studies, we calculated the AIS 3+ rib fracture injury risk for a mid-sized male involved in a 56 km/h frontal collision, calculated for ages 25, 45, and 65 years old. The range of risks calculated from those two studies are shown in Figure 78, with an estimated risk of approximately 3 to 6% for a 65-year-old. Figure 78 also shows the predicted injury risks calculated with the Strain IRFs for THUMS v4.1 and GHBMC v6.0, where the upper bound of the range represents the calculated risk of 3+ fractures, and the lower bound of the range represents calculated risk of 7+ rib fractures. These predicted ranges of risk are compared to the range of AIS 3+ rib fracture risk estimated from the field data studies.

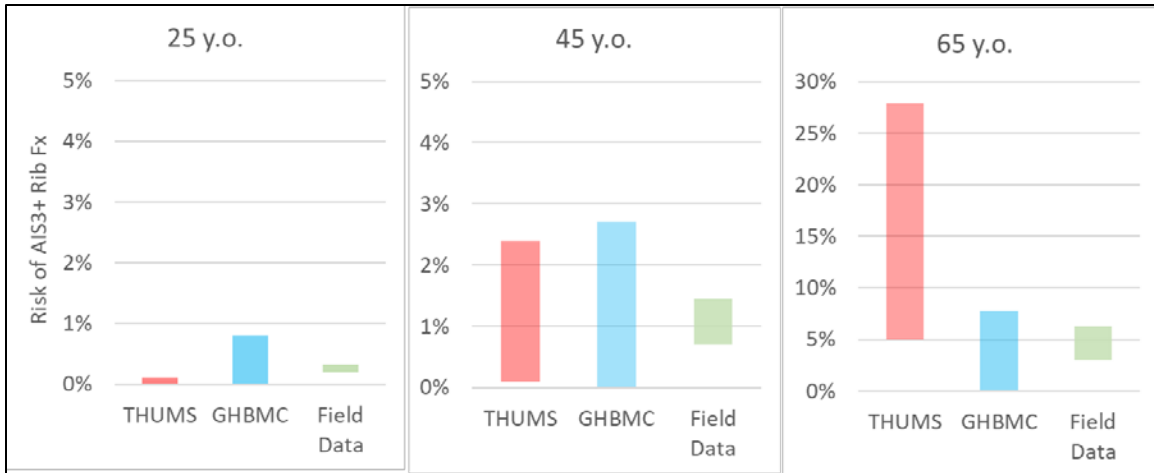


Figure 78 Ranges of AIS 3+ thoracic injury risk in 56 km/h frontal collision estimated from the strain-based predictions of THUMS and GHBM, compared to risk estimates from field data (Forman et al. 2019 and subsequent follow-up study).

The comparison to the field data is confounded by the definition of AIS 3+ rib fracture injury: Rib fracture severity definitions have changed with different versions of AIS. In addition, past interpretations seeking to compare to PMHS results have suggested a shift of 1-2 fractures to account for differences in diagnosis sensitivity between living humans and PMHS (Laituri et al. 2005). As a result, AIS 3+ can be interpreted as anything between 3 and 7 rib fractures, depending on the version of AIS used and the shift suggested in the literature to account for diagnostic sensitivity. So, when comparing to field data, the AIS 3+ rib fracture risk estimated from the field data should lie somewhere between the risk of 3+ fractures and 7+ fractures estimated from the human body models. As can be seen in Figure 78, the risk ranges estimated from the HBMs tend to overlap with the range from the field data (except for the 25 y.o. case, where the risk is very low from all estimates). The ranges estimated from the THUMS and GHBM results differ somewhat, but in general they are both reasonable compared to the range and precision expected from the field data.

In contrast, Figure 79 shows the risk estimates if the Larsson et al. (2021) rib cortical bone ultimate strain distributions were applied directly to both models. As expected from the component simulations, the THUMS tended to result in less rib strain than the GHBMC in the vehicle-occupant simulations. As a result, if the same strain-based IRF were used for both models, the THUMS would result in far less predicted risk than the GHBMC, well below the risk estimates indicated from the field data (Figure 79). This further highlights the utility of the method developed here, demonstrating the need to tune IRF for each human body model to arrive at comparable injury prediction.

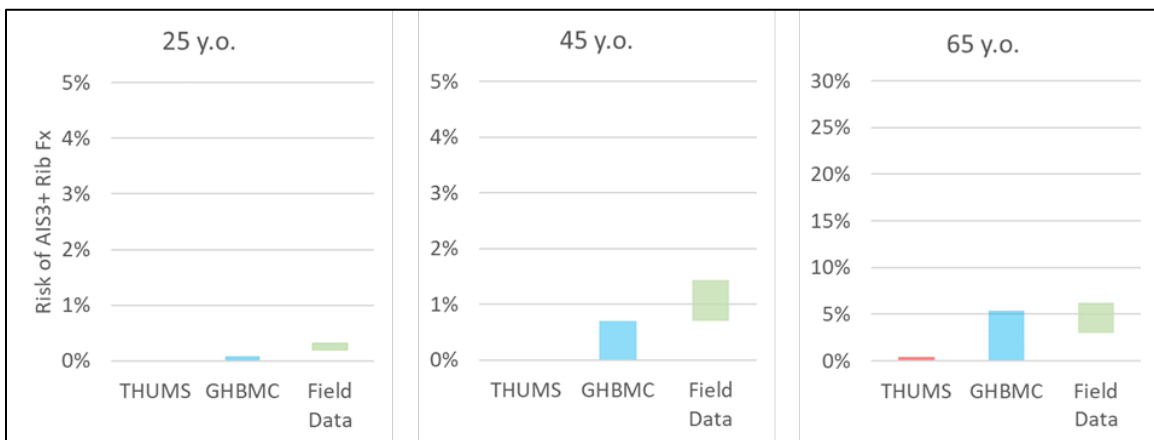


Figure 79 AIS 3+ thoracic injury risk in 56 km/h frontal collision, estimated if the Larsson (2021) strain IRF curves were applied to both HBMs (compared to the field risk estimates).

5.3 Summary

In this task, the thoracic injury risk functions developed in previous chapters were exercised by applying to simulations with the THUMS v4.1 and GHBMC v6.0 in exemplar simulations in a realistic vehicle environment. Simulations of the NCAP 56 kph frontal collision mode were performed in an environment based on NHTSA’s publicly available FE model of a mid-sized sedan (2014 Honda Accord). The THUMS and the GHBMC models were seated in the

driver position, with restraint provided by a seatbelt, airbag, seat, and instrument panel. From these simulations, injury risk was calculated based on the injury risk functions tuned for each model. These predictions were also compared to field data describing risk from comparable collisions, to give context to general reasonableness of the risks predicted by the models. Using the tuned strain-based chest IRFs, the THUMS and GHBMC both predicted rib fracture risks that were generally consistent with the field data for 56 km/h frontal collisions. The THUMS predicted a rib fracture risk on the high-end of the range indicated by the field data, whereas GHBMC predicted a risk that was on the low-end of the range described by the field data. Although, application of the model-specific strain-based IRFs resulted in comparable prediction between the two models. In contrast, the deflection-based chest IRF tuned for THUMS resulted in a predicted rib fracture risk that was considerably above the risks indicated by the field data. This suggests that model-tuned strain-based IRFs may provide more robust chest injury prediction that is less sensitive to the loading-mode differences between component-level tests and in-vehicle applications.

CHAPTER 6: Discussion and Conclusions

6.1 Discussion

The overall objective of this thesis was to develop a framework for generating injury risk functions for predicting risk of thoracic injury in frontal impacts using human body models. Detailed guidelines and instructions required to setup the simulations of the loadcases in this study using any other HBM are provided in Chapter 2. This is the largest-scale study to develop thoracic injury risk functions for specific human body models via simulations matched to individual PMHS tests. IRFs were developed using 170 unique matched-pair simulations consisting of 13 different loadcases. The loadcases or test series selected in this study comprised of different impact conditions as well as different impactors. The dataset consists of simulations with hub impact (Horsch, 1988; Kroell, 1971; Kroell et al., 1974; Yoganandan et al., 1997), rod impact (Hardy et al., 2001), steering wheel impact (Shaw et al., 2004) and table-top simulations with single diagonal belts (Cesari & Bouquet, 1990, 1994; Kemper et al., 2011; Kent et al., 2004; Salzar et al., 2009) as well as double diagonal belt and distributed loading belt (J. Forman et al., 2005; Kent et al., 2004). Additionally, 6 different sled simulations were also performed to validate the developed IRFs. Previous studies that have attempted to develop thoracic IRFs for HBMs in a similar way, use substantially smaller number of matched pair simulations. For example, Mendoza-Vazquez et al. reproduced 23 PMHS tests with the modified THUMS which included 10 impactor, 5 tabletop and 8 sled cases for developing injury risk curves for the DcTHOR injury criterion (Mendoza-Vazquez et al., 2013, 2015). Similarly, Song et al. performed 24 simulations with the HUMOS2LAB model in impactor and sled conditions to develop the Dc injury criterion and

related injury risk curves (Song et al., 2011). Pipkorn et al. used 5 PMHS tests (2 tabletop and 3 sled) and 20 detailed accident reconstruction simulations to validate the SAFER HBM's capability to predict two or more rib fractures using the strain-based rib fracture prediction method (Iraeus & Pipkorn, 2019; Pipkorn et al., 2019). These studies, while having a smaller dataset, also fail to provide detailed guidelines to setup the same simulations with other HBMs. This information is particularly critical for setting up same loadcase simulation setups for different HBMs and developing model-specific injury risk functions that provide comparable risk prediction for those different HBMs, despite the differences in the models. In contrast, the current study provides all the information required to replicate the simulations using a different HBM and have comparable loading and boundary conditions setup for the same dataset.

The current study also included a good proportion of injurious and non-injurious PMHS tests. Out of the 170 impactor and table-top tests (excluding the sled cases), 69 tests had injurious outcome at the 3+ rib fractures injury level (40.6% injurious tests). Since the sizes of the PMHSs in the tests were different to the size of the THUMSv4.1 model (50th percentile male), scaling of the test conditions was performed. To maximize the dataset for injury risk function development and to capture the PMHS size variability, test-specific simulations are setup corresponding to each individual test by modifying the loading conditions, targeting the test inputs applied to the PMHS. This was implemented in the impactor cases by applying a scaling law to the impactor mass without making any changes to the impactor velocities. For the table-top cases, this was achieved by normalizing the prescribed displacement curves by PMHS chest depth and then rescaling them back using the HBM chest depth to use as simulation input. The sled tests were not scaled in any way since it is the inertia of the HBM or the PMHS that loads the ribcage in these test cases. This

exercise allowed for the use of the full dataset of the PMHS tests without having to morph the HBM or exclude any tests due differences in the size of the PMHS and HBM.

- ***Deflection Based IRF***

The dataset of impactor and table-top cases used in the current study contains some cases where multiple tests were performed on the same PMHS, for example, Salzar 2009 Single Belt or the Forman 2005 Double Belt case. The Kent 2004 study had tests in different loading configurations performed on the same cadaver. Therefore it was necessary to use an approach which captured this phenomenon while developing the deflection based IRF. The use of survival analysis would have required reducing the dataset to only one test per PMHS and then censoring the data. This would have greatly reduced the dataset and the underlying information pool. Hence the novel approach of Generalized Estimating Equations (GEE) was used, as it accounts for clustering of data and seeks to model a population average based on a specified correlation structure. This approach allowed us to use all the PMHS tests and their matched-pair simulations from our dataset for developing IRFs. Age was found to be a significant covariate and contributor to thoracic injury risk in frontal impacts from the deflection based IRF models in this study. This is consistent with the existing knowledge on how age affects the thoracic injury tolerance and whenever it is considered, age has consistently appeared as a significant covariate in thoracic injury risk functions (J. L. Forman et al., 2012; Kent & Patrie, 2005; Laituri et al., 2005; Poplin et al., 2017).

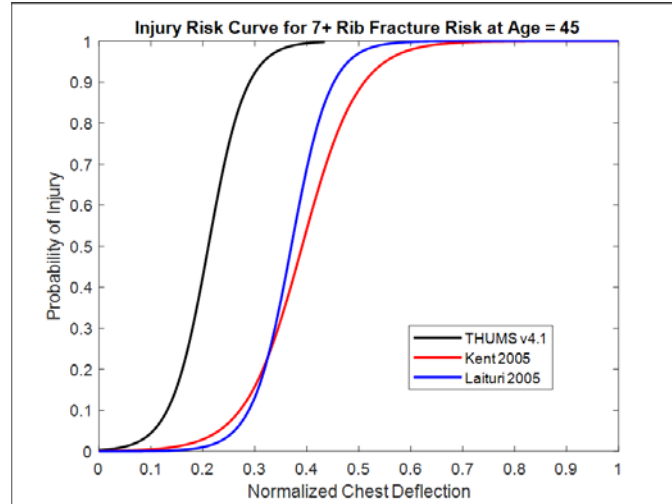


Figure 80 Comparison of deflection based IRF for 7+ rib fractures tuned for THUMS v4.1 with chest deflection IRFs for PMHS proposed by Kent et al. 2003 and Laituri et al. 2005

Figure 80 shows the comparison of the mid-sternum deflection based IRF tuned for THUMS v4.1 in this study with IRFs developed for PMHS chest deflection by Kent et al. 2005 (Kent & Patrie, 2005) and Laituri et al. 2005 (Laituri et al., 2005). Both the PMHS IRFs were developed considering 7+ rib fractures and so the 7+ rib fractures risk curve for THUMS v4.1 is used for comparison. As all these IRFs are age-dependent, a nominal age of 45 years old is selected for comparison. It is seen that the risk curve for the THUMS v4.1 model is significantly to the left of the PMHS curves. This means that the THUMS v4.1 chest has a stiffer response than the PMHS, with less deflection for similar loads. This is also observed in the biofidelity plots in Section 2.2.2 (sub-sections “HBM Biofidelity”). This also means that direct application of these PMHS IRF to the THUMS model would result in an underprediction of rib fracture risk.

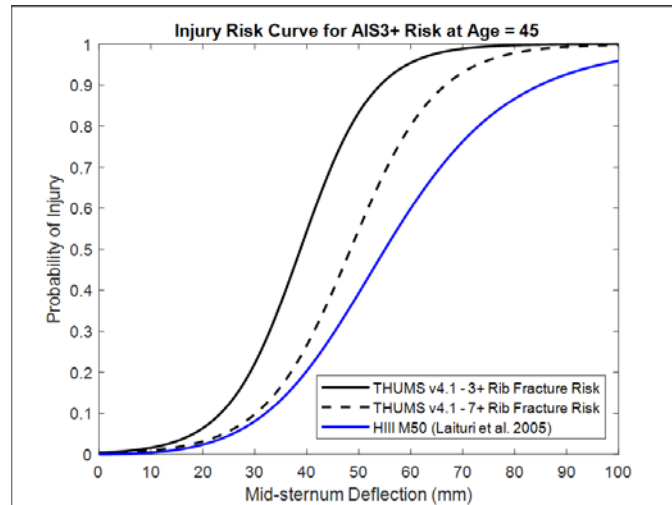


Figure 81 Comparison of mid-sternum deflection based injury risk curves tuned for THUMS v4.1 model with that developed for the HIII M50 dummy model (Laituri et al. 2005).

Similarly, application of an IRF developed for an ATD like the HIII M50 to the THUMS model would also likely result in incorrect thoracic injury risk prediction. This can be seen in Figure 81, where both the injury risk curves of 3+ and 7+ rib fractures tuned for THUMS are significantly to the left the injury risk curve for the HIII M50 dummy model. These comparisons highlight the need to tune specific IRFs for human body models, and the utility of the framework developed in the current study.

- ***Stain Based IRF***

The current study is the first one to develop a novel method to tune a strain-based injury risk function for a specific human body model, using optimization with a combined probability approach. Forman et al. 2012 developed a probabilistic framework for translating injury risk for an individual rib calculated from a fracture risk function (e.g. developed using survival analysis) to a risk of sustaining a certain number of rib fractures in HBM simulations (J. L. Forman et al., 2012). The framework included an age adjusted rib cortical bone strain based injury risk function developed from dynamic test data from twelve human subjects (Kemper et al., 2005, 2007) and

was presented as an empirical cumulative distribution function. The drawback of cumulative distribution function was that a very small increase in strain led to a large increase in predicted risk of fracture. To overcome this limitation, the framework was updated with a smooth risk curve derived by fitting Weibull distribution over the original empirical curve (Iraeus & Lindquist, 2021). In a recent study, Larsson et al. 2021 developed age-dependent rib strain-based fracture risk function from data from material coupon testing performed on rib cortical bone samples from 61 PMHSs (Katzenberger et al., 2020; Larsson et al., 2021), updating the original framework with the new fracture risk function. The new functions are in the form of analytical equations, thus making the risk curves smooth and continuous and easier to optimize if required. Pipkorn et al. 2019 validated the SAFER HBM model against the original probabilistic framework from Forman 2012, by using sled simulations and detailed accident reconstructions (Pipkorn et al., 2019). No changes to the underlying rib fracture risk function were made by Pipkorn et al., rather the HBM's ribcage and thorax were modified so as to obtain similar strains to PMHS (Iraeus & Pipkorn, 2019).

However, this approach may not always work, as different HBMs have subtle differences in the geometry and material properties of the ribcage and thorax. At the same time, they are surrogates, and rib fracture risk functions developed using data from PMHS tests may not directly work with HBMs and may lead to incorrect injury risk prediction. For example, consider the ribcage geometries of the THUMSv4.1 and GHBMCv6.0 models (**Figure 82**). Differences in the geometry can be clearly seen as well as the difference in the proportion of rib cartilage. The mesh size and material properties are also different between the two models. Hence, the strains generated in the ribs of these models may be different even if the models are setup in identical boundary and loading condition simulations. This may result in different risk predictions by these models in identical loading scenarios. This was highlighted in Section 5.2, where we see that application of

the original Larsson 2021 curves resulted in different injury risks predicted by the THUMS and the GHBMC models in the same vehicle environment and collision loadcase (**Figure 79**).

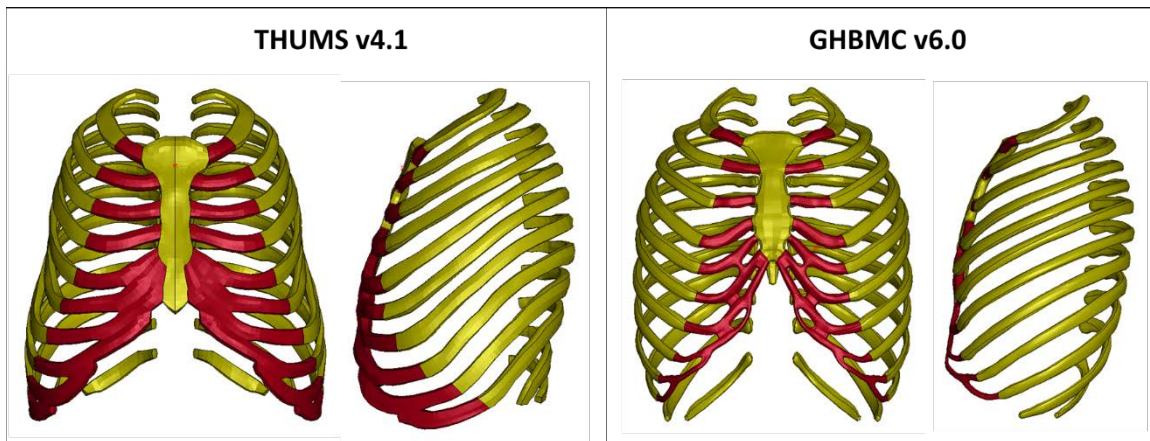


Figure 82 Comparison between ribcages of THUMS v4.1 and GHBMC v6.0 models.

Thus, a methodology was needed to modify or optimize the rib fracture risk function to work with the strains produced by a particular HBM. This research question led us to develop the optimization methodology to tune or calibrate the rib fracture risk function for application with a particular HBM. The probability framework provided the flexibility to predict the risk of multiple rib fractures, and so it was possible to optimize the fracture risk curve to give reasonable prediction at multiple injury levels (3+ and 7+ rib fractures in this study). As seen in **Figure 83**, the tuned strain-based IRF for THUMS resulted in a curve substantially to the left of the original Larsson (2021) curve, meaning that direct application of ultimate strain data from rib cortical bone coupon tests would result in an underprediction of rib fracture risk with THUMS v4.1. In other words, THUMS tends to systematically experience less rib strains than would be expected to cause fracture in actual rib cortical bone, and a different local IRF is needed to arrive at comparable injury prediction with it. In contrast, the tuned strain-based IRF for GHBMC resulted in a curve identical to that of the Larsson 2021 curve. This does not necessarily mean a limitation in the biofidelity of the THUMS model. Rather the THUMS model has been shown to be biofidelic in

the force-compression response of its chest under multiple impactor and belt loading modes. However, strain-based injury prediction is also dependent on the relationship between gross ribcage deflection and strain induced in models of the ribs. This is partially dependent on the fundamental mechanics of the rib models, but also is partially dependent on model-specific factors such as the mesh density. By taking the IRF-tuning approach developed here, a model does not necessarily need to replicate rib strains that an actual vehicle occupant would experience. It is sufficient instead for the model to be biofidelic in its gross response and for the relative magnitude of strain in its ribs to be sensitive to the severity and pattern of loading in a manner consistent with PMHS. This potentially provides a means to tune injury prediction across models of differing complexity, without needing to validate each down to the rib-strain level. The comparison of injury predictions of THUMS and GHBM in in-vehicle simulations with the field data (Section 5.2, Figure 78) highlight the utility of this framework, providing guidelines to tune local rib fracture risk functions for application to specific HBMs to arrive at comparable injury prediction.

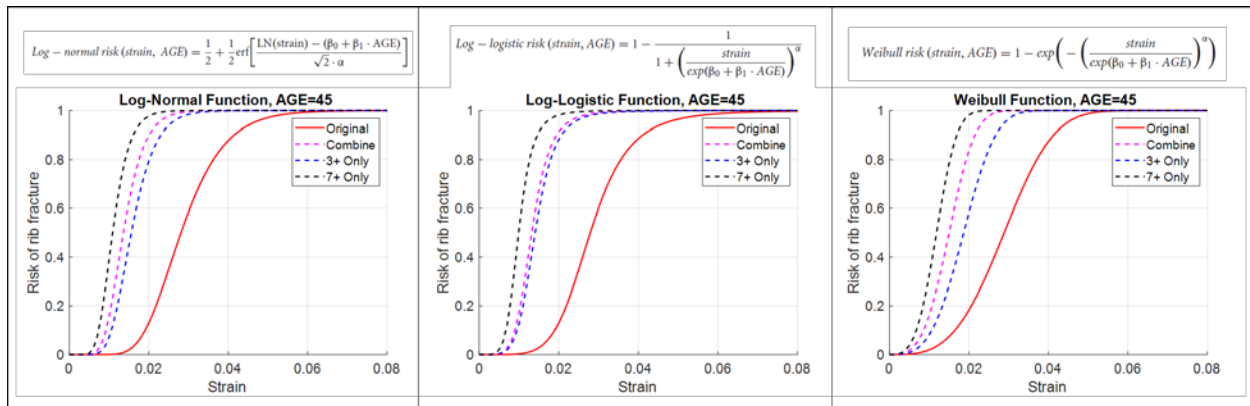


Figure 83 Comparison of original fracture risk curves from Larsson et al. 2021 and calibrated fracture risk curves for THUMS v4.1 for age of 45 years old.

For the strain-based IRF, two different optimization strategies were applied – independent and the combined optimization. The results from THUMS v4.1 suggested that better-fitting prediction may be achieved by fitting injury risk curves for prediction of 3+ and 7+ rib fractures.

This is to be expected, since by fitting separate functions we are essentially doubling the number of degrees of freedom (i.e., function coefficients) in the prediction model, which by definition will always result in a better fit (when evaluated against the data that is used in the model fitting). For the THUMS v4.1, the independently optimized IRFs being different implies that the relationship between the observed strains in the model and the predicted severity of injury is non-linear. The local strain IRF tuned for prediction of 7+ fractures is to the left of the local strain function tuned for the prediction of 3+ fractures. This means that less incremental increase in strain per rib is needed to escalate from 3 fractures to 7 fractures, compared to the strain needed to escalate from 0 fractures to 3 fractures. This can be attributed to the loss of stability in the ribcage that may occur due to multiple rib fractures. In PMHS, as ribs begin to fracture, the loads are transferred to the surrounding ribs, which causes more stress and strains in the ribcage. The simulations performed in this study are without any material failure defined in the ribs, and hence this phenomenon of ribs breaking and loads transferring may not be captured. As the structural stability of the ribcage is increasingly compromised in PMHS, a modest increase in overall loading severity may result in continuing accumulation of more fractures. In the THUMS (which maintains ribcage stability throughout), this translates to needing lesser incremental increase in per-rib strain to continue to accumulate predicted risk of more rib fractures.

- *Effect of Rib Cartilage*

Although developed on the same dataset of PMHS tests and matched simulations, there were some differences between the injury prediction from the deflection based IRF (mid-sternum deflection) and strain based IRF for the THUMS v4.1 model. This may be attributed to the proportion of rib cartilage in the THUMS v4.1 model. Consider, for example, the ribcage deformations and the subsequent rib strains produced in four different loadcases in **Figure 84**. It

is observed that in all four cases the mid-sternum deflection is approximately 45mm. However, the overall ribcage deformation and the generated rib strains differ substantially. It can also be seen that in some cases, most of the deformation is carried by the rib cartilage leading to less strain in the ribs.

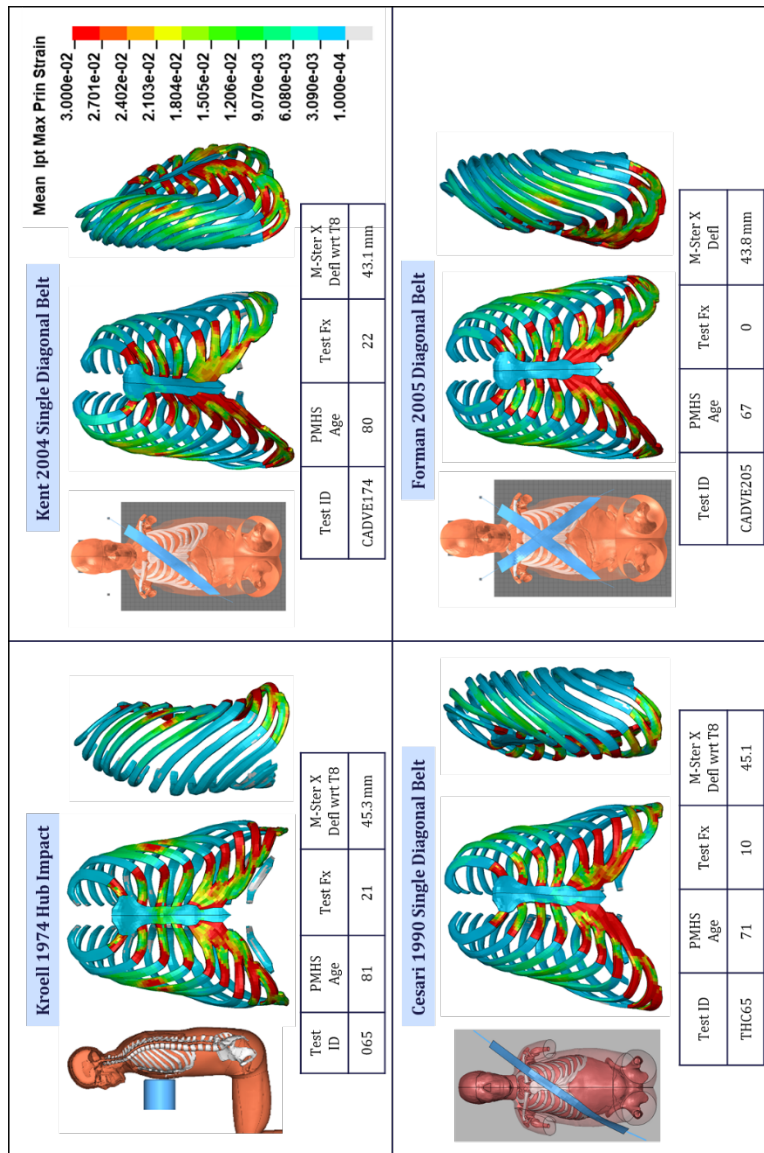


Figure 84 Ribcage deformation patterns and generated rib strains in example impactor and table-top simulations with THUMSv4.1.

This effect is also observed in the sled cases where the ribcage deforms under asymmetrical loading from the seatbelt and most of the deformation is borne by the cartilage (**Figure 85**). This effect is due to the specific construction of the THUMS model and may not be observed in simulations with other HBMs, such as the GHBMC model which do not have such a proportionately large rib cartilage (**Figure 82**). It is also likely one of the reasons why the tuned strain-based IRF for THUMS resulted in a curve which is to the left of the original Larsson (2021) curve. As the deformation is borne largely by the rib cartilage, the strains developed in the ribs are substantially less. A future research scope to extend the probabilistic rib fracture risk prediction framework is to include the fracture risk function for the rib cartilage in the analysis. This will require cartilage fracture risk functions along with rib fracture risk functions but will make the algorithm more robust in predicting the risk of fracture in the overall ribcage. However this was out of scope of the current study. Hence, for the THUMS v4.1 model, both deflection and strain-based IRFs should be used in combination to predict the risk of thoracic injury in frontal impacts.

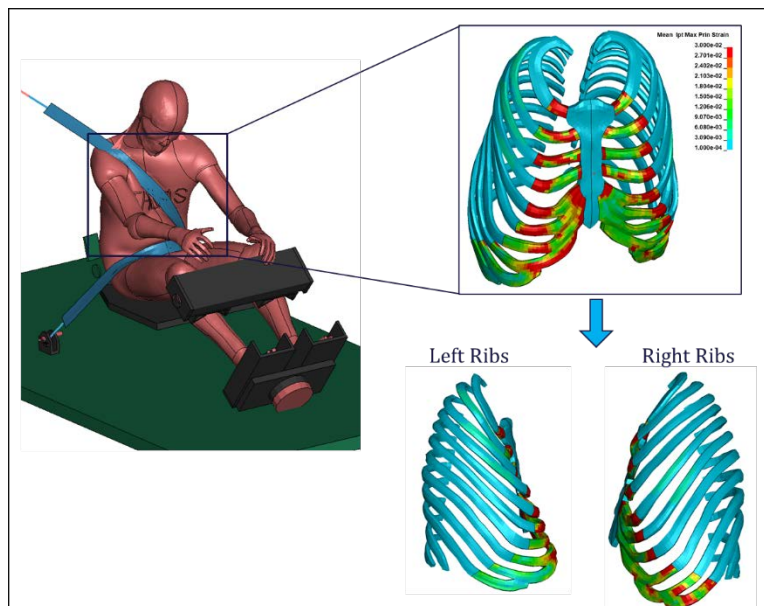


Figure 85 THUMSv4.1 ribcage deformation and generated strains in Gold Standard sled simulation.

6.2 Future Research Directions

The current study focused on developing a framework for thoracic injury risk functions in frontal impacts, as this is one of the main applications of HBMs in virtual assessments in vehicle simulations. However, this methodology can be extended to include PMHS tests under other loading conditions, including different directions and patterns of loading such as lateral impacts. The strategy would be similar to this study as in identifying the PMHS test series of primarily lateral loading direction for which sufficient information is available such that they can be setup and replicated in simulation environment with HBMs. Checking the basic biofidelity of the HBM to ensure that it interacts with the loading environment in a reasonable way. Then performing matched-pair simulations and developing models relating the HBM output with the injury information in the PMHS tests. Similar methodology as in frontal impacts can be followed to develop deflection and strain-based IRFs.

Another avenue of research is incorporating the rib cartilage in the probabilistic rib fracture risk prediction framework. This will involve developing a fracture risk curve for the cartilage similar to the one developed for rib fracture by Larsson et al. 2021. Once this is available, it can be used to predict local fracture risk in the cartilage similar to the vector of 24 probabilities of fracture for the 24 ribs in the current framework. Then the vector of cartilage plus rib fracture probabilities can be used to calculate the probability of sustaining multiple fractures throughout the ribcage in the same way as is done currently (using the generalized binomial equation) in probabilistic framework. Including cartilage in the calculation will make the algorithm more robust and able to capture the entire deformation of the ribcage irrespective of the size or proportion of the cartilage to ribs in the human body model.

Further, this framework may also be applied to tune strain-based IRFs for other body regions, particularly those that may benefit from a combined probability approach due to complex structures, strain fields, and the potential for different types of fracture that may occur (for example, tuning local strain IRFs for a combined probability approach in the pelvis).

6.3 Concluding Remarks

The main objective of this thesis was to develop a set of guidelines and framework which standardizes the methodology for developing thoracic injury risk functions for human body models in frontal impacts and drives towards consistent injury risk prediction even across different models. This goal was achieved in this study and Chapters 2 and 3 of this thesis form the framework and include detailed guidelines on setting up the simulations and developing injury risk functions. The entire process was demonstrated using the THUMS v4.1 50th percentile male human body model. A total of 176 unique matched pair simulations (55 impactor cases, 115 table-top cases and 6 sled cases) from 19 different loadcases were performed in this study. This makes this the largest-scale study of this kind. The impactor and tabletop simulations were used for IRF generation and the sled simulations for IRF validation. Two types of injury risk functions, deflection based and rib strain based were developed for the THUMS v4.1 model. For the deflection based IRF, multiple injury criteria were explored using the novel method of Generalized Estimating Equations to form models and the best one (mid-sternum deflection) was selected using statistical selection criteria of QIC and AUROC. Age was found to be a significant covariate to the mid-sternum deflection in this model. For the strain based IRF, the underlying rib fracture risk curve of Larsson et al. 2021 was calibrated to be used with the THUMSv4.1 model in the probabilistic rib fracture risk prediction framework developed by Forman et al. 2012. This is the first study to develop this

methodology to optimize strain-based fracture risk curve to be used with a specific human body model. Finally, these guidelines and framework can be applied to any different HBM to develop thoracic injury risk functions for frontal impacts. Further, the developed framework was verified and improved by applying to a different HBM, namely the GHBMC v6.0 (discussed in Chapter 4). To verify the objective of this study to drive towards consistent injury prediction across different HBMs, the two models were exercised in a realistic vehicle environment subjected to 56 kph frontal collision. The subsequent injury risk prediction from the models was compared to field data describing risk from comparable collisions. Application of the model-specific strain-based IRFs resulted in comparable prediction between the two models, despite the two models exhibiting considerably different strains. In contrast, the deflection-based chest IRF tuned for THUMS resulted in a predicted rib fracture risk that was considerably above the risks indicated by the field data. This suggests that model-tuned strain-based IRFs may provide more robust chest injury prediction that is less sensitive to the loading-mode differences between component-level tests and in-vehicle applications.

References

- Acosta, S. M., Ash, J. H., Lessley, D. J., Shaw, C. G., Heltzel, S. B., & Crandall, J. R. (2016). Comparison of whole body response in oblique and full frontal sled tests. In Proceedings of IRCOBI Conference.
- Albert, D., Kang, Y.-S., Agnew, A., & Kemper, A. (2017). *A Comparison of Rib Structural and Material Properties from Matched Whole Rib Bending and Tension Coupon Tests*.
- Cesari, D., & Bouquet, R. (1990). Behaviour of human surrogates thorax under belt loading (No. 902310). SAE Technical Paper.
- Cesari, D., & Bouquet, R. (1994). Comparison of Hybrid III and human cadaver thorax deformations loaded by a thoracic belt. SAE transactions, 1633-1644.
- Danelson, K. A., Golman, A. J., Kemper, A. R., Scott Gayzik, F., Clay Gabler, H., Duma, S. M., & Stitzel, J. D. (2015). Finite element comparison of human and Hybrid III responses in a frontal impact. *Accident Analysis & Prevention*, 85, 125–156. <https://doi.org/10.1016/j.aap.2015.09.010>
- Forman, J., Kent, R., Ali, T., Crandall, J., Bostrom, O., & Haland, Y. (2005). Biomechanical considerations for the optimization of an advanced restraint system: assessing the benefit of a second shoulder belt. In IRCOBI Conference on the Biomechanics of Impact.
- Forman, J. L., del Pozo de Dios, E., Dalmases, C. A., & Kent, R. W. (2010). The Contribution of the Perichondrium to the Structural Mechanical Behavior of the Costal-Cartilage. *Journal of Biomechanical Engineering*, 132(9), 094501. <https://doi.org/10.1115/1.4001976>
- Forman, J. L., Kent, R. W., Mroz, K., Pipkorn, B., Bostrom, O., & Segui-Gomez, M. (2012, October). Predicting rib fracture risk with whole-body finite element models: development

- and preliminary evaluation of a probabilistic analytical framework. In *Annals of Advances in Automotive Medicine/Annual Scientific Conference* (Vol. 56, p. 109). Association for the Advancement of Automotive Medicine.
- Forman, J. L., & McMurry, T. L. (2018). Nonlinear models of injury risk and implications in intervention targeting for thoracic injury mitigation. *Traffic Injury Prevention, 19*(sup2), S103–S108. <https://doi.org/10.1080/15389588.2018.1528356>
- Forman, J., Lessley, D., Shaw, C. G., Evans, J., Kent, R., Rouhana, S. W., & Prasad, P. (2006). Thoracic response of belted PMHS, the Hybrid III, and the THOR-NT mid-sized male surrogates in low-speed, frontal crashes (No. 2006-22-0009). SAE Technical Paper.
- Forman, J., Lopez-Valdes, F., Lessley, D., Kindig, M., Kent, R., Ridella, S., & Bostrom, O. (2009). Rear seat occupant safety: an investigation of a progressive force-limiting, pretensioning 3-point belt system using adult PMHS in frontal sled tests. *Stapp car crash journal, 53*, 49.
- Forman, J., Poplin, G. S., Shaw, C. G., McMurry, T. L., Schmidt, K., Ash, J., & Sunnevang, C. (2019). Automobile injury trends in the contemporary fleet: Belted occupants in frontal collisions. *Traffic Injury Prevention, 20*(6), 607–612. <https://doi.org/10.1080/15389588.2019.1630825>
- Gayzik, F. S., Moreno, D. P., Vavalle, N. A., Rhyne, A. C., & Stitzel, J. D. (2012). *Development of a Full Human Body Finite Element Model for Blunt Injury Prediction Utilizing a Multi-Modality Medical Imaging Protocol*. 14.
- Guleyupoglu, B., Koya, B., Barnard, R., & Gayzik, F. S. (2018). Failed rib region prediction in a human body model during crash events with precrash braking. *Traffic Injury Prevention, 19*(sup1), S37–S43. <https://doi.org/10.1080/15389588.2017.1395873>

- Guleyupoglu, B., Koya, B., & Gayzik, F. S. (2018). Development of Component Level Transfer Equations of Simplified Human and ATD Occupant Models. *SAE International Journal of Transportation Safety*, 6(1), 55–68. <https://doi.org/10.4271/09-06-01-0005>
- Hardy, W. N., Schneider, L. W., & Rouhana, S. W. (2001). Abdominal impact response to rigid-bar, seatbelt, and airbag loading. *Stapp car crash journal*, 45, 1-32.
- Horsch, J. D., & Schneider, D. (1988). Biofidelity of the Hybrid III Thorax in high-velocity frontal impact. *SAE transactions*, 169-176.
- Iraeus, J., & Lindquist, M. (2021). Analysis of minimum pulse shape information needed for accurate chest injury prediction in real life frontal crashes. *International Journal of Crashworthiness*, 26(6), 684–691. <https://doi.org/10.1080/13588265.2020.1769004>
- Iraeus, J., & Pipkorn, B. (2019). *Development and Validation of a Generic Finite Element Ribcage to be used for Strain-based Fracture Prediction*. <http://www.ircobi.org/wordpress/downloads/irc19/pdf-files/35.pdf>
- Iwamoto, M., Kisanuki, Y., Watanabe, I., Furusu, K., Miki, K., & Hasegawa, J. (2002). *Development of a Finite Element Model of the Total Human Model for Safety (THUMS) and Application to Injury Reconstruction*. 12.
- Kato, D., Nakahira, Y., Atsumi, N., & Iwamoto, M. (2018). *Development of Human-Body Model THUMS Version 6 containing Muscle Controllers and Application to Injury Analysis in Frontal Collision after Brake Deceleration*. 17.
- Katzenberger, M. J., Albert, D. L., Agnew, A. M., & Kemper, A. R. (2020). Effects of sex, age, and two loading rates on the tensile material properties of human rib cortical bone. *Journal of the mechanical behavior of biomedical materials*, 102, 103410.

- Kemper, A. R., Kennedy, E. A., McNally, C., Manoogian, S. J., Stitzel, J. D., & Duma, S. M. (2011). Reducing chest injuries in automobile collisions: rib fracture timing and implications for thoracic injury criteria. *Annals of biomedical engineering*, 39(8), 2141-2151.
- Kemper, A. R., McNally, C., Kennedy, E. A., & Manoogian, S. J. (2005). Material Properties of Human Rib Cortical Bone from Dynamic Tension Coupon Testing. *Stapp Car Crash Journal*, 49, 199.
- Kemper, A. R., McNally, C., Pullins, C. A., Freeman, L. J., Duma, S. M., & Rouhana, S. W. (2007). The biomechanics of human ribs: material and structural properties from dynamic tension and bending tests (No. 2007-22-0011). SAE Technical Paper.
- Kent, R. (2008). Frontal thoracic response to dynamic loading: The role of superficial tissues, viscera and the rib cage. *International Journal of Crashworthiness*, 13(3), 289–300. <https://doi.org/10.1080/13588260801933725>
- Kent, R., Lessley, D., & Sherwood, C. (2004). Thoracic response to dynamic, non-impact loading from a hub, distributed belt, diagonal belt, and double diagonal belts. *Stapp car crash journal*, 48, 495.
- Kent, R., & Patrie, J. (2005). Chest deflection tolerance to blunt anterior loading is sensitive to age but not load distribution. *Forensic science international*, 149(2-3), 121-128.
- Kindig, M., Lau, A., Forman, J., & Kent, R. (2010). Structural response of cadaveric ribcages under a localized loading: Stiffness and kinematic trends. *Stapp Car Crash Journal*, 54, 337–380.
- Kroell, C. (1971). Impact tolerance and response of the human thorax. In Proc. 15th Stapp Car Crash Conference, 1971 (pp. 84-134).

- Kroell, C. K., Schneider, D. C., & Nahum, A. M. (1974). Impact tolerance and response of the human thorax II. *SAE Transactions*, 3724-3762.
- Kullgren, A., Axelsson, A., Stigson, H., & Ydenius, A. (2019). *DEVELOPMENTS IN CAR CRASH SAFETY AND COMPARISONS BETWEEN RESULTS FROM EURO NCAP TESTS AND REAL-WORLD CRASHES*. 11.
- L'Abbe, R. j., Dainty, D. A., & Newman, J. A. (1982). An experimental analysis of thoracic deflection response to belt loading. *Proceedings of the International Research Council on the Biomechanics of Injury Conference*, 10, 184–194.
- Laituri, T. R., Prasad, P., Sullivan, K., Frankstein, M., & Thomas, R. S. (2005). Derivation and evaluation of a provisional, age-dependent, AIS3+ thoracic risk curve for belted adults in frontal impacts. *SAE Technical Paper*, (2005-01), 0297.
- Larsson, K. J., Blennow, A., Iraeus, J., Pipkorn, B., & Lubbe, N. (2021). Rib cortical bone fracture risk as a function of age and rib strain: updated injury prediction using finite element human body models. *Frontiers in bioengineering and biotechnology*, 9, 412.
- Lebarbe. (2005). *Thoracic Injury Investigation using PMHS in Frontal Airbag Out-of-Position Situations*.
<https://www.proquest.com/openview/80a1f7ad144120f3cd72878664c59856/1.pdf?pq-origsite=gscholar&cbl=29197>
- Lopez-Valdes, F. J., Lau, A., Lamp, J., Riley, P., Lessley, D. J., Damon, A., Kindig, M., Kent, R., Balasubramanian, S., Seacrist, T., Maltese, M. R., Arbogast, K. B., Higuchi, K., & Tanji, H. (2010). Analysis of spinal motion and loads during frontal impacts. Comparison between PMHS and ATD. *Annals of Advances in Automotive Medicine / Annual Scientific Conference*, 54, 61–78.

- Martynenko, O. V., Neininger, F. T., & Schmitt, S. (2019). *DEVELOPMENT OF A HYBRID MUSCLE CONTROLLER FOR AN ACTIVE FINITE ELEMENT HUMAN BODY MODEL IN LS-DYNA CAPABLE OF OCCUPANT KINEMATICS PREDICTION IN FRONTAL AND LATERAL MANEUVERS*. 12.
- Mendoza-Vazquez, M., Brodin, K., Davidsson, J., & Wisman, J. (2013). Human rib response to different restraint systems in frontal impacts: A study using a human body model. *International Journal of Crashworthiness*, 18(5), 516–529. <https://doi.org/10.1080/13588265.2013.815019>
- Mendoza-Vazquez, M., Davidsson, J., & Brodin, K. (2015). Construction and evaluation of thoracic injury risk curves for a finite element human body model in frontal car crashes. *Accident Analysis & Prevention*, 85, 73–82. <https://doi.org/10.1016/j.aap.2015.08.003>
- Mertz, H. J. (1984). A procedure for normalizing impact response data. *SAE transactions*, 351-358.
- Michaelson, J., Forman, J., Kent, R., & Kuppa, S. (2008). Rear seat occupant safety: kinematics and injury of PMHS restrained by a standard 3-point belt in frontal crashes (No. 2008-22-0012). SAE Technical Paper.
- Pipkorn, B., Iraeus, J., Björklund, M., Bunketorp, O., & Jakobsson, L. (2019). Multi-scale validation of a rib fracture prediction method for human body models. In *Proceedings of the IRCOBI Conference* (pp. 175-192).
- Pipkorn, B., Iraeus, J., Lindkvist, M., Puthan, P., & Bunketorp, O. (2020). Occupant injuries in light passenger vehicles—A NASS study to enable priorities for development of injury prediction capabilities of human body models. *Accident Analysis & Prevention*, 138, 105443. <https://doi.org/10.1016/j.aap.2020.105443>

- Pipkorn, B., & Kent, R. (2011). *Validation of a Human Body Thorax Model and its Use for Force, Energy and Strain Analysis in Various Loading Conditions*. 14.
- Poplin, G. S., McMurry, T. L., Forman, J. L., Ash, J., Parent, D. P., Craig, M. J., ... & Crandall, J. (2017). Development of thoracic injury risk functions for the THOR ATD. *Accident Analysis & Prevention*, 106, 122-130.
- Roberts, C., Forman, J., & Kerrigan, J. (2018). *Injury Risk Functions for 5th Percentile Females: Ankle Inversion and Eversion*. 16.
- Roberts, C., Forman, J., Kerrigan, J., & Pipkorn, B. (2020). Sensitivity of scale factor choice on injury response for equal-stress equal-velocity scaling. *Traffic Injury Prevention*, 21(sup1), S168–S170. <https://doi.org/10.1080/15389588.2020.1829919>
- Salzar, R. S., Bass, C. R., Lessley, D., Crandall, J. R., Kent, R. W., & Bolton, J. R. (2009). Viscoelastic response of the thorax under dynamic belt loading. *Traffic injury prevention*, 10(3), 290-296.
- Shaw, G., Lessley, D., Bolton, J., & Crandall, J. (2004). Assessment of the THOR and Hybrid III crash dummies: Steering wheel rim impacts to the upper abdomen (No. 2004-01-0310). SAE Technical Paper.
- Shaw, G., Parent, D., Purtsezov, S., Lessley, D., Crandall, J., Kent, R., ... & Martin, P. (2009). Impact response of restrained PMHS in frontal sled tests: skeletal deformation patterns under seat belt loading. *Stapp Car Crash Journal*, 53, 1.
- Shigeta, K., Kitagawa, Y., & Yasuki, T. (2009). Development of next generation human FE model capable of organ injury prediction. *Proceedings of the 21st Annual Enhanced Safety of Vehicles*, 15-18.

- Singh, H., Ganesan, V., James, D., Paramasuwom, M., & Gradischnig, L. (2018). *Vehicle Interior and Restraints Modeling Development of Full Vehicle Finite Element Model Including Vehicle Interior and Occupant Restraints Systems for Occupant Safety Analysis Using THOR Dummies* (DOT HS 812 545). Article DOT HS 812 545. <https://trid.trb.org/view/1662795>
- Song, E., Lecuyer, E., & Trosseille, X. (2011, June). Development of injury criteria for frontal impact using a human body FE model. In International Technical Conference on the Enhanced Safety Vehicles Conference, June (pp. 13-16).
- Yoganandan, N., Pintar, F. A., Kumaresan, S., Haffner, M., & Kuppa, S. (1997). Impact biomechanics of the human thorax-abdomen complex. *International journal of crashworthiness*, 2(2), 219-228.

APPENDIX A: PMHS details and injury information for all tests

Loadcase	PMHS_ID	Test_ID	Age	Sex	Height (cm)	Weight (kg)	Total Rib Fractures	3+ Rib Fractures	7+ Rib Fractures
01_Horsch_1988	119FM	218	69	M	178.3	65	11	1	1
	121FM	219	66	M	185.5	68.2	6	1	0
	123FM	220	58	M	173.7	72.3	7	1	1
02_Yoganandan_1997	1	1	72	M	170	82	5	1	0
	2	2	81	M	175	63	4	1	0
	3	3	84	M	168	68	0	0	0
	4	4	86	M	170	56	2	0	0
	5	5	62	M	174	61	3	1	0
	6	6	70	M	169	91	4	1	0
	7	7	68	M	178	83	11	1	1
03_Hardy_2001	28800	GI5	65	F	164	61	13	1	1
	29084	GI10	64	M	180	65	20	1	1
	29115	GI11	74	M	168	75	16	1	1
04_Shaw_2004	2000-FRM-135	Cad1	63	M	172.6	69.1	3	1	0
	2002-FRM-159	Cad2	66	M	166.5	65.9	2	0	0
	2001-FRM-149	Cad3	40	M	158.3	43.1	1	0	0
	2002-FRM-161	Cad4	61	M	181.7	65.8	16	1	1
05_Kroell_1974	11FF	60	60	F	160	58.9	11	1	1
	12FF	61	67	F	162.5	62.6	24	1	1
	13FM	65	81	M	167.6	76.2	21	1	1
	14FF	66	76	F	157.5	57.6	7	1	1
	15FM	69	80	M	165.1	53	13	1	1
	18FM	76	78	M	175.3	65.7	16	1	1
	19FM	77	19	M	NA	65.7	1	0	0
	20FM	79	29	M	180.3	56.7	0	0	0
	21FF	82	45	F	172.7	68.5	19	1	1
	22FM	83	72	M	182.9	74.8	17	1	1
	23FF	85	58	F	162.5	61.2	23	1	1
	24FM	86	65	M	182.9	81.6	6	1	0
	25FM	87	65	M	167.6	54.4	18	1	1
	26FM	88	75	M	172.7	63.5	0	0	0
	28FM	90	54	M	182.9	68	0	0	0
	30FF	92	52	F	156	40.8	3	1	0
	31FM	93	51	M	183	74.8	15	1	1
	32FM	94	75	M	171	54.4	21	1	1
34FM	96	64	M	178	59	13	1	1	
36FM	99	52	M	183	74.8	7	1	1	

	37FM	104	48	M	179	73.9	10	1	1
	42FM	171	61	M	183	54.4	0	0	0
	43FM	172	59	M	178	54.4	4	1	0
	45FM	177	64	M	181	64	11	1	1
	46FM	178	46	M	178	94.8	0	0	0
	48FM	182	69	M	170	64.4	0	0	0
	50FM	186	66	M	181	59.9	13	1	1
	51FM	187	60	M	185	82.1	0	0	0
	52FM	188	65	M	175	51.7	12	1	1
	53FM	189	75	M	174	77.1	3	1	0
	54FF	190	49	F	163	37.2	7	1	1
	55FF	191	46	F	177	81.2	8	1	1
	56FM	192	65	M	177	73.9	3	1	0
	58FM	196	68	M	179	68.9	4	1	0
	60FM	200	66	M	180	79.4	9	1	1
	62FM	202	76	M	174	50.3	10	1	1
	63FM	203	53	M	183	88	5	1	0
	64FM	204	72	M	163	63	6	1	0
06_Kent_2004_Hub	147	Cadve42	63	F	161	45	0	0	0
	145	Cadve62	54	M	192	87.7	0	0	0
	145	Cadve64	54	M	192	87.7	6	1	0
	155	Cadve67	71	F	166	54.4	0	0	0
	170	Cadve87	75	M	178	65	0	0	0
	173	Cadve103	67	F	162	57.2	0	0	0
	178	Cadve127	73	M	182	80.7	0	0	0
	177	Cadve146	79	F	161	47.6	0	0	0
	177	Cadve149	79	F	161	47.6	24	1	1
	176	Cadve152	85	F	157	58.2	0	0	0
	182	Cadve171	80	F	157	65.3	0	0	0
	157	Cadve179	55	F	168	74.4	0	0	0
	186	Cadve197	58	F	178	61.2	0	0	0
	186	Cadve201	58	F	178	61.2	8	1	1
	188	Cadve203	71	M	173	85.3	0	0	0
	187	Cadve217	54	M	178	112.7	1	0	0
	190	Cadve230	79	M	173	73.5	0	0	0
189	Cadve248	79	M	159	56.7	0	0	0	
07_Kent_2004_Dist	147	Cadve45	63	F	161	45	0	0	0
	145	Cadve57	54	M	192	87.7	0	0	0
	155	Cadve73	71	F	166	54.4	0	0	0
	170	Cadve96	75	M	178	65	0	0	0
	170	Cadve98	75	M	178	65	11	1	1
	173	Cadve100	67	F	162	57.2	0	0	0

	178	Cadve120	73	M	182	80.7	0	0	0
	177	Cadve143	79	F	161	47.6	0	0	0
	176	Cadve155	85	F	157	58.2	0	0	0
	182	Cadve167	80	F	157	65.3	0	0	0
	157	Cadve176	55	F	168	74.4	0	0	0
	186	Cadve195	58	F	178	61.2	0	0	0
	188	Cadve207	71	M	173	85.3	0	0	0
	187	Cadve221	54	M	178	112.7	0	0	0
	190	Cadve232	79	M	173	73.5	0	0	0
	189	Cadve250	79	M	159	56.7	0	0	0
08_Kent_2004_SB	147	Cadve50	63	F	161	45	1	0	0
	145	Cadve54	54	M	192	87.7	0	0	0
	155	Cadve69	71	F	166	54.4	1	0	0
	170	Cadve93	75	M	178	65	1	0	0
	173	Cadve105	67	F	162	57.2	0	0	0
	178	Cadve124	73	M	182	80.7	1	0	0
	177	Cadve139	79	F	161	47.6	1	0	0
	176	Cadve159	85	F	157	58.2	0	0	0
	176	Cadve161	85	F	157	58.2	8	1	1
	182	Cadve163	80	F	157	65.3	0	0	0
	182	Cadve174	80	F	157	65.3	22	1	1
	157	Cadve182	55	F	168	74.4	1	0	0
	186	Cadve192	58	F	178	61.2	1	0	0
	188	Cadve209	71	M	173	85.3	1	0	0
	187	Cadve225	54	M	178	112.7	0	0	0
	187	Cadve228	54	M	178	112.7	1	0	0
	190	Cadve234	79	M	173	73.5	0	0	0
189	Cadve246	79	M	159	56.7	0	0	0	
09_Kent_2004_DB	155	Cadve71	71	F	166	54.4	0	0	0
	170	Cadve90	75	M	178	65	0	0	0
	173	Cadve107	67	F	162	57.2	0	0	0
	178	Cadve122	73	M	182	80.7	1	0	0
	177	Cadve141	79	F	161	47.6	0	0	0
	176	Cadve157	85	F	157	58.2	0	0	0
	182	Cadve165	80	F	157	65.3	0	0	0
	157	Cadve184	55	F	168	74.4	0	0	0
	157	Cadve188	55	F	168	74.4	27	1	1
	186	Cadve190	58	F	178	61.2	0	0	0
	188	Cadve211	71	M	173	85.3	0	0	0
	187	Cadve223	54	M	178	112.7	0	0	0
190	Cadve236	79	M	173	73.5	0	0	0	
190	Cadve240	79	M	173	73.5	12	1	1	

	189	Cadve242	79	M	159	56.7	0	0	0
10_Kemper_2011	1	01Male	65	M	183	76.8	14	1	1
	2	02Female	69	F	155	50.9	8	1	1
11_Salzar_2009	412	12	62	M	175	68	0	0	0
	412	13	62	M	175	68	0	0	0
	413	22	54	M	175	68	0	0	0
	413	23	54	M	175	68	0	0	0
	419	33	31	M	193	90	0	0	0
	419	34	31	M	193	90	0	0	0
12_Forman_2005	207	cadve205	67	F	160	49.9	0	0	0
	207	cadve206	67	F	160	49.9	0	0	0
	207	cadve207	67	F	160	49.9	0	0	0
	207	cadve208	67	F	160	49.9	0	0	0
	207	cadve209	67	F	160	49.9	0	0	0
	207	cadve210	67	F	160	49.9	0	0	0
	207	cadve212	67	F	160	49.9	8	1	1
	194	cadve217	38	F	170	94.8	0	0	0
	194	cadve218	38	F	170	94.8	0	0	0
	194	cadve219	38	F	170	94.8	0	0	0
	194	cadve220	38	F	170	94.8	0	0	0
	194	cadve221	38	F	170	94.8	0	0	0
	194	cadve222	38	F	170	94.8	0	0	0
	194	cadve223	38	F	170	94.8	0	0	0
	194	cadve225	38	F	170	94.8	0	0	0
	195	cadve227	67	F	173	58.9	0	0	0
	195	cadve229	67	F	173	58.9	0	0	0
	195	cadve230	67	F	173	58.9	0	0	0
	195	cadve231	67	F	173	58.9	0	0	0
	195	cadve232	67	F	173	58.9	0	0	0
195	cadve233	67	F	173	58.9	0	0	0	
195	cadve234	67	F	173	58.9	0	0	0	
195	cadve238	67	F	173	58.9	21	1	1	
13_Cesari_1990	THC11	thc11	47	F	170	92.5	8	1	1
	THC12	thc12	17	F	164	58.5	0	0	0
	THC13	thc13	86	F	160	43	2	0	0
	THC14	thc14	69	M	173	82	17	1	1
	THC15	thc15	60	M	177	69	3	1	0
	THC16	thc16	59	M	170	62	4	1	0
	THC17	thc17	71	M	177	75	7	1	1
	THC18	thc18	67	M	174	47	6	1	0
	THC19	thc19	83	F	155	43	4	1	0
	THC20	thc20	70	M	160	63	18	1	1

	THC62	thc62	72	M	183	53	4	1	0
	THC65	thc65	71	M	170	41	10	1	1
	THC69	thc69	40	M	183	56	1	0	0
	THC75	thc75	60	M	160	44.5	6	1	0
	THC77	thc77	64	F	164	49.5	6	1	0
	THC79	thc79	43	M	186	54	3	1	0
	THC93	thc93	63	M	176	56	10	1	1
Gold Standard 1	411	1294	76	M	178	70	8	1	1
	403	1295	47	M	177	68	29	1	1
	425	1358	54	M	177	79	16	1	1
	426	1359	49	M	184	76	11	1	1
	428	1360	57	M	175	64	6	1	0
	443	1378	72	M	184	81	10	1	1
	433	1379	40	M	179	88	11	1	1
	441	1380	37	M	180	78	2	0	0
Gold Standard 2	494	UVAS028	59	M	178	68	0	0	0
	492	UVAS029	66	M	179	70	0	0	0
	674	UVAS0302	67	M	177	68	4	1	0
	736	UVAS0303	67	M	173	68	8	1	1
	695	UVAS0304	74	M	183	70	0	0	0
Gold Standard 3	632	UVAS0313	69	M	173	69	7	1	1
	750	UVAS0314	66	M	171.5	76	8	1	1
	767	UVAS0315	67	M	176.5	64	0	0	0
Rear Seat (Forman 2009)	1	1386	67	M	175	69	12	1	1
	2	1387	69	M	171	67	3	1	0
	3	1389	72	M	183	72	17	1	1
Rear Seat (Michaelson 2008)	1	1262	51	M	175	54.9	14	1	1
	2	1263	57	F	165	108.9	30	1	1
	3	1264	57	M	179	59	14	1	1
Low Speed Frontal	322	1094	49	M	178	58.1	0	0	0
	327	1096	39	M	184	79.4	0	0	0
	323	1095	44	M	172	77.1	0	0	0

APPENDIX B: Impactor masses and velocities for Impactor Cases

Loadcase	PMHS_ID	Test_ID	Test Impactor Mass (kg)	Test Impactor Initial Velocity (m/s)	Scaled impactor mass for THUMS v4.1 (kg)
01_Horsch_1988	119FM	218	4.25	13.4	5.03
	121FM	219	4.25	13.4	4.80
	123FM	220	4.25	13.4	4.53
02_Yoganandan_1997	1	1	23.5	4.3	22.07
	2	2	23.5	4.3	28.72
	3	3	23.5	4.3	26.61
	4	4	23.5	4.3	32.31
	5	5	23.5	4.3	29.66
	6	6	23.5	4.3	19.88
	7	7	23.5	4.3	21.80
03_Hardy_2001	28800	GI5	48	6	60.59
	29084	GI10	48	8.9	56.86
	29115	GI11	48	6.2	49.28
04_Shaw_2004	2000-FRM-135	Cad1	64	4	71.32
	2002-FRM-159	Cad2	64	4	74.78
	2001-FRM-149	Cad3	64	4	114.34
	2002-FRM-161	Cad4	64	4	74.89
05_Kroell_1974	11FF	60	19.5	6.3	25.49
	12FF	61	22.8	7.2	28.04
	13FM	65	22.8	7.4	23.04
	14FF	66	22.8	7.3	30.48
	15FM	69	23.6	6.9	34.29
	18FM	76	23.6	6.7	27.66
	19FM	77	23.6	6.7	27.66
	20FM	79	23.6	6.7	32.05
	21FF	82	23.6	6.8	26.53
	22FM	83	23.6	6.7	24.29
	23FF	85	19.5	7.7	24.53
	24FM	86	22.8	9.6	21.51
	25FM	87	5.5	13.8	7.78
	26FM	88	1.8	11.1	2.18
	28FM	90	1.6	14.5	1.81
30FF	92	15.9	13.23	30.01	

	31FM	93	23.04	10.19	23.72
	32FM	94	22.86	9.92	32.36
	34FM	96	18.96	8.23	24.74
	36FM	99	18.96	7.2	19.52
	37FM	104	22.86	9.83	23.82
	42FM	171	22.86	4.87	32.36
	43FM	172	22.86	4.83	32.36
	45FM	177	23	5.05	27.67
	46FM	178	19.28	7.33	15.66
	48FM	182	10.43	7.06	12.47
	50FM	186	10.43	7.29	13.41
	51FM	187	10.43	6.66	9.78
	52FM	188	10.43	7.2	15.53
	53FM	189	22.95	5.23	22.92
	54FF	190	19.55	6.71	40.47
	55FF	191	19.55	9.92	18.54
	56FM	192	10.43	6.93	10.87
	58FM	196	10.43	6.75	11.66
	60FM	200	22.95	4.34	22.26
	62FM	202	9.98	6.93	15.28
	63FM	203	23	6.93	20.13
	64FM	204	23	6.93	28.11

APPENDIX C: Mid-sternum deflections and Probabilities of injury

calculated with Deflection IRF for all cases

Loadcase	PMHS_ID	Test_ID	Mid-Sternum X deflection wrt T8 (mm)	Risk of 3+ Rib fractures	Risk of 7+ Rib Fractures
01_Horsch_1988	119FM	218	41.013	0.800	0.482
	121FM	219	40.190	0.756	0.432
	123FM	220	39.195	0.651	0.340
02_Yoganandan_1997	1	1	26.160	0.355	0.146
	2	2	29.268	0.565	0.253
	3	3	28.314	0.565	0.250
	4	4	30.778	0.670	0.325
	5	5	29.706	0.366	0.157
	6	6	25.325	0.308	0.126
	7	7	26.067	0.311	0.129
03_Hardy_2001	28800	GI5	19.777	0.138	0.059
	29084	GI10	21.712	0.168	0.071
	29115	GI11	19.797	0.195	0.078
04_Shaw_2004	2000-FRM-135	Cad1	18.483	0.108	0.047
	2002-FRM-159	Cad2	18.497	0.123	0.052
	2001-FRM-149	Cad3	18.568	0.041	0.022
	2002-FRM-161	Cad4	30.240	0.373	0.162
05_Kroell_1974	11FF	60	41.618	0.743	0.425
	12FF	61	48.554	0.915	0.684
	13FM	65	45.339	0.928	0.703
	14FF	66	50.831	0.958	0.795
	15FM	69	50.709	0.964	0.814
	18FM	76	45.512	0.920	0.685
	19FM	77	45.512	0.433	0.227
	20FM	79	48.400	0.647	0.369
	21FF	82	45.176	0.707	0.405
	22FM	83	42.757	0.855	0.560
	23FF	85	48.386	0.874	0.610
	24FM	86	54.149	0.956	0.799
	25FM	87	48.682	0.909	0.673
	26FM	88	24.427	0.330	0.133
	28FM	90	26.640	0.205	0.089
30FF	92	61.567	0.972	0.863	

	31FM	93	57.497	0.949	0.788
	32FM	94	58.889	0.986	0.909
	34FM	96	51.197	0.932	0.729
	36FM	99	42.219	0.686	0.377
	37FM	104	56.727	0.935	0.753
	42FM	171	37.855	0.639	0.326
	43FM	172	37.630	0.609	0.306
	45FM	177	36.455	0.624	0.312
	46FM	178	40.453	0.562	0.285
	48FM	182	37.014	0.694	0.365
	50FM	186	38.610	0.712	0.386
	51FM	187	32.939	0.455	0.205
	52FM	188	39.912	0.740	0.416
	53FM	189	35.731	0.713	0.376
	54FF	190	52.251	0.889	0.648
	55FF	191	51.994	0.870	0.617
	56FM	192	35.064	0.588	0.283
	58FM	196	35.221	0.626	0.309
	60FM	200	31.288	0.465	0.206
	62FM	202	38.750	0.800	0.473
	63FM	203	41.519	0.674	0.365
	64FM	204	47.085	0.916	0.683
06_Kent_2004_Hub	147	Cadve42	22.639	0.180	0.076
	145	Cadve62	29.967	0.293	0.128
	145	Cadve64	57.190	0.953	0.798
	155	Cadve67	15.830	0.107	0.045
	170	Cadve87	33.505	0.644	0.315
	173	Cadve103	35.932	0.639	0.320
	178	Cadve127	27.630	0.416	0.174
	177	Cadve146	25.495	0.408	0.167
	177	Cadve149	87.685	1.000	0.997
	176	Cadve152	20.371	0.304	0.117
	182	Cadve171	20.478	0.261	0.101
	157	Cadve179	29.002	0.274	0.119
	186	Cadve197	14.075	0.049	0.024
	186	Cadve201	54.745	0.945	0.771
	188	Cadve203	29.956	0.475	0.207
	187	Cadve217	22.533	0.125	0.056
	190	Cadve230	13.103	0.105	0.043
	189	Cadve248	23.394	0.338	0.134
07_Kent_2004_Dist	147	Cadve45	18.061	0.103	0.045
	145	Cadve57	23.195	0.136	0.061

	155	Cadve73	16.217	0.113	0.047
	170	Cadve96	19.906	0.205	0.082
	170	Cadve98	33.860	0.655	0.325
	173	Cadve100	33.558	0.557	0.261
	178	Cadve120	21.087	0.218	0.087
	177	Cadve143	10.936	0.079	0.033
	176	Cadve155	16.255	0.195	0.074
	182	Cadve167	10.897	0.082	0.034
	157	Cadve176	24.880	0.173	0.076
	186	Cadve195	6.318	0.017	0.010
	188	Cadve207	14.944	0.096	0.041
	187	Cadve221	18.787	0.077	0.037
	190	Cadve232	6.169	0.042	0.019
	189	Cadve250	13.178	0.106	0.043
08_Kent_2004_SB	147	Cadve50	17.712	0.098	0.043
	145	Cadve54	25.406	0.178	0.078
	155	Cadve69	21.450	0.211	0.085
	170	Cadve93	29.908	0.519	0.230
	173	Cadve105	39.137	0.737	0.409
	178	Cadve124	32.506	0.588	0.276
	177	Cadve139	17.012	0.170	0.067
	176	Cadve159	19.695	0.284	0.108
	176	Cadve161	42.114	0.907	0.647
	182	Cadve163	16.310	0.163	0.064
	182	Cadve174	43.086	0.899	0.635
	157	Cadve182	26.455	0.208	0.090
	186	Cadve192	9.679	0.027	0.014
	188	Cadve209	25.631	0.328	0.134
	187	Cadve225	18.986	0.079	0.037
	187	Cadve228	28.589	0.254	0.111
	190	Cadve234	17.791	0.187	0.073
189	Cadve246	23.880	0.354	0.141	
09_Kent_2004_DB	155	Cadve71	29.776	0.469	0.204
	170	Cadve90	40.138	0.823	0.507
	173	Cadve107	50.137	0.931	0.724
	178	Cadve122	38.686	0.776	0.446
	177	Cadve141	23.824	0.352	0.140
	176	Cadve157	32.059	0.699	0.352
	182	Cadve165	25.305	0.413	0.168
	157	Cadve184	36.116	0.511	0.242
	157	Cadve188	44.173	0.768	0.459
	186	Cadve190	17.462	0.077	0.036

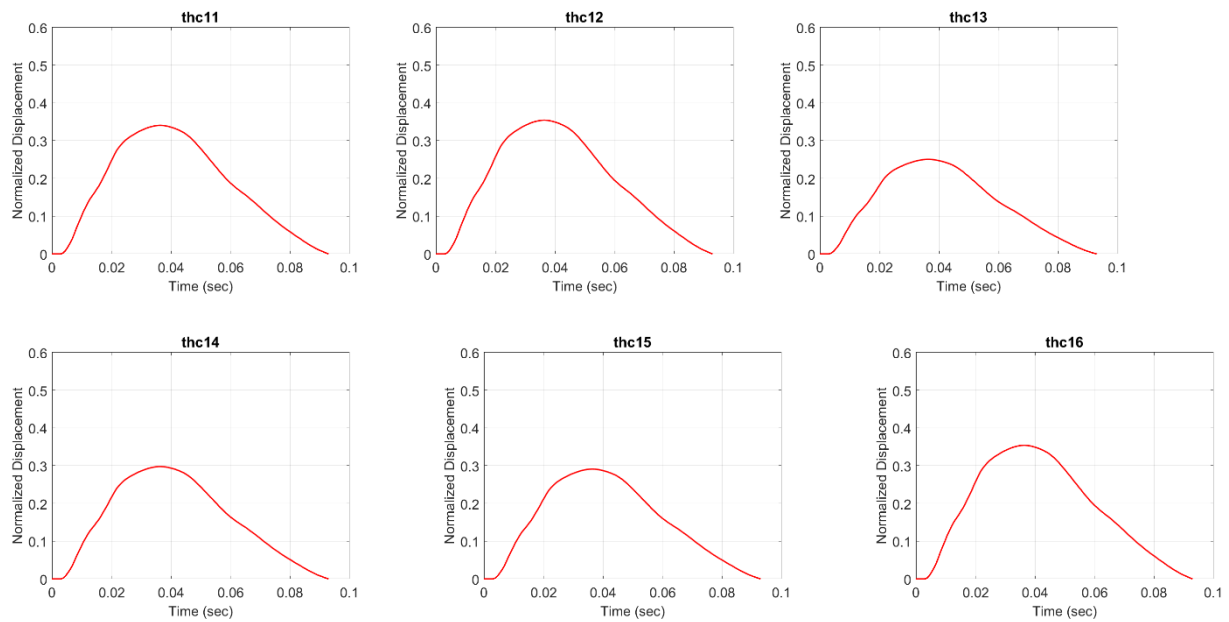
	188	Cadve211	33.569	0.603	0.288
	187	Cadve223	29.109	0.268	0.117
	190	Cadve236	26.849	0.456	0.191
	190	Cadve240	32.971	0.668	0.331
	189	Cadve242	31.625	0.624	0.296
10_Kemper_2011	1	01Male	23.205	0.207	0.086
	2	02Female	31.391	0.503	0.225
11_Salzar_2009	412	12	6.191	0.020	0.011
	412	13	11.799	0.043	0.021
	413	22	5.243	0.012	0.007
	413	23	9.347	0.021	0.012
	419	33	9.933	0.008	0.006
	419	34	13.552	0.014	0.009
12_Forman_2005	207	cadve205	43.791	0.845	0.549
	207	cadve206	33.846	0.568	0.268
	207	cadve207	35.694	0.631	0.314
	207	cadve208	34.869	0.603	0.293
	207	cadve209	35.169	0.613	0.300
	207	cadve210	34.689	0.597	0.288
	207	cadve212	49.437	0.924	0.707
	194	cadve217	27.014	0.115	0.056
	194	cadve218	27.993	0.130	0.063
	194	cadve219	28.827	0.144	0.069
	194	cadve220	7.161	0.008	0.005
	194	cadve221	29.507	0.157	0.075
	194	cadve222	27.733	0.126	0.061
	194	cadve223	36.201	0.326	0.153
	194	cadve225	37.608	0.372	0.177
	195	cadve227	36.289	0.651	0.329
	195	cadve229	33.901	0.570	0.269
	195	cadve230	27.743	0.354	0.149
	195	cadve231	29.114	0.400	0.171
	195	cadve232	29.225	0.404	0.173
	195	cadve233	29.107	0.400	0.171
	195	cadve234	29.751	0.422	0.182
	195	cadve238	54.304	0.961	0.813
13_Cesari_1990	THC11	thc11	43.501	0.675	0.373
	THC12	thc12	44.574	0.379	0.196
	THC13	thc13	38.193	0.854	0.541
	THC14	thc14	41.772	0.817	0.505
	THC15	thc15	41.152	0.730	0.411
	THC16	thc16	45.010	0.818	0.518

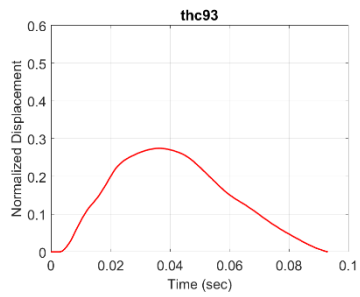
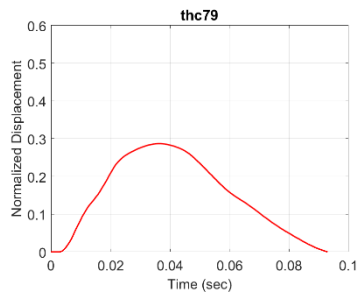
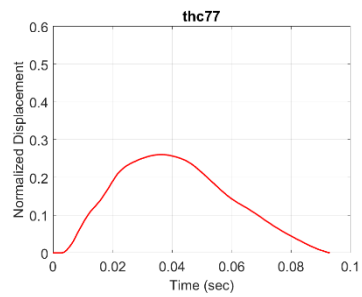
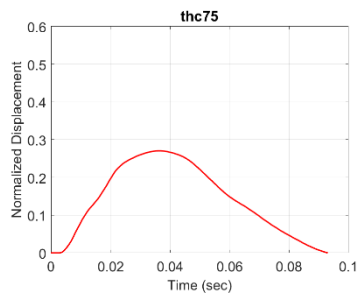
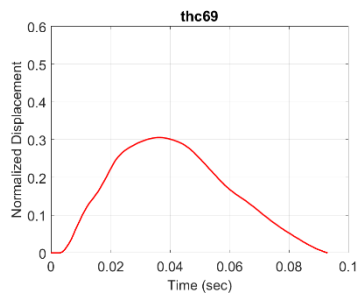
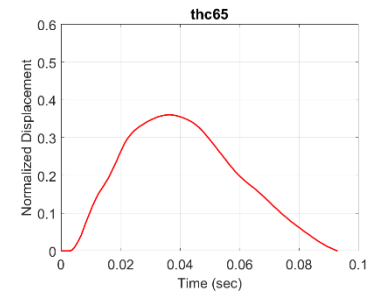
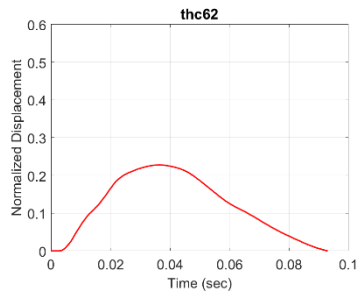
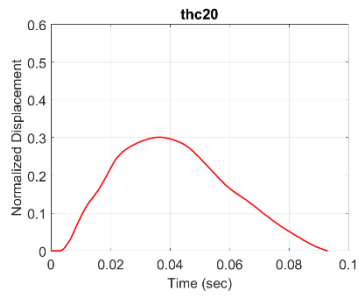
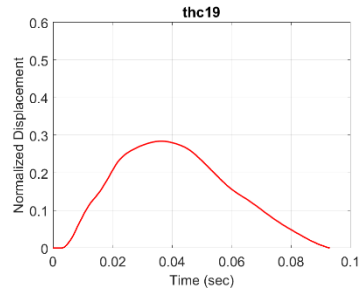
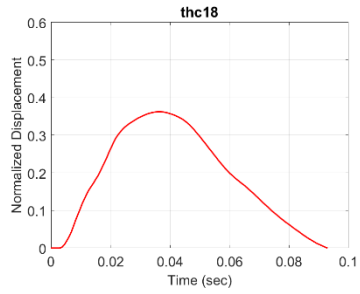
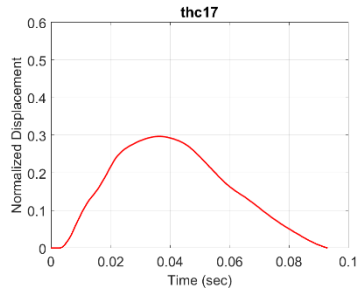
	THC17	thc17	41.520	0.825	0.514
	THC18	thc18	45.357	0.872	0.595
	THC19	thc19	40.804	0.881	0.594
	THC20	thc20	41.749	0.823	0.513
	THC62	thc62	36.449	0.706	0.372
	THC65	thc65	45.126	0.888	0.621
	THC69	thc69	42.215	0.556	0.287
	THC75	thc75	39.658	0.686	0.368
	THC77	thc77	38.949	0.703	0.380
	THC79	thc79	40.950	0.546	0.276
	THC93	thc93	40.137	0.729	0.406
Gold Standard 1	411	1294	40.399	0.835	0.523
	403	1295	40.399	0.572	0.290
	425	1358	40.399	0.648	0.342
	426	1359	40.399	0.594	0.305
	428	1360	40.399	0.679	0.365
	443	1378	40.399	0.808	0.489
	433	1379	40.399	0.492	0.244
	441	1380	40.399	0.457	0.226
Gold Standard 2	494	UVAS028	29.347	0.323	0.139
	492	UVAS029	29.347	0.397	0.170
	674	UVAS0302	29.347	0.408	0.175
	736	UVAS0303	29.347	0.408	0.175
	695	UVAS0304	29.347	0.488	0.212
Gold Standard 3	632	UVAS0313	21.212	0.191	0.078
	750	UVAS0314	21.212	0.171	0.071
	767	UVAS0315	21.212	0.177	0.073
Rear Seat (Forman 2009)	1	1386	35.293	0.617	0.303
	2	1387	35.293	0.639	0.318
	3	1389	35.293	0.670	0.340
Rear Seat (Michaelson 2008)	1	1262	41.194	0.643	0.340
	2	1263	41.194	0.703	0.388
	3	1264	41.194	0.703	0.388
Low Speed Frontal	322	1094	32.416	0.319	0.143
	327	1096	32.416	0.228	0.106
	323	1095	32.416	0.271	0.123

APPENDIX D: Normalized input displacement curves for Table Top

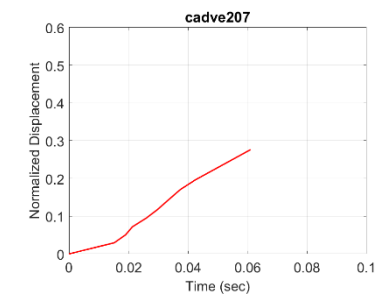
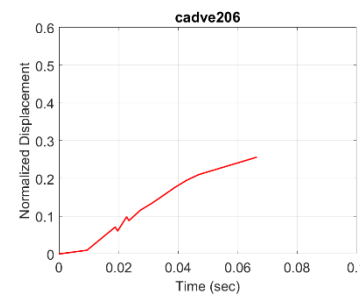
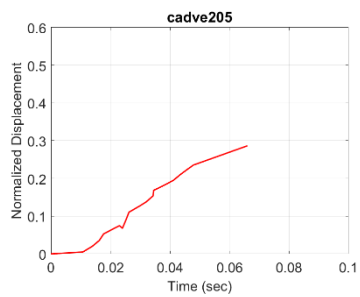
Tests

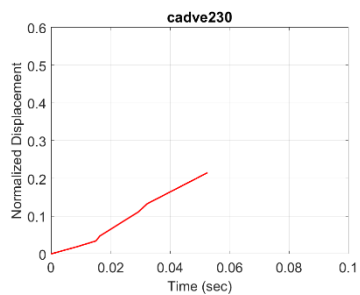
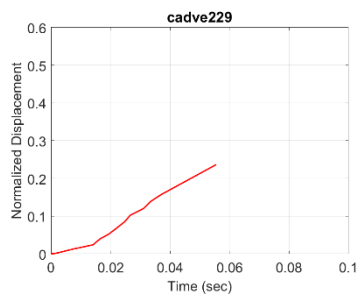
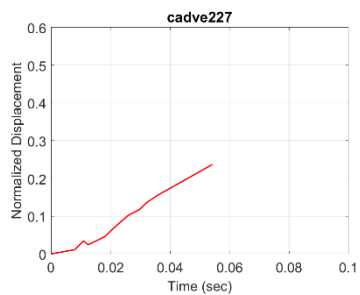
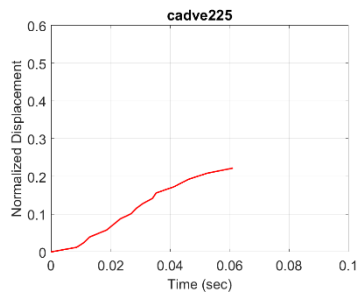
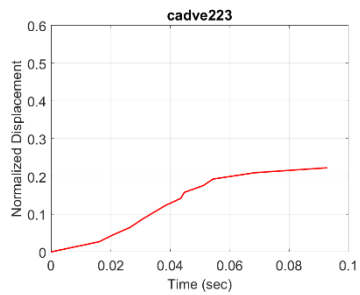
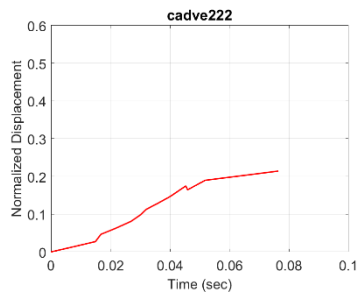
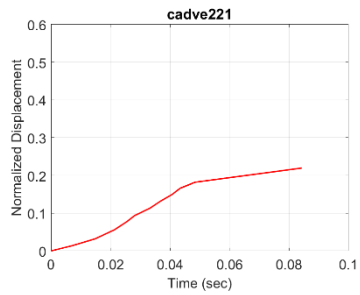
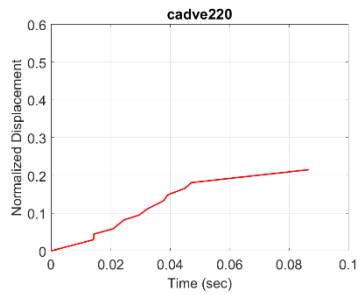
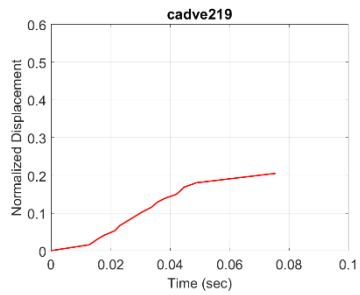
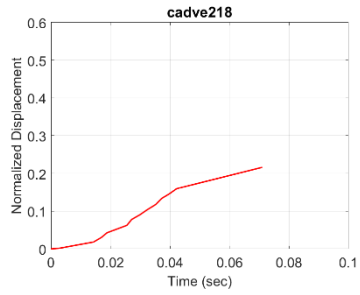
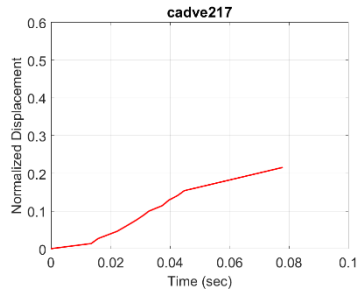
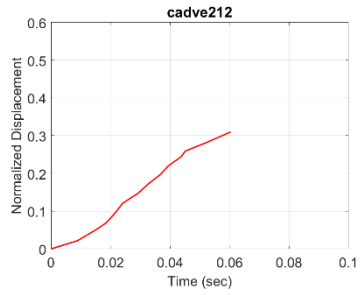
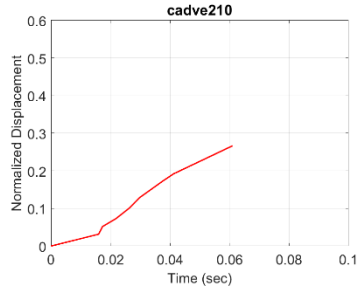
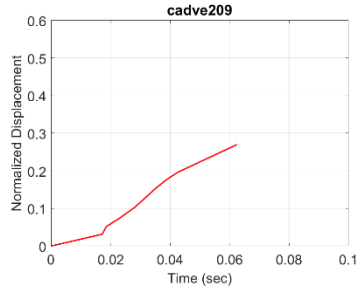
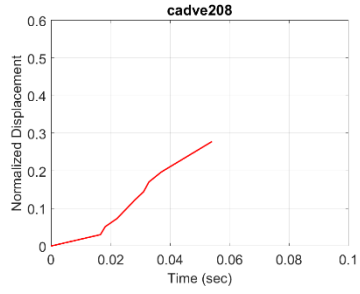
- Cesari 1990, 1994

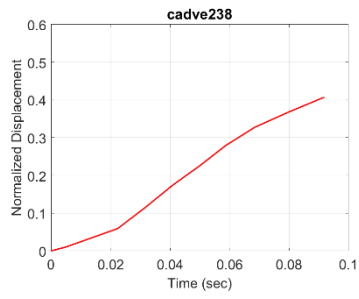
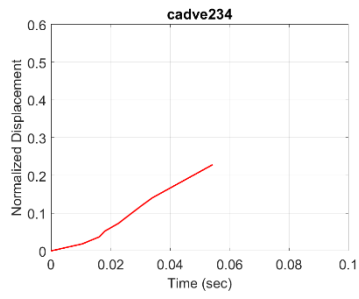
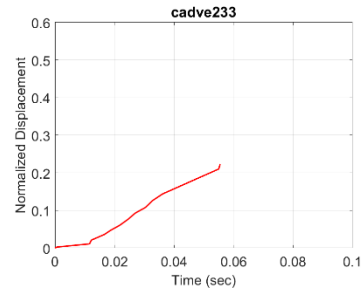
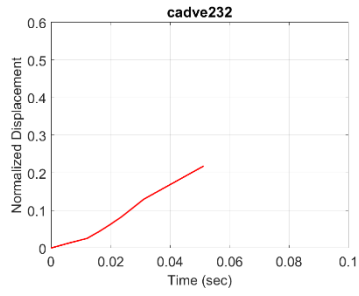
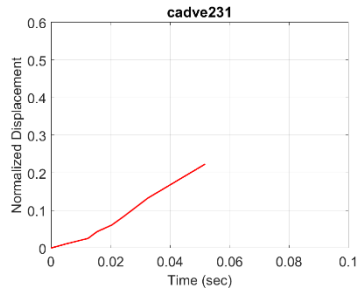




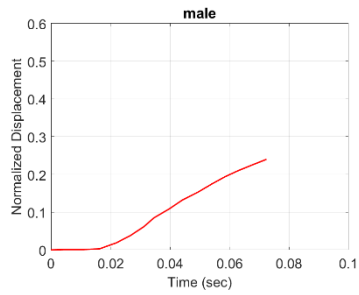
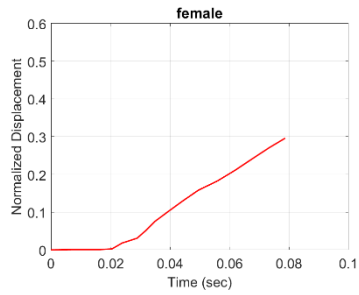
● Forman 2005



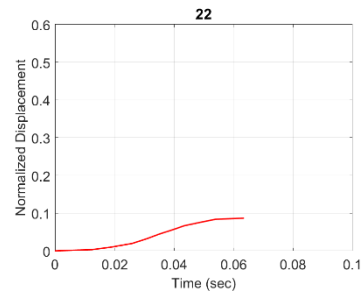
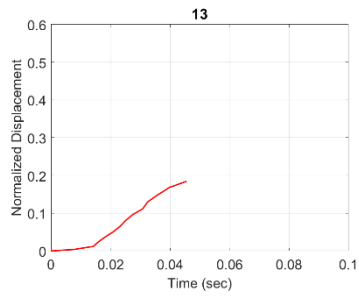
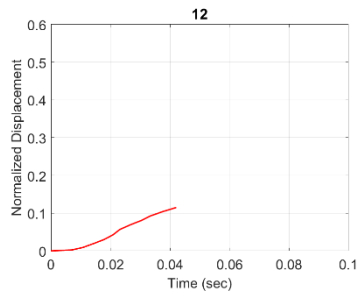


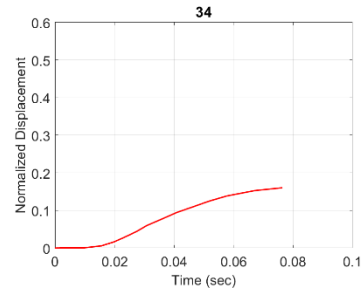
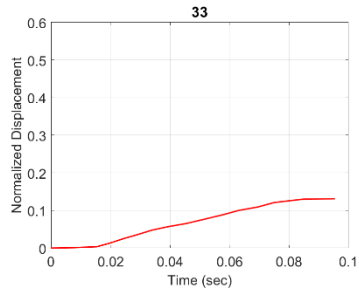
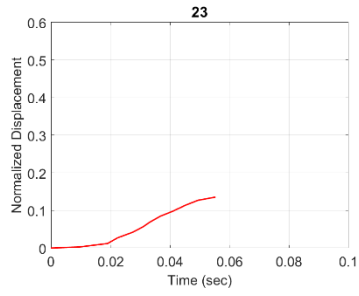


- **Kemper 2011**

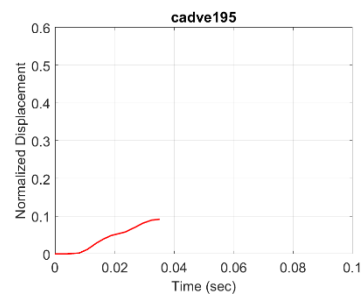
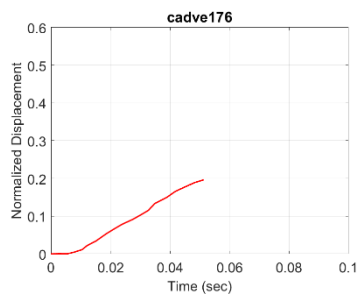
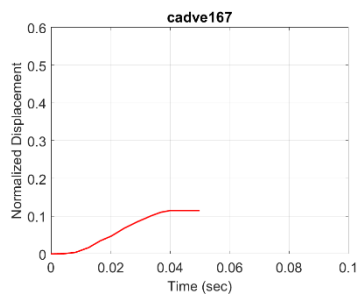
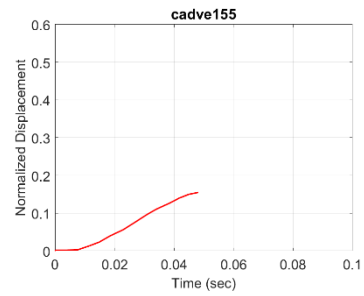
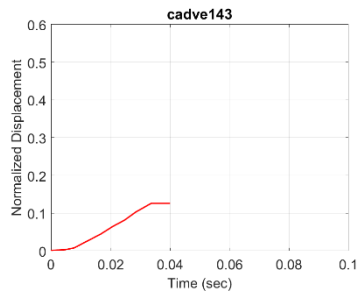
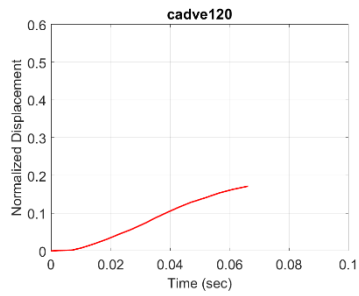
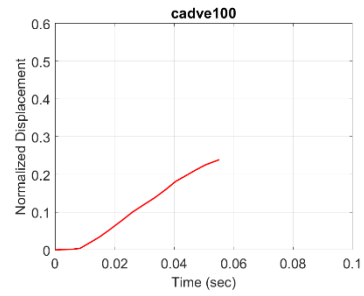
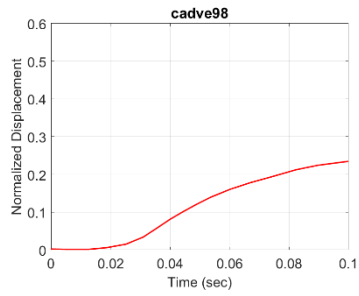
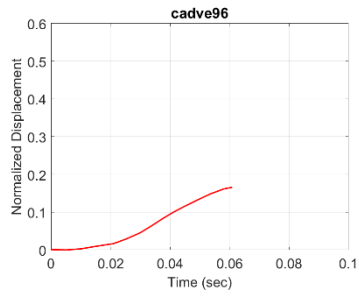
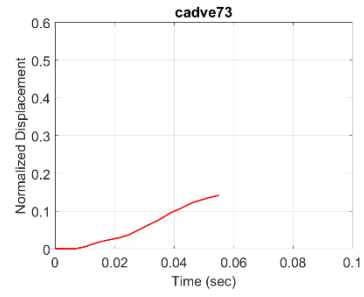
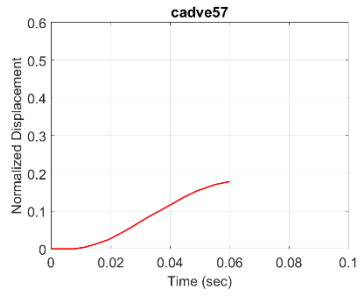
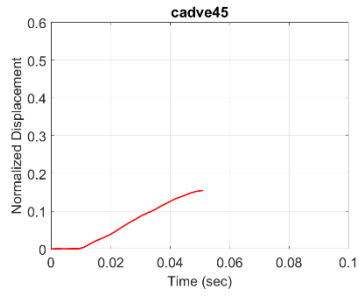


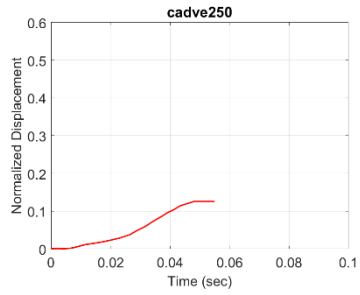
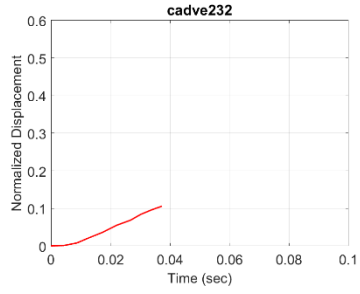
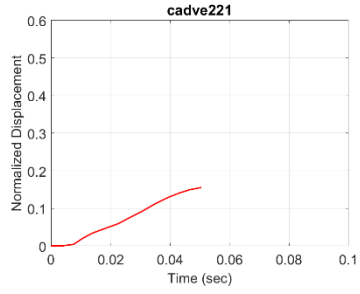
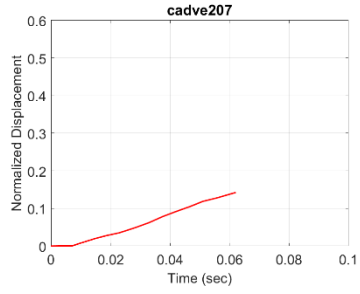
- **Salzar 2009**



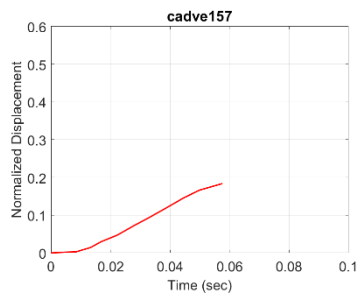
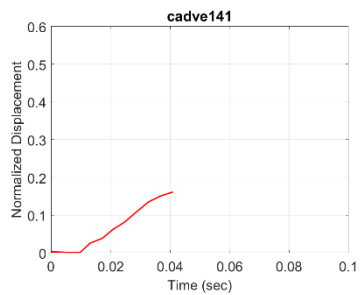
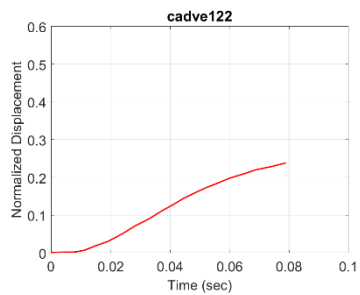
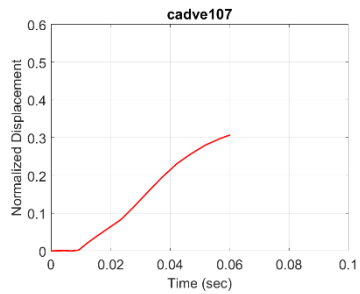
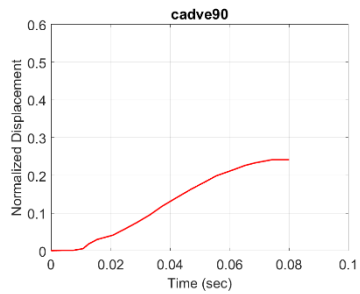
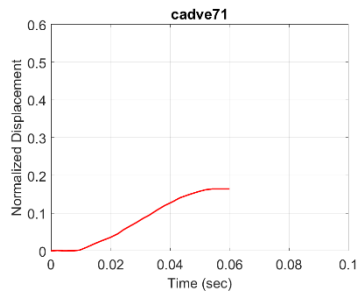


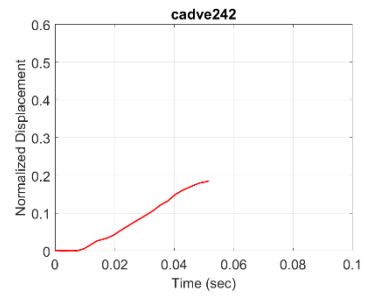
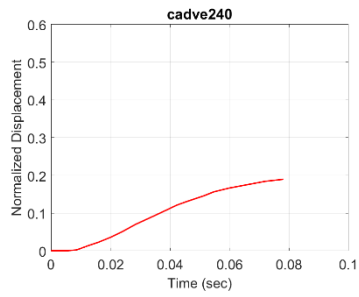
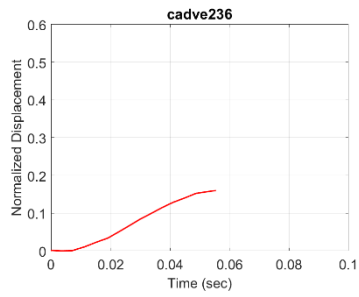
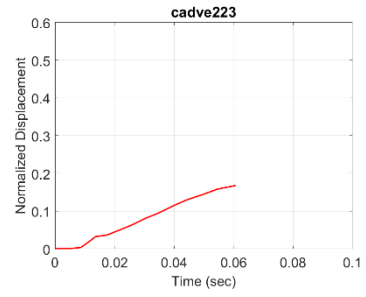
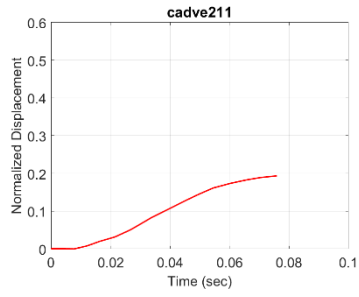
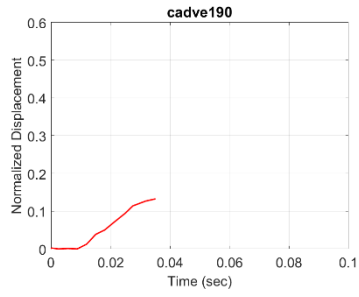
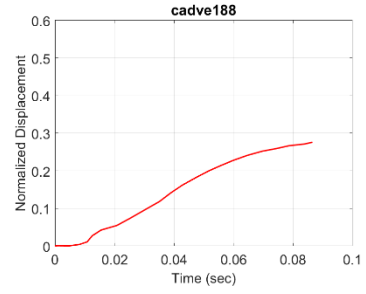
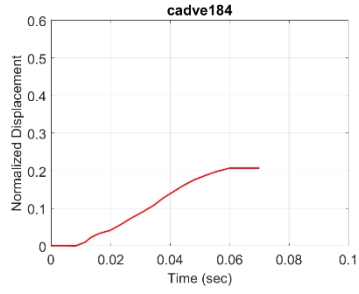
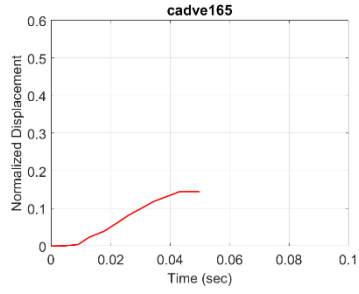
• Kent 2004 Distributed



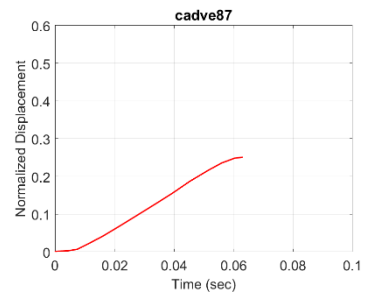
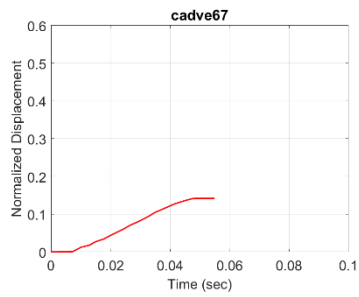
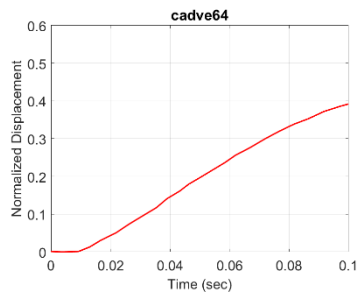
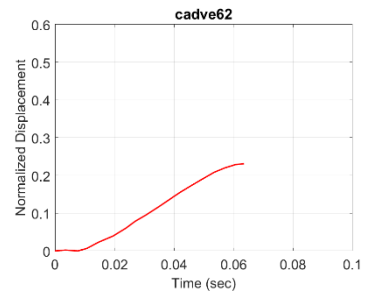
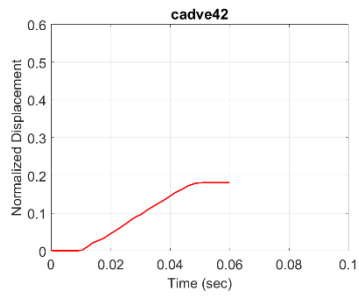
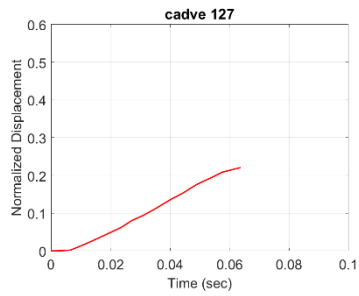


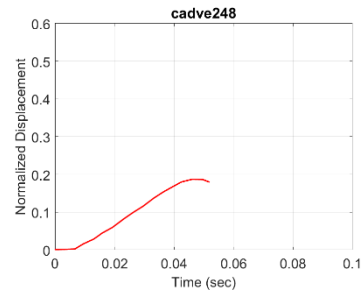
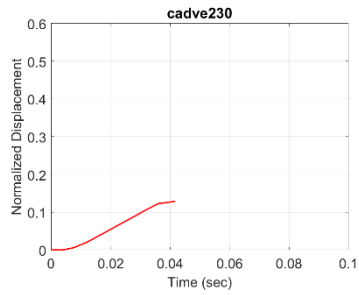
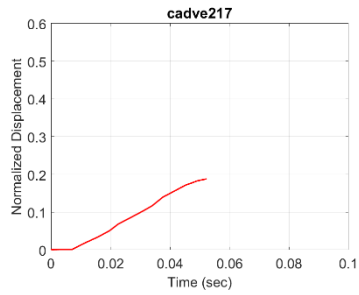
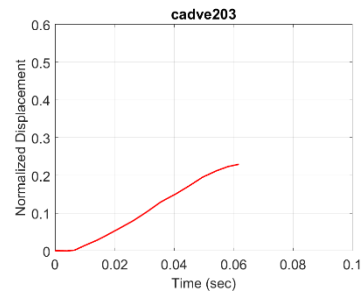
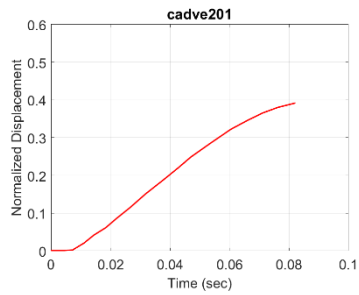
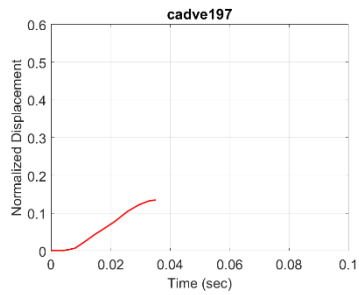
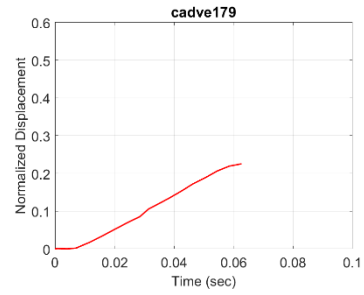
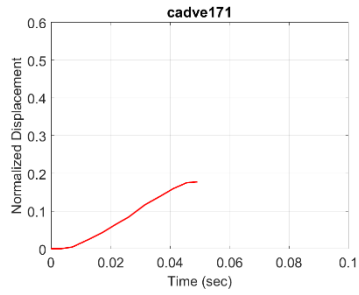
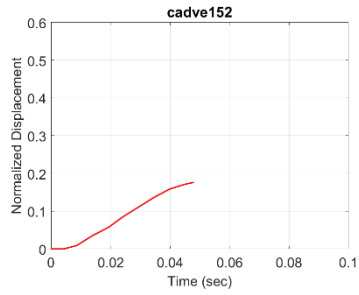
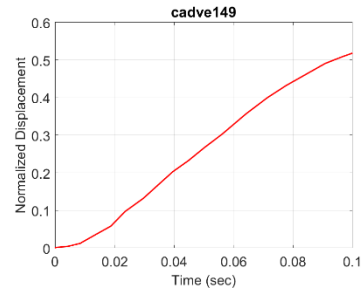
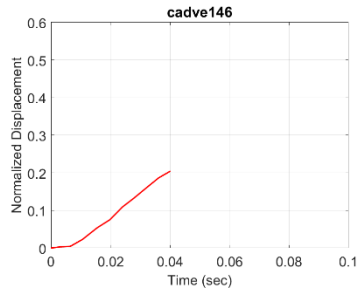
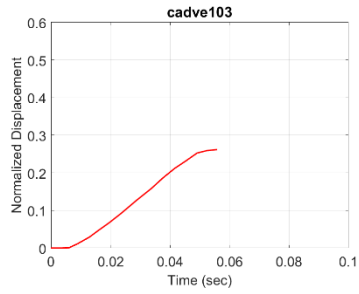
- Kent 2004 Double belt





● Kent 2004 Hub





● Kent 2004 Single Belt

